The University Of Sheffield.

White Noise Reduction for Wideband Sensor Array Signal Processing

Mohammad Reza Anbiyaei

Supervisors:

Dr. Wei Liu

and

Dr. Xiaoli Chu

Thesis submitted in candidature
for graduating with degree of doctor of philosophy

March 2018

Abstract

The performance of wideband array signal processing algorithms is dependant on the noise level in the system. In this thesis, a method is proposed for reducing the level of white noise in wideband arrays via a judiciously designed spatial transformation followed by a bank of high-pass filters. The method is initially introduced for uniform linear arrays (ULAs) and analysed in detail. The spectrum of the signal and noise after being processed by the proposed noise reduction method is analysed, and the correlation matrix of the processed noise is derived.

The reduced noise level leads to a higher signal-to-noise ratio (SNR) for the system, which can have a significant effect on the performance improvement of various beamforming methods and other array signal processing applications such as direction of arrival (DOA) estimation.

The performance of two well-known beamformers, the reference signal based (RSB) beamformer and the linearly constrained minimum variance (LCMV) beamformer is reviewed. Then, the theoretical effect of applying the proposed noise reduction method as a pre-processing step on the performance enhancement of RSB and LCMV beamformers is studied. The theoretical results are then confirmed by simulation. As a representative example of wideband DOA estimation application, a compressive sensing-based DOA estimation method is employed to demonstrate the improved estimation by applying the pre-processing noise reduction method, which is confirmed by simulation.

Next, the idea is extended to wideband non-uniform linear arrays (NLAs). Since, NLA does not have a uniform spacing, the beam response of the row vectors of the transformation is distorted. Therefore, the transformation is re-designed using the least squares method to satisfy the band-pass requirements of the transformation. Simulation results show a satisfactory improvement in the the performance of RSB and LCMV beamformers for the NLA structure.

The idea is further extended to uniform rectangular arrays (URAs) and uniform circular arrays (UCAs), as two major types of the planar arrays. Two methods are proposed for reducing the effect of white noise in wideband URAs and for each one, a different transformation is designed. The first one is based on a two-dimensional (2D) transformation and the second one is an adaptation of the method developed for the ULA case. The developed method for the UCA structure is based on a one-dimensional (1D) transformation, with modified modulation for the transformation to satisfy the required band-pass characteristics of the transformation. Same as linear array structures, the RSB and LCMV beamformers are used to demonstrate the performance enhancement of the method for planar arrays.

Contents

List of Abbreviations:

ANC	Active Noise Control
CRB	Cramer-Rao Bound
CS	Compressive Sensing
CSSM	Coherent Signal Subspace Method
DFT	Discrete Fourier Transform
DTFT	Discrete-Time Fourier Transform
DOA	Direction of Arrival
ESPRIT	Estimation of Signal Parameters via Rotational Invariance Techniques
FFT	Fast Fourier Transform
FIR	Finite Impulse Response
ISSM	Incoherent Signal Subspace Method
LCMV	Linearly Constrained Minimum Variance
MSE	Mean Square Error
MUSIC	MUltiple Signal Classification
NLA	Non-uniform Linear Array
NP	Non-deterministic Polynomial-time
NR	Noise Reduction
PSD	Power Spectral Density
RMSE	Root Mean Square Error
RSB	Reference Signal Based
SBL	Sparse Bayesian Learning
SINR	Signal-to-Interference plus Noise Ratio
SIR	Signal-to-Interference Ratio
SNR	Signal-to-Noise Ratio
SRACV	Sparse Representation of Array Covariance Vector

SVD	Singular Value Decomposition
TDL	Tapped Delay-Line
TOPS	Test of Orthogonality of Projected Subspaces method
TSNR	Total Signal-to-Noise Ratio
ULA	Uniform Linear Array
UCA	Uniform Circular Array
URA	Uniform Rectangular Array
ZP	Zero Phase

List of Figures

List of Tables

List of Publications:

Journal papers:

1. M. R. Anbiyaei, W. Liu, and D. C. McLernon, " White noise reduction for wideband linear array signal processing", *IET Signal Processing*, DOI: 10.1049/iet-spr.2016.0730, accepted, yet to appear in the printed journal.

Conference papers:

1. M. R. Anbiyaei, W. Liu, and D. C. McLernon, "Performance improvement for wideband beamforming with white noise reduction based on sparse arrays", in *Proc. 25th European Signal Processing Conference*, pp. 2433-2437, Greece, September 2017.

2. M. R. Anbiyaei, W. Liu, and D. C. McLernon, "White noise reduction for wideband beamforming based on uniform rectangular arrays", in *Proc. 22nd Digital Signal Processing Conference*, pp. 1-5, London, UK, August 2017.

3. M. R. Anbiyaei, W. Liu, and D. C. McLernon, "Performance improvement for wideband DOA estimation with white noise reduction based on uniform linear arrays," in *Proc. IEEE, 9th Sensor Array and Multichannel Signal Processing Workshop (SAM)*, pp. 1-5, Rio de Janeiro, Brazil, July 2016.

Acknowledgements:

I would like to take this opportunity to express my deepest gratitude to my supervisor Dr. Wei Liu for his persistent encouragement, guidance and support, and also for giving me the opportunity to pursue my PhD studies under his supervision.

I also thank my second supervisor Dr. Xiaoli Chu for her help and support regarding the doctoral development program.

Finally, I would like to thank my parents for their continuous encouragement and support.

Chapter 1

Introduction

1.1 Introduction

Wideband array signal processing, including beamforming and direction of arrival (DOA) estimation, has various applications in radar, sonar and wireless communications, and has been studied extensively in the past.

In [1], different adaptive beamformer methods and parameter estimation is reviewed thoroughly. Wei et. al [2] has reviewed different methods of beamforming and array structures. Krim and Vberg review background material and of the basic problem formulation of the parameter estimation in [3]. They introduce spectral-based algorithmic solutions to the signal parameter estimation problem, and the suboptimal solutions are compared to the parametric methods. Allen and Ghavami review the fundamentals of array signal processing in [4], and they review different adaptive beamforming and estimation methods considering both narrowband and wideband cases. Some difficulties and practical techniques related to sensor

arrays are addressed in [5]. Such as, placing sensors as an array for accurate measurement, calibrating a sensor array by experiment and etc.

The performance of wideband array signal processing algorithms is dependent on the level of noise in the system, and normally the lower the level of noise, the better the performance is. Many methods have been developed in the past to reduce the noise level, such as adaptive noise cancellation (ANC) [6], the Wiener filters [7, 8], and zero phase (ZP) noise reduction methods [9, 10]. The ANC uses a reference undesired noise source and a primary source contaminated by noise, and then adaptive filtering is employed to produce a cleaned result [11]. The Wiener filter produces an estimate of the desired signal by minimising the mean squared error (MSE) between the noisy signal and a reference [12, 13]. The ANC and Wiener filter methods have proved to work well in specific applications but due to their adaptive nature, they have high computational complexity. ZP noise reducers can reduce the noise without the need to know a priori information of the signal [14, 15]. The limitation of ZP noise reducers is that, the signal has to be periodic [16], and it is mainly applied to speech signals. In this thesis, a novel non-adaptive white noise reduction approach is developed with low computational complexity, and relatively good performance, with no limitation on the received wideband signal.

In addition to the wideband beamforming, the wideband DOA estimation is also a field of interest in this thesis. Many DOA methods have been proposed for both narrowband and wideband signals, and two rep-

resentative ones are the multiple signal classification (MUSIC) [17] and the estimation of signal parameters via rotational invariance techniques (ESPRIT) [18] algorithms, which were originally proposed for narrowband signals. For wideband signals, a commonly used approach is to decompose the wideband signal into different frequency bins and transform the wideband problem into a narrowband one through various focusing or interpolation algorithms [19, 20]. In addition, methods such as incoherent signal subspace method (ISSM) [21], coherent signal subspace method (CSSM) [22] and test of orthogonality of projected subspaces method (TOPS) [23] have also been proposed.

Recently, with the development of compressive sensing theory [24, 25], many sparsity based DOA estimation methods were developed. A source localization method based on a sparse representation of sensor measurements is introduced in [26]. In [27], a DOA estimation method is proposed based on a novel data model using the concept of a sparse representation of array covariance vectors (SRACV), in which DOA estimation is achieved by jointly finding the sparsest coefficients of the array covariance vectors. The sparse spectrum fitting algorithm for the estimation of DOAs of multiple sources is introduced in [28], and its asymptotic consistency and effective regularization under both asymptotic and finite sample cases are studied. In [29], the authors propose co-prime arrays for effective DOA estimation.

In addition, various extensions of the above methods are developed for

the wideband case. A method named wideband covariance matrix sparse representation (W-CMSR) is proposed in [30]. In this method, the lower left triangular elements of the covariance matrix are aligned to form a new measurement vector, then DOA estimation is achieved by representing this vector on an over-complete dictionary under the constraint of sparsity. In [31], the sparse Bayesian learning (SBL) technique is used to estimate the DOAs of independent narrowband/wideband signals by reconstructing the covariance vectors with high computational efficiency. In [32], a class of low-complexity compressive sensing-based DOA estimation methods for wideband co-prime arrays is proposed, which is based on the narrowband DOA estimation method for co-prime arrays [29].

Wideband arrays are affected by noise from different sources. These noise sources include the voltages due to thermal noise [33] also known as Johnson-Nyquist noise [34], the shot noise [35], the cosmic black-body radiation [36] and etc. The classical central limit theorem [37] asserts that the distribution of the summation of different random variables converges to a normal, Gaussian distribution with mean 0, which is the definition of the white noise. Therefore, one common assumption for noise in wideband arrays is that it is spatially (and in many cases also temporally) white. That is, the noise at one array sensor is uncorrelated with that at other sensors. Under this assumption, it seems that there is not much can be done about it and simply it has to be accepted whatever is left of the noise component after processing the signals. For example, in the simplest beamforming

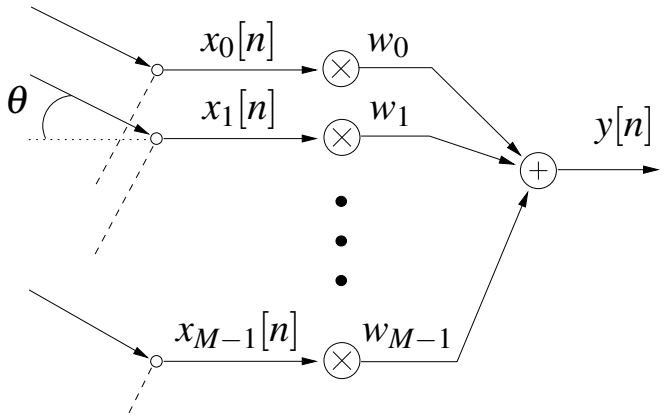

Fig. 1.1: A simple beamformer with its output $y[n]$ given by a linear combination of the received array signals $x_0[n], x_1[n], \cdots, x_{M-1}[n]$ weighted with the coefficients w_0, w_1, $\cdots$, w_{M-1}.

structure shown in Fig. 1.1, the beamformer output $y[n]$ is a linear combination of the received array signals $x_0[n], x_1[n], \cdots, x_{M-1}[n]$ weighted with the coefficients w_0, w_1, $\cdots$, w_{M-1}, where n is the discrete time index, M is the number of sensors in the array and θ is the angle of arrival of the impinging signal. The values of these coefficients are obtained based on some criterion such as maximising the output signal-to-interference plus noise ratio (SINR).

The question here is, whether there is anything that can be done to reduce the effect of the white noise in a wideband array system (without attenuating the directional signals) so that the performance of the subsequent processing (such as DOA estimation and beamforming) can be improved.

In this thesis, the aim is to answer that question by developing a novel method to reduce the white noise level of a wideband array using a combi-

nation of a set of judiciously designed spatial transformations and a bank of high-pass filters, and the key is to realise that the white noise and the directional wideband signals received by the array have different spatial characteristics. Based on this difference, and motivated by the low-complexity subband-selective adaptive beamformer proposed in [38], first the received wideband sensor signals is transformed into a new domain where the directional signals are decomposed in such a way that their corresponding outputs are associated with a series of tighter and tighter high-pass spectra, while the spectrum of noise still covers the full band from $-\pi$ to π in the normalised frequency domain. Then, a series of high-pass filters with different cut-off frequencies are applied to selectively remove part of the noise spectrum while keeping the directional signals unchanged. Finally, an inverse transformation is applied to the filtered outputs to recover the original sensor signals, where compared to the original set of received sensor signals, the directional signals are left intact while the noise power has been reduced.

One condition placed on the transformation matrix is that it must be invertible. It has been further assumed that it is also unitary and thus the discrete Fourier transform (DFT) matrix is used as a representative example for the uniform linear array (ULA) case and a least squares based design is introduced for the non-uniform linear array (NLA) case. Detailed analysis shows that the signal-to-noise ratio (SNR) of the array after the proposed processing can be improved by about 3 dB in the ideal case. This

is then translated into improved performance for beamforming, as demonstrated by both theoretical analysis and simulation results. This work is focused on two well-known beamformers, namely the reference signal based (RSB) [39, 40], and the linearly constrained minimum variance (LCMV) beamformers [41].

The method is also extended to uniform rectangular arrays (URAs), and uniform circular arrays (UCAs) as examples of planar arrays.

1.2 Original Contributions

The original contributions of this work to the field of array signal processing are listed as follows,

- The SNR of the received signal can be improved by a maximum of 3 dB using the proposed noise reduction method for different array structures such as ULA, NLA, URA and UCA which have been presented in this work.

- Using the developed noise reduction method an increased output SINR performance is achieved for the classic RSB and LCMV beamformers, for different array structures.

- Simulation results show an improved estimation accuracy for the compressive sensing based DOA estimation for the ULA structure.

- The method provides an alternative approach to beamforming with

reduced computational complexity and more robustness.

- No prior information of the impinging signal is needed and the method is quite flexible. Therefore, it can be used for different array signal processing applications, such as beamforming and DOA estimation.

In the following, the contributions of the work are explained in greater detail.

1.2.1 White noise reduction for wideband uniform linear array signal processing with applications in beamforming and DOA estimation

A novel method is proposed for reducing the level of white noise in wideband ULAs via a judiciously designed spatial transformation followed by a bank of high-pass filters. 3 dB improvement in total SNR is achieved by this method. A detailed analysis of the method and its effect on the spectrum of the signal and noise is presented. The reduced noise level leads to a higher SNR for the system, which can have significant effect on the performance of various beamforming methods and other signal processing applications, such as DOA estimation.

The improved performance of two well-known beamformers, namely, the RSB and the LCMV beamformers is analysed. Initially, a detailed theoretical performance analysis is presented, and then, the improved performance is confirmed using simulation.

A compressive sensing based method employing the group sparsity concept is employed to analyse the performance improvement for DOA estimation. The performance is evaluated by calculating the error between the estimated and the actual DOA angles of the received signals. By applying the noise reduction method, the error between the estimated and the actual DOA angles was reduced. Therefore, the estimation accuracy has been improved by employing the noise reduction method. The improved estimation accuracy is confirmed by simulation.

By studying the structure of the method further, it is understood that if a classic beamformer is applied to a set of array signals which have been processed by the noise reduction method, the pre-processing and the classic beamformer can be modelled as an equivalent beamformer with longer TDLs. Additionally, the complexity of the noise reduction method including the beamformer part is less than the direct implementation with equivalent length. Also, with the noise reduction method, a more robust beamforming can be achieved, since by using the noise reduction pre-processing the numerical issues due to calculating the optimum beamforming coefficients based on inversion of correlation matrices can be avoided.

1.2.2 Extension of the white noise reduction method for non-uniform linear arrays

The idea is extended to the NLAs by redesigning the transformation using least squares filter design method. Therefore, the noise reduction method

is adjusted to be applicable to the non-uniform sensor layout of NLAs. A prototype filter using least squares method is designed, and modulated to different frequency subbands to cover the whole normalised spectrum. A low condition number is crucial, to be certain that the transformation is invertible. Initially, the diagonal loading method is used to keep the condition number low. Similar to the ULA case, 3 dB improvement in total SNR is achieved, which leads to the performance enhancement for beamforming. This enhancement is demonstrated by simulation, using RSB and LCMV beamformers.

Also, for reducing the condition number of the designed transformation matrix, a modification method is proposed based on replacing the small singular values of the transformation. The effect of this modification method on the beam-pattern and the condition number of the transformation is presented, and the beamforming performance of the noise reduction method using the modified transformation is investigated using simulation.

1.2.3 Extension of the white noise reduction method for planar arrays

The idea is also extended to two major types of planar arrays, namely, URAs and UCAs.

In case of the URA, two design methods are introduced for the noise reduction method, and for each one the transformation is redesigned. The first method is based on a two-dimensional (2D) transformation, and the

second one is an adaptation of the ULA noise reduction method, which is based on one-dimensional (1D) transformation of the received signals.

For the UCA case, a 1D transformation is presented, which is almost similar to the ULA case, and the difference is in modulating the prototype filter to different subbands. Due to the sparse nature of circular arrays, the condition number of the transformation might be high, which is in this case, and the condition number is reduced by replacing the small singular values of the transformation, same as in the NLA case.

The effect of the noise reduction methods for the planar arrays on performance improvement of RSB and LCMV beamformers is confirmed by simulation.

1.3 Outline

This thesis is organised as follows.

In Chapter 2, the wideband beamforming is briefly reviewed and a detailed theoretical performance analysis is provided for the two well-known classic beamformers, namely, RSB and LCMV beamformers. These two beamformers are used for different applications in this thesis.

The white noise reduction method based on the ULA structure is proposed in Chapter 3, with a detailed analysis of the spectrum and correlation matrix of the noise after the proposed processing, when DFT matrix is used as transformation. Then, the effect of the noise reduction method on

the performance enhancement of the RSB and LCMV beamformers and a compressive sensing based DOA estimation is presented, and confirmed by simulation results.

The idea is extended to the structure of the NLAs in Chapter 4. The least squares approach is used for designing the transformation with satisfactory band-pass response.

The idea is further extended to the URA and UCA structures as examples of the planar arrays in Chapter 5, where two methods are presented for the URA case, one based on 2D filtering and one by directly adopting the method developed for the ULA structure. For the UCA case, the modulation of the row vectors of the transformation is modified to satisfy the structure of the UCA.

In Chapter 6, it is shown that the proposed noise reduction method is equivalent to a traditional tapped delay-line (TDL) system. The performance and computational complexity of the beamformers are compared, with the proposed pre-processing and without any pre-processing with the same length.

Finally, conclusions are drawn in Chapter 7, with possible topics for future work.

Chapter 2

Adaptive Wideband Beamforming

In this chapter, the general idea of wideband beamforming is briefly reviewed. The RSB and LCMV beamformers are reviewed as examples for adaptive wideband beamforming, and a detailed analysis of their performance is provided.

2.1 Wideband Beamforming

For wideband beamforming, a TDL is normally employed, with Fig. 2.1 showing a general structure, where M is the number of sensors, J is the length of the TDL and Δ denotes a tapped delay. The coefficient for the m-th sensor at the k-th position of the TDL is denoted by $w_{m,k}$, $m = 0, \cdots, M-1$, $k = 0, \cdots, J-1$. All J weights at the m-th TDL form an *element* weight vector $\mathbf{w}_m$, $m = 0, \cdots, M-1$, and all M element weight vectors form a $MJ \times 1$ *total* weight vector $\mathbf{w}$, and they are defined as:

$$\mathbf{w}_m = [w_{m,0}, w_{m,1}, \cdots, w_{m,J-1}]^T, \tag{2.1}$$

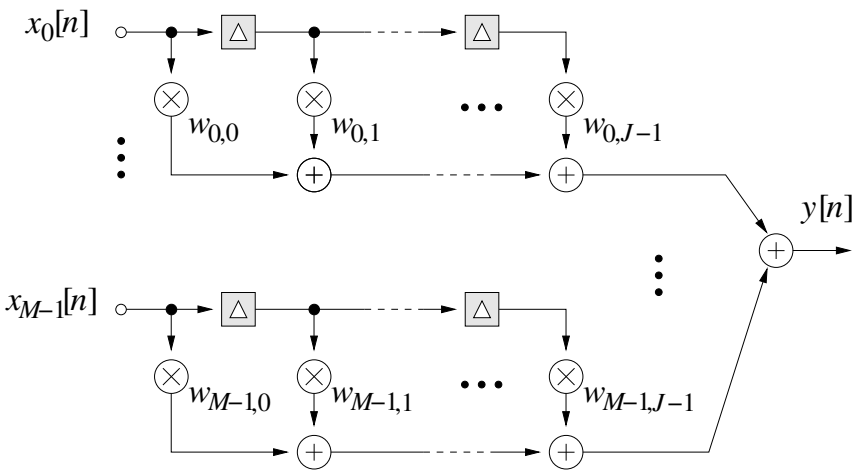

Fig. 2.1: A general wideband beamformer with M sensors and J taps.

$$\mathbf{w} = \left[\mathbf{w}_0^T, \mathbf{w}_1^T, \cdots \mathbf{w}_{M-1}^T\right]^T \ , \tag{2.2}$$

where $\{\cdot\}^T$ denotes the transpose. The received signal by the m-th sensor at the k-th position of the TDL is denoted by $x_{m,k}[n]$, $m = 0, \cdots, M-1$, $k = 0, \cdots, J-1$. All J received signals at the m-th TDL form an *element signal vector* $\mathbf{x}_m$, $m = 0, \cdots, M-1$ and all M element signal vectors form the total input signal vector $\mathbf{x}$, which are defined as:

$$\mathbf{x}_m = \left[x_{m,0}[n], x_{m,1}[n], \cdots, x_{m,M-1}[n]\right]^T , \tag{2.3}$$

$$\mathbf{x} = \left[\mathbf{x}_0^T, \mathbf{x}_1^T, \cdots, \mathbf{x}_{M-1}^T\right]^T \ . \tag{2.4}$$

Finally, the beamformer output $y[n]$ is given by

$$y[n] = \mathbf{w}^T \mathbf{x} \ . \tag{2.5}$$

The idea is to process the received array signals by the noise reduction method, so that the noise level in the received signals will be reduced. Then, the new set of array signals with reduced noise level will be fed to the

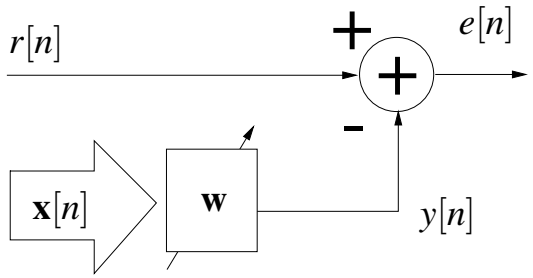

Fig. 2.2: The RSB adaptive beamforming structure.

following beamformers. In the following, two widely-used adaptive beamforming methods are briefly reviewed and the theoretical performance results are then derived based on the proposed noise reduction method.

2.2 Reference Signal Based Adaptive Beamformer

The reference signal based (RSB) beamformer is normally employed when a reference signal $r[n]$ is available, where the weight vector of the beamformer can be adjusted to minimise the MSE between the reference signal and the beamformer output $y[n]$ [39,40], as shown in Fig. 2.2. The $MJ \times 1$ optimal weight vector is given by:

$$\mathbf{w}_{opt} = \mathbf{\Phi}_x{}^{-1}\mathbf{s}_d \ , \tag{2.6}$$

where $\{\cdot\}^{-1}$ denotes the inverse operator, $\mathbf{\Phi}_x$ is the signal correlation matrix with size $MJ \times MJ$, and is defined by:

$$\mathbf{\Phi}_x = E\left[\mathbf{x}^*\mathbf{x}^T\right] \ , \tag{2.7}$$

where $E\{\cdot\}$ denotes the mathematical expectation, $\{\cdot\}^*$ denotes the complex conjugate, and $\mathbf{s}_d$ is the reference correlation vector with size $MJ \times 1$,

$$\mathbf{s}_d = E\left[\mathbf{x}^* r_0[n]\right] \ , \tag{2.8}$$

with $r_0[n]$ being the normalised reference signal with unit power.

There are three components for each of the received sensor signals: desired signal $x_d[n]$, interference $x_i[n]$ and noise $x_v[n]$. The desired signal $x_d[n]$ is a deterministic signal received from the intended transmitter. The interference $x_i[n]$ is a deterministic or random signal received by the array transmitted from a source but it does not have the characteristics of the desired signal. The interference can be a deterministic signal transmitted from the same source as the desired signal, which is the case for the multipath reflection [42]. Otherwise, the source of interference can be from different transmitters, which is the case when there are different transmitters in the range. This can happen when multiple transmitters and receivers are trying to communicate in the same area. Also, disturbance signals transmitted from the jammers are considered as interference [43]. The jammers may transmit deterministic or random signals to interrupt the communication between the transmitter based on their design. The noise $x_v[n]$ is a random signal which come from different sources such as the voltages due to thermal noise [33] also known as Johnson-Nyquist noise [34], the shot noise [35], the cosmic black-body radiation [36] and etc.

The total signal absorption at any time in an array is the linear superpo-

sition of the absorption associated with all the impinging signals and the noise [44, 45]. Therefore, the signal available at the m-th sensor and k-th tap is,

$$x_{m,k}[n] = x_{d_{m,k}}[n] + x_{i_{m,k}}[n] + x_{v_{m,k}}[n] \; . \tag{2.9}$$

So, the total signal vector $\mathbf{x}$ can also be decomposed into three corresponding parts:

$$\mathbf{x} = \mathbf{x}_d + \mathbf{x}_i + \mathbf{x}_v. \tag{2.10}$$

Since the desired signal, interference and noise are independent and so, uncorrelated with each other, $\mathbf{\Phi}_x$ is also a linear superposition of the corresponding parts and can be decomposed into three $MJ \times MJ$ correlation matrices corresponding to the desired signal, interference and white noise components, respectively. i.e.,

$$\mathbf{\Phi}_x = \mathbf{\Phi}_d + \mathbf{\Phi}_i + \mathbf{\Phi}_v \; . \tag{2.11}$$

In the following, each of the correlation matrices from (2.11) are determined.

First, the desired signal part is considered. To simplify the theoretical calculations, it is assumed that the desired signal $x_d[n]$ has a flat power spectral density (PSD) equal to $2\pi p_d/\Delta\omega_d$, where p_d, ω_d and $\Delta\omega_d$ are the power, frequency, and bandwidth of the desired signal, respectively. The PSD of the desired signal $S_d(\omega)$ is illustrated in Fig. (2.3) with ω_0 being the centre frequency.

The auto-correlation is a measure of the correlation between the values

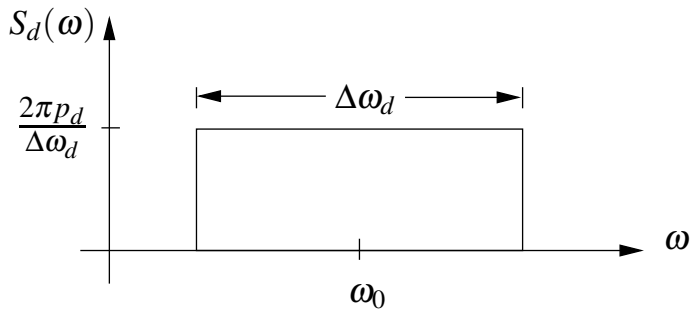

Fig. 2.3: PSD of the desired signal.

of a signal at different times. Therefore, the auto-correlation function of the desired signal $x_d[n]$ is

$$R_d[\tau] = E\left[x_d[n]\, x_d[n+\tau]\right] , \tag{2.12}$$

where τ is the time delay. According to the Wiener-Khinchin theorem [46] the auto-correlation function $R_d(\tau)$ is the inverse Fourier transform of the PSD $S_d(\omega)$. Therefore,

$$R_d(\tau) = \frac{1}{2\pi}\int_{\Delta\omega_d} S_d(\omega) e^{j\omega\tau} d\omega , \tag{2.13}$$

where $j = \sqrt{-1}$.

By taking the inverse Fourier transform from $S_d(\omega)$, the auto-correlation function of the desired signal can be obtained as [40]:

$$R_d(\tau) = p_d \,\mathrm{sinc}\left(\frac{\Delta\omega_d \tau}{2}\right) e^{j\omega_0\tau} . \tag{2.14}$$

Next, the desired signal correlation matrix $\mathbf{\Phi}_d$ is separated into $M \times M$

sub-matrices as:

$$\mathbf{\Phi}_d = \begin{bmatrix} \mathbf{\Phi}_{d_{0,0}} & \cdots & \mathbf{\Phi}_{d_{0,M-1}} \\ \vdots & \ddots & \vdots \\ \mathbf{\Phi}_{d_{M-1,0}} & \cdots & \mathbf{\Phi}_{d_{M-1,M-1}} \end{bmatrix}, \tag{2.15}$$

where each correlation sub-matrix is a $J \times J$ matrix and corresponds to the correlation of the desired signal of two different element signal vectors. Therefore,

$$\mathbf{\Phi}_{d_{m_1,m_2}} = E\left[\mathbf{x}^*_{d_{m_1}} \mathbf{x}^T_{d_{m_2}}\right] . \tag{2.16}$$

Note that the correlation between the desired signal at the k_1-th tap of the m_1-th element and the k_2-th tap of m_2-th element is given by:

$$\left[\mathbf{\Phi}_{d_{m_1,m_2}}\right]_{k_1,k_2} = E\left[x^*_{d_{m_1,k_1}}[n]\, x_{d_{m_2,k_2}}[n]\right] . \tag{2.17}$$

The desired signal received at the m-th element and the k-th tap is a copy of the original desired signal with a delay among the array elements, as well a delay among taps. So

$$x_{d_{m,k}}[n] = x_d\left[n - mT_e - kT_0\right] , \tag{2.18}$$

where T_e is the unit propagation delay between elements, and T_0 is the propagation delay between adjacent taps. So, (2.17) can be written as:

$$\left[\mathbf{\Phi}_{d_{m_1,m_2}}\right]_{k_1,k_2} = R_d\left[(m_1 - m_2)T_e + (k_1 - k_2)T_0\right] . \tag{2.19}$$

It is assumed that the adjacent array sensor spacing is half a wavelength of the maximum frequency ω_{max} to avoid the spatial aliasing [47]. There-

fore, the propagation delay between adjacent sensors can be expressed as

$$T_e = \frac{L}{c} sin(\theta_d) = \frac{\pi}{\omega_{max}} \sin(\theta_d) \,, \tag{2.20}$$

where L is the array spacing, c is the wave propagation speed, and θ_d is the DOA of the desired signal. Next step is to define the delay between two adjacent taps T_0. It is normally assumed that the delay between the adjacent taps is r times the delay associating with a quarter wavelength corresponding to the maximum frequency [48], which is equal to a delay associated with 90° phase shift at ω_{max} . Therefore,

$$T_{90} = \frac{\pi}{2\omega_{max}} \,. \tag{2.21}$$

So, the delay T_0 can be written as

$$T_0 = rT_{90} = \frac{\pi r}{2\omega_{max}} \,. \tag{2.22}$$

Now, from (2.14) and (2.19),

$$\left[\mathbf{\Phi}_{d_{m_1,m_2}}\right]_{k_1,k_2} = p_d \,\mathrm{sinc}\left\{\frac{\Delta\omega_d}{2}\left[(m_1-m_2)T_e + (k_1-k_2)T_0\right]\right\} \times e^{j\omega_0[(m_1-m_2)T_e+(k_1-k_2)T_0]} \,. \tag{2.23}$$

For an easier representation, the above equation is simplified by replacing the bandwidth $\Delta\omega_d$ and centre frequency ω_0 with $B_d = \Delta\omega_d/\omega_{max}$ and $\Omega_0 = \omega_0/\omega_{max}$, respectively. Consequently, the terms $\Delta\omega_d T_e$ and $\omega_0 T_e$ can be written as,

$$\Delta\omega_d T_e = \frac{\Delta\omega_d}{\omega_{max}}\pi\sin(\theta_d) = B_d\pi\sin(\theta_d) \,, \tag{2.24}$$

$$\omega_0 T_e = \frac{\omega_0}{\omega_{max}}\pi\sin(\theta_d) = \Omega_0\pi\sin(\theta_d) \,. \tag{2.25}$$

Similarly, $\Delta\omega_d T_0$ and $\omega_0 T_0$ are written as,

$$\Delta\omega_d T_0 = \frac{\Delta\omega_d}{\omega_{max}} \cdot \frac{\pi r}{2} = B_d \frac{\pi r}{2} , \tag{2.26}$$

$$\omega_0 T_0 = \frac{\omega_0}{\omega_{max}} \cdot \frac{\pi r}{2} = \Omega_0 \frac{\pi r}{2} . \tag{2.27}$$

Therefore, in the simplified form, the correlation of the desired signal at the k_1-th tap of the m_1-th element and the k_2-th tap of the m_2-th element can be expressed as,

$$\left[\mathbf{\Phi}_{d_{m_1,m_2}}\right]_{k_1,k_2} = p_d \,\mathrm{sinc}\left\{\frac{B_d}{2}\tau_d\right\} e^{j\Omega_0\tau_d} , \tag{2.28}$$

where τ_d is,

$$\tau_d = \pi\left[(m_1 - m_2)\sin(\theta_d) + (k_1 - k_2)\frac{r}{2}\right] . \tag{2.29}$$

Next step is to determine the interference correlation matrix $\mathbf{\Phi}_i$ using the same approach. The DOA θ_i of the interference is different from θ_d. Same as before, to simplify the theoretical calculations, it is been assumed that the interference signal $x_i[n]$ has a flat PSD, equal to $2\pi p_i/\Delta\omega_i$, where p_i, ω_i and $\Delta\omega_i$ are the power, frequency and bandwidth of the interference signal, respectively. Same as (2.15), the interference correlation matrix $\mathbf{\Phi}_i$ is separated into $M \times M$ sub-matrices as:

$$\mathbf{\Phi}_i = \begin{bmatrix} \mathbf{\Phi}_{i_{0,0}} & \cdots & \mathbf{\Phi}_{i_{0,M-1}} \\ \vdots & \ddots & \vdots \\ \mathbf{\Phi}_{i_{M-1,0}} & \cdots & \mathbf{\Phi}_{i_{M-1,M-1}} \end{bmatrix} , \tag{2.30}$$

where each correlation sub-matrix is a $J \times J$ matrix, corresponding to the correlation of the interference of two different element interference signal

vectors,

$$\mathbf{\Phi}_{i_{m_1,m_2}} = E\left[\mathbf{x}^*_{i_{m_1}}\mathbf{x}^T_{i_{m_2}}\right] . \tag{2.31}$$

The correlation between the interference at the k_1-th tap of the m_1-th element and the k_2-th tap of the m_2-th element is:

$$\left[\mathbf{\Phi}_{i_{m_1,m_2}}\right]_{k_1,k_2} = E\left[x^*_{i_{m_1,k_1}}[n]\;\; x_{i_{m_2,k_2}}[n]\right] . \tag{2.32}$$

Similar to the desired signal in (2.28), in the simplified form, the correlation of the interference at the k_1-th tap of the m_1-th element and the k_2-th tap of the m_2-th element can be expressed as:

$$\left[\mathbf{\Phi}_{i_{m_1,m_2}}\right]_{k_1,k_2} = p_i \,\mathrm{sinc}\left\{\frac{B_i}{2}\tau_i\right\} e^{j\Omega_0\tau_i} , \tag{2.33}$$

where $B_i = \Delta\omega_i/\omega_0$ and τ_i is

$$\tau_i = \pi\left[(m_1 - m_2)\sin(\theta_i) + (k_1 - k_2)\frac{r}{2}\right] . \tag{2.34}$$

Since it is assumed that the noise available at each sensor is temporally and also spatially white, so the noise is mathematically independent between the sensors in the TDL. Therefore, the noise correlation products of the correlation matrix in (2.11) are zero, apart from the product of the same delay-line. Similar to (2.15) and (2.30), the noise correlation matrix $\mathbf{\Phi}_v$ is also separated into $M \times M$ sub-matrices, so:

$$\mathbf{\Phi}_v = \begin{bmatrix} \mathbf{\Phi}_{v_{0,0}} & 0 & \cdots & 0 \\ 0 & \mathbf{\Phi}_{v_{1,1}} & \cdots & 0 \\ \vdots & \vdots & \ddots & \vdots \\ 0 & 0 & \cdots & \mathbf{\Phi}_{v_{M-1,M-1}} \end{bmatrix}, \tag{2.35}$$

where each non-zero noise correlation sub-matrix is a $J \times J$ matrix. It is assumed the white noise has a flat PSD equal to $2\pi\sigma_v^2/\Delta\omega_v$, where σ_v^2 is the noise variance and $\Delta\omega_v$ is the bandwidth of the noise. Therefore, as in (2.28) and (2.33), the correlation of the noise at the k_1-th and k_2-th tap of the same m_1-th element is

$$[\mathbf{\Phi}_{v_{m_1,m_1}}]_{k_1,k_2} = \sigma_v^2 \,\mathrm{sinc}\left\{\frac{B_v}{2}\tau_v\right\} e^{j\Omega_0\tau_v}, \tag{2.36}$$

where $B_v = \Delta\omega_v/\omega_0$ and τ_v is

$$\tau_v = \pi\left[(k_1 - k_2)\frac{r}{2}\right]. \tag{2.37}$$

Finally, the reference correlation vector $\mathbf{s}_d$ is determined. Assuming the reference signal $r_o[n]$ is the same as the desired signal $x_d[n]$, $\mathbf{s}_d$ in (2.8) can be written as

$$\mathbf{s}_d = E[\mathbf{x}^* r_o[n]] = E[\mathbf{x}^* x_{d_o}[n]]\,. \tag{2.38}$$

where $x_{d_o}[n]$ is the same as $x_d[n]$, with unit power. It has been assumed that the desired signal, interferences and the noise are uncorrelated with each other. Therefore, (2.38) can be expressed as:

$$\mathbf{s}_d = E[\mathbf{x}_d^* x_{d_o}[n]]\,. \tag{2.39}$$

Furthermore, $\mathbf{s}_d$ can be expanded as:

$$\mathbf{s}_d = \left[s_{d_{0,0}}, \cdots, s_{d_{0,J-1}}, \cdots, s_{d_{M-1,0}}, \cdots, s_{d_{M-1,J-1}}\right]^T, \tag{2.40}$$

where $s_{d_{m,k}}$, $m = 0, \cdots, M-1$, $k = 0, \cdots, J-1$, indicates the correlation of the reference and the desired signal at the m-th element and k-th tap, given

by:

$$s_{d_{m,k}} = \sqrt{p_d}\,\mathrm{sinc}\left\{\frac{B_d}{2}\tau_s\right\} e^{j\Omega_0\tau_s}, \tag{2.41}$$

with

$$\tau_s = \pi\left[m\sin(\theta_d) + k\frac{r}{2}\right]. \tag{2.42}$$

Since $\mathbf{\Phi}_x$ and $\mathbf{s}_d$ are fully determined, using (2.6), $\mathbf{w}_{opt}$ can be calculated for the RSB beamformer.

The beamformer output can be calculated from (2.5), and the output power is:

$$P = \frac{1}{2}E\left[\|y[n]\|_2^2\right] = \frac{1}{2}\mathbf{w}_{opt}^H\mathbf{\Phi}_x\mathbf{w}_{opt}, \tag{2.43}$$

where $\|\cdot\|_2$ is the l_2 norm and $\{\cdot\}^H$ denotes the Hermitian transpose. As denoted in (2.11), $\mathbf{\Phi}_x$ can be expressed as desired, interference and noise parts. Therefore, the output power can also be expressed as:

$$P_d = \frac{1}{2}\mathbf{w}_{opt}^H\mathbf{\Phi}_d\mathbf{w}_{opt}, \tag{2.44}$$

$$P_i = \frac{1}{2}\mathbf{w}_{opt}^H\mathbf{\Phi}_i\mathbf{w}_{opt}, \tag{2.45}$$

$$P_v = \frac{1}{2}\mathbf{w}_{opt}^H\mathbf{\Phi}_v\mathbf{w}_{opt}. \tag{2.46}$$

Finally, the output SINR of the beamformer is:

$$\mathrm{SINR} = \frac{P_d}{P_i + P_v}. \tag{2.47}$$

This concludes the performance analysis for the RSB beamformer.

2.3 Linearly Constrained Minimum Variance Adaptive Beamformer

In practice, the reference signal $r[n]$ may be unavailable. However, when some information on the DOAs as well as the bandwidth limits of the desired signal and/or the interferences is available, a linearly constrained minimum variance (LCMV) beamformer can be employed for effective beamforming [2, 49].

$$\min_{\mathbf{w}} \mathbf{w}^H \mathbf{\Phi}_x \mathbf{w} \qquad \text{subject to} \qquad \mathbf{C}^H \mathbf{w} = \mathbf{f}\,, \tag{2.48}$$

where $\mathbf{w}$ and $\mathbf{\Phi}_x$ are defined as before in Section 2.2, $\mathbf{C}$ is the $MJ \times J$ constraint matrix and $\mathbf{f}$ is the $J \times 1$ response vector. The beamformer will always have the desired response set out by the constraint equation $\mathbf{C}^H\mathbf{w} = \mathbf{f}$, no matter how the weights are adjusted. The structure of the LCMV beamformer is shown in Fig. 2.4. The solution to (2.48) can be obtained using the Lagrange multipliers method [49],

$$\mathbf{w}_{opt} = \mathbf{\Phi}_x^{-1}\mathbf{C}(\mathbf{C}^H\mathbf{\Phi}_x^{-1}\mathbf{C})^{-1}\mathbf{f}\,. \tag{2.49}$$

The correlation matrix $\mathbf{\Phi}_x$ is determined in the same way as in Sec. 2.2. So, only the constraint matrix $\mathbf{C}$ and the response vector $\mathbf{f}$ need to be defined. In the following, $\mathbf{C}$ and $\mathbf{f}$ are defined for the case when the desired signal is coming from the broadside, i.e., $\theta_d = 0^\circ$.

In this case, the desired signal components are received at the same time at the array elements, and so there would be no delay between the

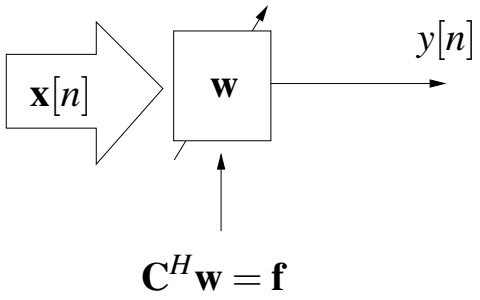

Fig. 2.4: The LCMV adaptive beamforming structure.

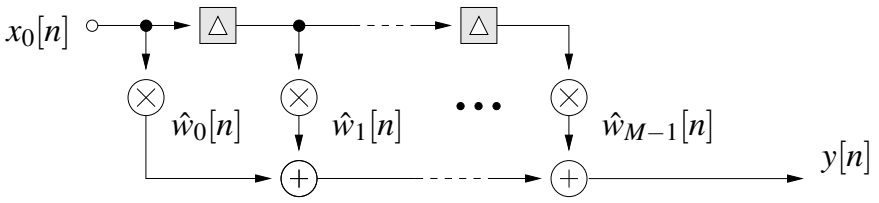

Fig. 2.5: The equivalent single TDL beamformer for LCMV when the desired signal is arriving from broadside.

desired signal components received by the array elements. Therefore, the beamformer can be considered as a single TDL, where each weight is the sum of the weights in the corresponding column. Thus, the single TDL coefficients are defined as:

$$\hat{w}_k = \sum_{m=0}^{M-1} w_{m,k} \tag{2.50}$$

where $k = 0, \cdots, M-1$, this single TDL structure is shown in Fig. 2.5.

In order to have a distortion-less response to the desired signal, the beamformer response should only be a delay. Therefore, only one of the coefficients of the structure in Fig. 2.5, $\hat{w}_k$, $k = 0, \cdots, J-1$, is 1 and the rest are zero. So, the constraint matrix $\mathbf{C}$ is expressed as M identity matrices

$\mathbf{I}_J$, with size $J \times J$. Thus, $\mathbf{C}$ is:

$$\mathbf{C} = [\mathbf{I}_J, \cdots, \mathbf{I}_J]^T. \tag{2.51}$$

The response vector $\mathbf{f}$ is only a delay, so:

$$\mathbf{f} = [0, \cdots, 1, \cdots, 0]^T. \tag{2.52}$$

After defining $\mathbf{C}$ and $\mathbf{f}$, using (2.49), $\mathbf{w}_{opt}$ can be obtained and the output SINR can be calculated using (2.43)–(2.47) from Sec. 2.2.

2.4 Summary

The general area of adaptive wideband beamforming was reviewed in this chapter. First, the general structure of wideband beamformers using TDLs was studied and the signal model was introduced which will be used throughout the thesis. Then, the general structure of the two well-known beamformers, namely, RSB and LCMV adaptive beamformers was studied. Under the assumption that the received signals have flat PSDs, the theoretical values for correlation matrices of the beamformers were calculated. Using these correlation values the optimum weight vector $\mathbf{w}_{opt}$ was calculated for the beamformers. Since the optimum weight vector $\mathbf{w}_{opt}$ and the correlation matrices for desired, interference and the noise for each beamformer is known, the power of the desired signal P_d, the power of interference P_i and the power of noise P_n in the output was derived, hence, the output SINR can be calculated from these values. In the following chapters, a

method is developed to improve the output SINR by developing a white noise reduction pre-processing method for different array structures.

Chapter 3

White Noise Reduction for Wideband Uniform Linear Array Signal Processing

The most common array structure is the uniform linear array (ULA). The general idea of the proposed method is presented in this chapter in details based on a ULA structure for the sensors. Also, the effect of the noise reduction method on the performance of wideband beamforming and DOA estimation is shown with simulation. The contents of this chapter has been published in [50], and parts of the contents is presented at a conference [51].

3.1 General Structure of the Proposed Method

Consider an M-element ULA, a block diagram for the general structure of the proposed method is shown in Fig. 3.1. The M received array signals

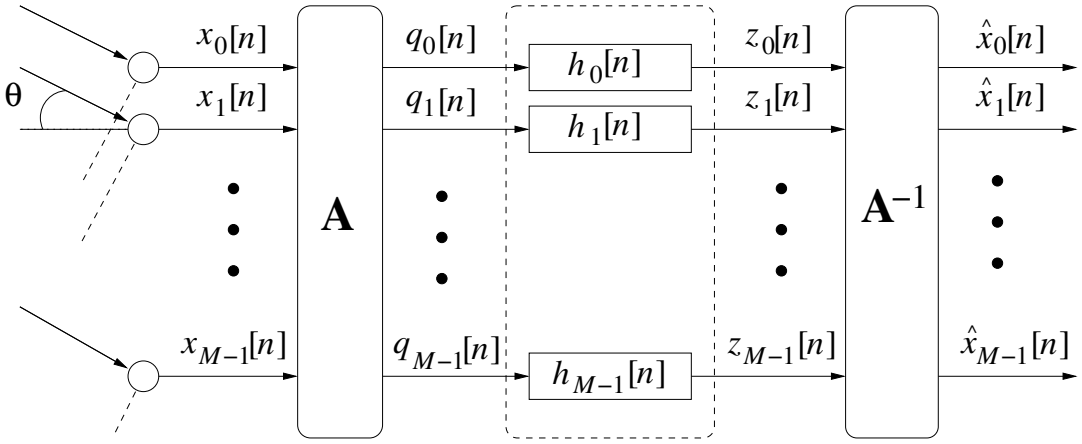

Fig. 3.1: A block diagram for the general structure of the proposed noise reduction approach.

$x_m[n]$, $m = 0,\ldots,M-1$, are first processed by an $M \times M$ transformation matrix $\mathbf{A}$, and then its outputs $q_m[n]$, $m = 0,\ldots,M-1$, pass through a bank of high-pass filters with impulse responses given by $h_m[n]$, $m = 0,\ldots,M-1$. The outputs of these filters are denoted by $z_m[n]$, $m = 0,\ldots,M-1$ and these are then transformed by the $M \times M$ inverse transformation $\mathbf{A}^{-1}$.

For simplicity it is assumed $\mathbf{A}$ is unitary. The matrix $\mathbf{A}$ is said to be unitary if $\mathbf{A}^H\mathbf{A} = \mathbf{A}\mathbf{A}^H = \mathbf{I}$, where $\mathbf{I}$ is the identity matrix [52]. Therefore, $\mathbf{A}^{-1} = \mathbf{A}^H$.

It is assumed there are K wideband signals $\bar{s}_k(t)$ (where t is the continuous time index) impinging on the array from different incident angles θ_k, $k = 0,\cdots,K-1$. The received array signal $x_m(t)$ at the m-th sensor consists of these wideband signals and white noise $v_m(t)$, i.e.,

$$x_m(t) = \sum_{k=0}^{K-1} \bar{s}_k\left[t - \tau_m(\theta_k)\right] + v_m(t), \tag{3.1}$$

where $\tau_m(\theta_k)$ represents the time delay (relative to a reference sensor) of

the k-th impinging signal with the incident angle θ_k arriving at the m-th sensor of the array. Taking the first sensor in the array as the reference point, hence $\tau_0(\theta_k) = 0$. So with

$$s_m(t) = \sum_{k=0}^{K-1} \bar{s}_k \left[t - \tau_m(\theta_k) \right], \tag{3.2}$$

(3.1) becomes

$$x_m(t) = s_m(t) + v_m(t) \ . \tag{3.3}$$

With a sampling frequency of f_s, the discrete version of the array vector snapshot is

$$\mathbf{x}[n] = \mathbf{s}[n] + \mathbf{v}[n] \ , \tag{3.4}$$

where

$$\mathbf{x}[n] = [x_0[n], x_1[n], \cdots, x_{M-1}[n]]^T,$$

$$\mathbf{s}[n] = [s_0[n], s_1[n], \cdots, s_{M-1}[n]]^T,$$

$$\mathbf{v}[n] = [v_0[n], v_1[n], \cdots, v_{M-1}[n]]^T.$$

Applying the $M \times M$ transformation matrix $\mathbf{A}$ to the signal vector $\mathbf{x}[n]$, the output signal vector $\mathbf{q}[n]$ is obtained as

$$\mathbf{q}[n] = \mathbf{A}\mathbf{x}[n], \tag{3.5}$$

where

$$\mathbf{q}[n] = [q_0[n], q_1[n], \cdots, q_{M-1}[n]]^T \ .$$

The element of $\mathbf{A}$ at the m-th row and l-th column is denoted by $a_{m,l}$, i.e., $[\mathbf{A}]_{m,l} = a_{m,l}$. Each row vector of $\mathbf{A}$ acts as a simple beamformer, and

its output $q_m[n]$ is given by

$$q_m[n] = \sum_{l=0}^{M-1} a_{m,l} x_l[n]. \tag{3.6}$$

The beam response $R_m(\Omega, \theta)$ of this simple beamformer as a function of the normalised angular frequency Ω and the DOA angle θ is [38, 53],

$$R_m(\Omega, \theta) = \sum_{l=0}^{M-1} a_{m,l} e^{-jl\mu\Omega\sin\theta}, \tag{3.7}$$

where $\mu = d/cT_s$ and $\Omega = \omega T_s$, with d being the spacing between the adjacent sensors, c the wave propagation speed, T_s the sampling period, and ω the angular frequency of signals.

Since the sampling frequency is $f_s = \frac{1}{T_s}$, the normalised angular frequency is $\Omega = \frac{\omega}{f_s} = \frac{2\pi f}{f_s}$, where f is the signal frequency. In this thesis, f_s is equal to the Nyquist frequency. Therefore, $f_s = 2f_{max}$, where f_{max} is the maximum frequency of the signal. So,

$$\Omega = \frac{2\pi f}{f_s} = \frac{2\pi f}{2f_{max}} = \frac{\pi f}{f_{max}}\,. \tag{3.8}$$

Assuming the range of the frequency f is $[-f_{max} : f_{max}]$, the range of normalised angular frequency Ω is $[-\pi : \pi]$.

With $\hat{\Omega} = \mu\Omega\sin\theta$, an alternative representation for $R_m(\Omega, \theta)$ can be obtained as follows

$$A_m(\hat{\Omega}) = \sum_{l=0}^{M-1} a_{m,l} e^{-jl\hat{\Omega}}, \tag{3.9}$$

where $\hat{\Omega}$ is representing the spatial frequency of the received signal, $A_m(\hat{\Omega})$ is the frequency response of the m-th row vector of the $M \times M$ transforma-

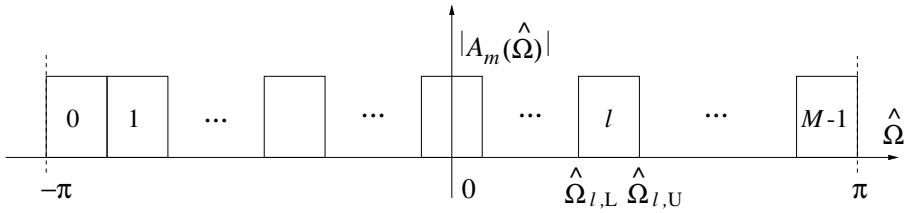

(a) Frequency responses of the row vectors of **A** in the ideal case for an odd number M.

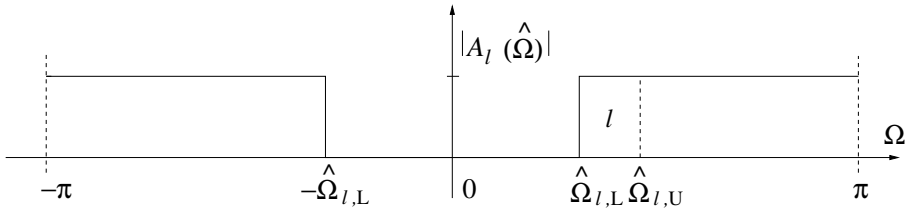

(b) The high-pass filtering effect of the l-th row vector in the ideal case.

Fig. 3.2: Frequency responses of the row vectors of **A** in the ideal case and the high-pass filtering effect of a sample row vector.

tion matrix **A** (if each row vector is considered as the impulse response of a finite impulse response (FIR) filter).

Since the structure of the array is a ULA and assuming that the sampling frequency is twice the highest frequency component of the wideband signal and the array spacing d is half the wavelength of the highest frequency component, hence $\mu = 1$. Therefore, $\hat{\Omega} = \Omega \sin\theta$.

Similar to [38], the frequency responses $A_m(\hat{\Omega})$, $m = 0, \cdots, M-1$, are arranged to be band-pass, each with a bandwidth of $2\pi/M$. The row vectors of **A** all together cover the whole normalised frequency range which is $[-\pi : \pi]$. An ideal example for an odd number M is shown in Fig. 3.2a.

The band-pass filters, which are used as row vectors of **A**, have a high-pass filtering effect on the received array signals. To examine this high-

pass behaviour, the l-th row vector is analysed. The frequency response of this row vector is shown in Fig. 3.2a, which is:

$$\left|A_l(\hat{\Omega})\right| = \begin{cases} 1, & \text{for } \hat{\Omega} \in [\hat{\Omega}_{l,L} : \hat{\Omega}_{l,U}] \\ 0, & \text{otherwise.} \end{cases} \tag{3.10}$$

Considering the above frequency response, the received array signal components with frequency of $\Omega \in [-\hat{\Omega}_{l,L} : \hat{\Omega}_{l,L}]$ will not "pass" through this row vector, since $\hat{\Omega} = \Omega \sin\theta$ does not fall into the passband of $[\hat{\Omega}_{l,L} : \hat{\Omega}_{l,U}]$, no matter what value the DOA angle θ takes. Therefore, the frequency range of the output is $|\Omega| \geq \hat{\Omega}_{l,L}$ and the lower bound is determined by $\hat{\Omega}_{l,L}$, when $\hat{\Omega}_{l,L} > 0$. Alternatively, the lower bound is determined by $|\hat{\Omega}_{l,U}|$, when $\hat{\Omega}_{l,L} < \hat{\Omega}_{l,U} < 0$.

As a result, the output spectrum of the directional signal part of $q_l[n]$ corresponding to the l-th row vector will then be high-pass filtered as shown in Fig. 3.2b. As the noise part in $\mathbf{x}[n]$ is spatially white, the output noise spectrum of the row vector is still a constant, covering the whole spectrum. As shown in Fig. 3.1, the output $q_l[n]$, $l = 0, \cdots, M-1$, of each row vector is the input to a corresponding high-pass filter $h_l[n]$, $l = 0, \cdots, M-1$. These high-pass filters should cover the whole bandwidth of the signal part of the output $q_l[n]$ and therefore have the same frequency response as specified in Fig. 3.2b. As a result, in the ideal case, the high-pass filters will not have any effect on the signal components and all the signal components will pass through the high-pass filters without any distortion. But then the frequency components of the white noise falling into

the stopband of these high-pass filters will be removed.

The output of the high-pass filters is the convolution of each row vector output and its corresponding high-pass filter,

$$\mathbf{z}[n] = \begin{bmatrix} z_0[n] \\ \vdots \\ z_{M-1}[n] \end{bmatrix} = \begin{bmatrix} q_0[n] \circ h_0[n] \\ \vdots \\ q_{M-1}[n] \circ h_{M-1}[n] \end{bmatrix}, \tag{3.11}$$

where $\circ$ denotes the convolution operator.

Considering the noise reduction effect of the high-pass filters, each filter removes part of the noise except for the filter corresponding to the row vector with a frequency response covering the zero frequency component, which should allow all frequencies to pass. Assuming that the size M of the array is an odd number, from Fig. 3.2, for the first row vector $A_0(\hat{\Omega})$, $2/M$ part of the noise passes, while for $A_1(\hat{\Omega})$, $4/M$ part of the noise passes, and so on. For the row vector with frequency response covering the zero frequency, all of the noise will pass. For the row vectors with frequency responses larger than the zero frequency, the high-pass filters are replicas of the high-pass filters regarding the row vectors with frequency responses lower than the zero frequency. Therefore, in the ideal case, the ratio between the total noise power after and before the processing of the M high-pass filters can be expressed as

$$\frac{P_{vo}}{P_{vi}} = \frac{1}{M}\left(1 + 2\left(\frac{2}{M} + \frac{4}{M} + \cdots + \frac{M-1}{M}\right)\right), \tag{3.12}$$

where P_{vo} is the total noise power at the output of the filters and P_{vi} is the

total noise power at their input. Following the same procedure, if the size of the array is an even number, then this ratio is given by

$$\frac{P_{vo}}{P_{vi}} = \frac{1}{M}\left(1+2\left(\frac{3}{M}+\frac{5}{M}+\cdots+\frac{M-1}{M}\right)+\frac{1}{M}\right). \tag{3.13}$$

As a result,

$$r(M) = \frac{P_{vo}}{P_{vi}} = \begin{cases} \frac{M^2+2M-1}{2M^2}, & \text{if } M \geqslant 1 \text{ is odd} \\ \frac{M^2+2M-2}{2M^2}, & \text{if } M \geqslant 2 \text{ is even.} \end{cases} \tag{3.14}$$

When $M \to \infty$, the noise power will be reduced by half in both cases. The output noise power to input noise power ratio versus the number of array sensors M is plotted in Fig. 3.3. Since the high-pass filters have no effect on the signal part, the ratio between the total signal power and the total noise power is improved by almost 3 dB in the ideal case. For a finite M, the improvement will be less than 3 dB. For example, when $M = 16$, it is about 2.53 dB.

Applying the inverse of the transformation matrix $\mathbf{A}^{-1} = \mathbf{A}^H$ (with size $M \times M$) to $\mathbf{z}[n]$, the estimates of the original input sensor signals $\hat{x}_m[n]$, $m = 0, \cdots, M-1$ is obtained. In vector form, it is represented as

$$\hat{\mathbf{x}}[n] = \mathbf{A}^{-1}\mathbf{z}[n], \tag{3.15}$$

where $\hat{\mathbf{x}}[n] = [\hat{x}_0[n], \hat{x}_1[n], \cdots, \hat{x}_{M-1}[n]]^T$.

After going through these processing stages, there is no change in the signal part at the final output $\hat{x}_l[n]$, $l = 0, \cdots, M-1$ compared to the original signal part in $x_l[n]$, $l = 0, \cdots, M-1$. On the contrary, since $\mathbf{A}^{-1}$ is

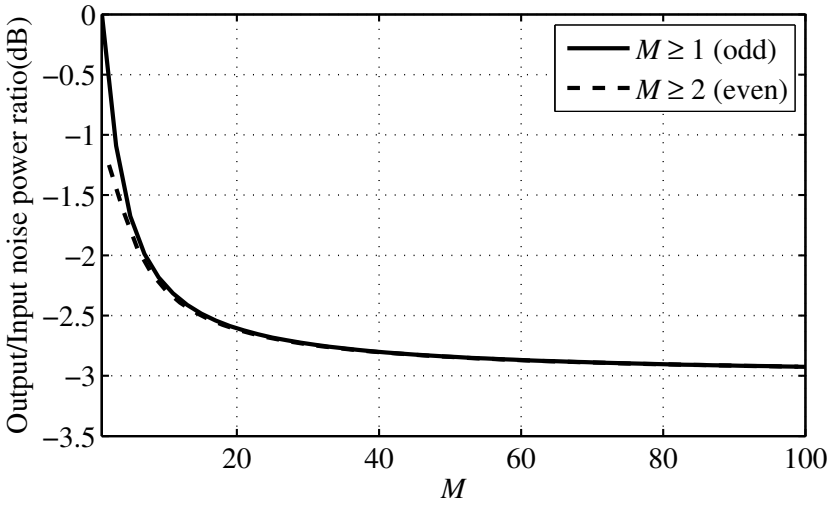

Fig. 3.3: Output to input noise power ratio for odd ($M \geqslant 1$) and even ($M \geqslant 2$) values of M.

also unitary, the total noise power stays the same between $\hat{\mathbf{x}}[n]$ and $\mathbf{z}[n]$, which is almost half the total noise power in $\mathbf{x}[n]$. Therefore, for a very large array size M,

$$\|\hat{\mathbf{x}}[n]\|_2^2 \approx \|\mathbf{s}[n]\|_2^2 + \frac{1}{2}\|\mathbf{v}[n]\|_2^2 \,. \tag{3.16}$$

Based on the above discussion, in terms of the total signal power to total noise power ratio (TSNR), the following relationship holds

$$\mathrm{TSNR}_{\hat{\mathbf{x}}} \approx \frac{\|\mathbf{s}[n]\|_2^2}{\frac{1}{2}\|\mathbf{v}[n]\|_2^2} = 2 \times \mathrm{TSNR}_{\mathbf{x}} \,. \tag{3.17}$$

So in the ideal case, for a very large M, the TSNR is almost doubled by the proposed noise reduction method. This can be translated into higher performance for different array processing applications such as higher output SINR for beamforming and increased accuracy for DOA estimation. In the following section, using the DFT-based transformation matrix for

ULAs, the theoretical result for two commonly used beamformers is analysed to show the performance improvement in the ideal case.

3.2 Analysis Based on the DFT Matrix for ULAs

The transformation matrix $\mathbf{A}$ is the most important part of the system. It should have a full rank so that an inverse transform can be applied at the end to recover the directional signals. Another key requirement is that the row vectors have the desired band-pass frequency responses shown in Fig. 3.2a. So, in general the design of the transformation matrix can be formulated as a constrained FIR filter design problem. This is similar to the beamspace transformation problem studied in [54, 55]. As pointed out there, a prototype low-pass filter could be designed and then it should be modulated to different frequency bands by a DFT operation or use the DFT matrix directly. In particular, the DFT matrix is unitary, which will simplify the theoretical analysis and provide with the crucial insight into the performance of the proposed structure.

Using the DFT matrix for an $M \times M$ transformation $\mathbf{A}$, with $\gamma = e^{-j(2\pi/M)}$,

$$\mathbf{A} = \frac{1}{\sqrt{M}} \begin{bmatrix} \gamma^{0\cdot 0} & \gamma^{0\cdot 1} & \cdots & \gamma^{0\cdot(M-1)} \\ \gamma^{1\cdot 0} & \gamma^{1\cdot 1} & \cdots & \gamma^{1\cdot(M-1)} \\ \vdots & \vdots & \ddots & \vdots \\ \gamma^{(M-1)\cdot 0} & \gamma^{(M-1)\cdot 1} & \cdots & \gamma^{(M-1)\cdot(M-1)} \end{bmatrix}. \tag{3.18}$$

Next, an analysis of the signal spectrum based on such a transformation

matrix at different stages of the proposed structure is provided.

3.2.1 Spectrum analysis with DFT matrix

The input-output relationship in the frequency domain based on the DFT matrix is studied in this section. Taking the discrete-time Fourier transform (DTFT) of (3.5), (3.11) and (3.15) yields respectively,

$$\mathbf{q}(\Omega) = \mathbf{A}\mathbf{x}(\Omega), \tag{3.19}$$

$$\mathbf{z}(\Omega) = \mathbf{H}\mathbf{q}(\Omega), \tag{3.20}$$

$$\hat{\mathbf{x}}(\Omega) = \mathbf{A}^{-1}\mathbf{z}(\Omega), \tag{3.21}$$

where $\mathbf{x}(\Omega)$, $\mathbf{q}(\Omega)$, $\mathbf{z}(\Omega)$ and $\hat{\mathbf{x}}(\Omega)$ are the vectors holding the DTFTs of the time-domain signal vectors $\mathbf{x}[n]$, $\mathbf{q}[n]$, $\mathbf{z}[n]$ and $\hat{\mathbf{x}}[n]$ respectively. $\mathbf{H}$ is an $M \times M$ real-valued diagonal matrix with its diagonal elements being the frequency responses $H_m(\Omega)$ of the corresponding filters $h_m[n]$, $m = 0, \cdots, M-1$, i.e.,

$$\mathbf{H} = \begin{bmatrix} H_0(\Omega) & 0 & \dots & 0 \\ 0 & H_1(\Omega) & \dots & 0 \\ \vdots & \vdots & \ddots & \vdots \\ 0 & 0 & \dots & H_{M-1}(\Omega) \end{bmatrix}. \tag{3.22}$$

Considering (3.19), (3.20) and (3.21) yields,

$$\hat{\mathbf{x}}(\Omega) = \mathbf{A}^{-1}\mathbf{H}\mathbf{A}\mathbf{x}(\Omega). \tag{3.23}$$

From (3.23), the transfer function of the system is:

$$\mathbf{T} = \mathbf{A}^{-1}\mathbf{H}\mathbf{A} =$$

$$\mathbf{A}^{-1}\frac{1}{\sqrt{M}}\begin{bmatrix} H_0(\Omega)\gamma^{0\cdot 0} & \cdots & H_0(\Omega)\gamma^{0\cdot(M-1)} \\ H_1(\Omega)\gamma^{1\cdot 0} & \cdots & H_1(\Omega)\gamma^{0\cdot(M-1)} \\ \vdots & \ddots & \vdots \\ H_{M-1}(\Omega)\gamma^{(M-1)\cdot 0} & \cdots & H_{M-1}(\Omega)\gamma^{(M-1)\cdot(M-1)} \end{bmatrix}. \tag{3.24}$$

Then, all the elements of $\mathbf{T}$ (complex-valued, with size $M \times M$) can be obtained. Considering the relationship between the terms, a general form for the elements of $\mathbf{T}$ can be derived and the element at the i_1-th row and i_2-th column is given by

$$T_{i_1,i_2} = \frac{1}{M}\sum_{l=0}^{M-1} H_l \gamma^{-li_1}\gamma^{li_2} = \frac{1}{M}\sum_{l=0}^{M-1} H_l \gamma^{l(i_2-i_1)}\,. \tag{3.25}$$

So,

$$\hat{\mathbf{x}}(\Omega) = \mathbf{T}\mathbf{x}(\Omega). \tag{3.26}$$

The spectrum of the noise at the output is in interest. The relationship between the input and output signals' spectrum is [56],

$$\mathbf{S}_{\hat{\mathbf{x}}}(\Omega) = \mathbf{T}\mathbf{T}^{*}(\Omega)\mathbf{S}_{\mathbf{x}}(\Omega), \tag{3.27}$$

where the asterisk $\{\cdot\}^*$ denotes the complex conjugate, and $\mathbf{S}_{\hat{\mathbf{x}}}(\Omega)$ and $\mathbf{S}_{\mathbf{x}}(\Omega)$ are $M \times M$ matrices, where each matrix element represents the cross-spectral density of the two corresponding signals. $\mathbf{S}_{\mathbf{x}}(i_1,i_2)$ is the (i_1,i_2)-th element of $\mathbf{S}_{\mathbf{x}}$ and it is the cross-spectral density between $x_{i_1}[n]$ and $x_{i_2}[n]$. It can be easily proved that the cross spectral density is equal to the DTFT of the cross correlation function of the two signals [57]. Then,

$$\mathbf{S}_{\mathbf{x}}(i_1,i_2) = x^{*}_{i_1}(\Omega)x_{i_2}(\Omega). \tag{3.28}$$

A detailed proof for (3.28) is provided in the Appendix. Similarly, $\mathbf{S}_{\hat{\mathbf{x}}}(i_1,i_2) = \hat{x}^*_{i_1}(\Omega)\hat{x}_{i_2}(\Omega)$.

Considering the noise part, the spectral density of the white noise is σ_v^2, where σ_v^2 is the variance of the white noise. Since the white noise received by each array sensor is uncorrelated, the noise spectral density of a sensor is $\mathbf{S}_{\mathbf{v}}(i_1,i_1) = \sigma_v^2$ and the noise cross spectral density between two sensors is $\mathbf{S}_{\mathbf{v}}(i_1,i_2) = 0$, the noise cross spectral density is the noise power shared by a given frequency between two sensors. It needs to be emphasised that, these assumptions are only valid in the presence of the white noise, and in other cases these assumptions do not hold. So, the spectrum of the white noise received by the array is:

$$\mathbf{S}_{\mathbf{v}}(\Omega) = \sigma_v^2 \begin{bmatrix} 1 & 0 & \cdots & 0 \\ 0 & 1 & \cdots & 0 \\ \vdots & \vdots & \ddots & \vdots \\ 0 & 0 & \cdots & 1 \end{bmatrix} = \sigma_v^2 \mathbf{I}\,, \tag{3.29}$$

where $\mathbf{I}$ is the $M \times M$ identity matrix. Therefore, (3.27) can be written as

$$\mathbf{S}_{\hat{\mathbf{v}}}(\Omega) = \mathbf{T}\mathbf{T}^*(\Omega)\sigma_v^2\mathbf{I}\,. \tag{3.30}$$

$\mathbf{S}_{\hat{\mathbf{v}}}(\Omega)$ is an $M \times M$ complex-valued matrix but with real values on the diagonal. Each term of $\mathbf{S}_{\hat{\mathbf{v}}}(\Omega)$ is given by:

$$\mathbf{S}_{\hat{\mathbf{v}}}(i_1,i_2)(\Omega) = \frac{\sigma_v^2}{M}\sum_{l=0}^{M-1} T_{i_1,l}T^*_{i_2,l}\,. \tag{3.31}$$

From (3.25) and (3.31),

$$\mathbf{S}_{\hat{\mathbf{v}}}(i_1,i_2)(\Omega) = \frac{\sigma_v^2}{M}\sum_{l=0}^{M-1} H_l(\Omega)e^{j\frac{2\pi}{M}(i_1-i_2)l}. \tag{3.32}$$

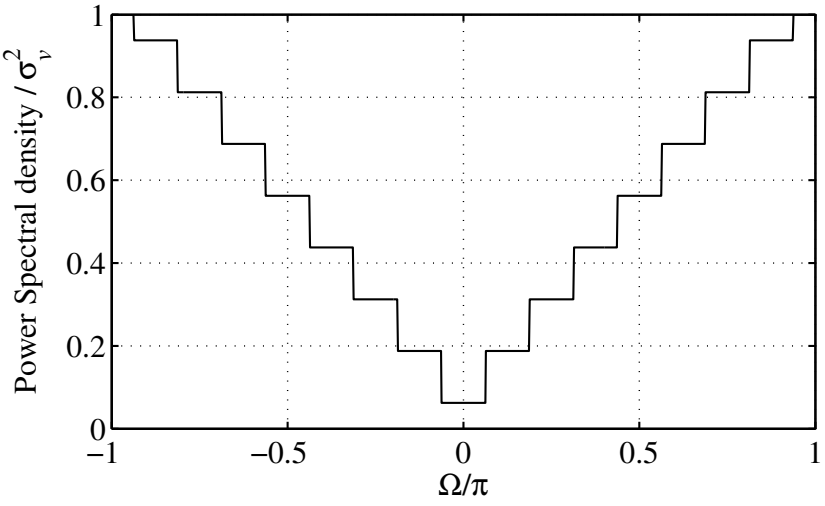

Fig. 3.4: Power spectrum of the output of the noise reduction system with M=16.

The spectrum of the noise for $M = 16$ is shown in Fig. 3.4 in the ideal case. The next step is to take the inverse DTFT from (3.32) to calculate the correlation function in the time domain. The inverse Fourier transform of (3.32) is:

$$\begin{aligned} R_{\hat{v}(i_1,i_2)}(\tau) &= \mathrm{DTFT}^{-1}\left\{\frac{\sigma_v^2}{M}\sum_{l=0}^{M-1} H_l(\Omega)e^{j\frac{2\pi}{M}(i_1-i_2)l}\right\} \\ &= \frac{\sigma_v^2}{M}\sum_{l=0}^{M-1} e^{j\frac{2\pi}{M}(i_1-i_2)l}\mathrm{DTFT}^{-1}\left\{H_l(\Omega)\right\}, \end{aligned} \tag{3.33}$$

where τ is an arbitrary delay and $R_{\hat{v}(i_1,i_2)}(\tau)$ is the correlation function between the filtered noise at the i_1-th and the i_2-th array elements after applying the noise reduction method. As the only term which is a function of frequency is $H_l(\Omega)$, the inverse DTFT only applies to this part. The frequency response of a single high-pass filter has the same form as that shown in Fig. 3.2b. To calculate $\mathrm{DTFT}^{-1}\{H_l(\Omega)\}$, (3.33) can be written

as

$$R_{\hat{v}(i_1,i_2)}(\tau) = \frac{\sigma_v^2}{M} \sum_{l=0}^{M-1} \frac{\pi - \hat{\Omega}_{l,L}}{\pi} e^{j\frac{2\pi}{M}(i_1-i_2)l} e^{j\frac{\pi+\hat{\Omega}_{l,L}}{2}\tau} \operatorname{sinc}(\frac{\pi - \hat{\Omega}_{l,L}}{2}\tau), \quad (3.34)$$

where π is the maximum normalised frequency and $\hat{\Omega}_{l,L}$ is the lower bound frequency of the l-th high-pass filter as was previously shown in Fig. 3.2b. The correlation values regarding different time delays can be calculated from (3.34) and will be used to derive the theoretical performance results for different wideband beamformers.

3.3 Performance Analysis of the Proposed Method for Adaptive Wideband Beamforming

In this section, the performance of the proposed noise reduction method for adaptive wideband beamforming is analysed.

3.3.1 Reference signal based adaptive beamformer

For the proposed noise reduction method, in the ideal case the directional signals (desired and interference) remain intact and only the noise part is reduced/changed. Then, the total signal vector $\hat{\mathbf{x}}$ corresponding to $\mathbf{x}$ after noise reduction can be expressed as:

$$\hat{\mathbf{x}} = \mathbf{x}_d + \mathbf{x}_i + \hat{\mathbf{x}}_v \, , \quad (3.35)$$

where $\hat{\mathbf{x}}_v$ is the part of $\hat{\mathbf{x}}$ corresponding to the reduced noise after the proposed processing.

Similarly, the correlation matrices $\mathbf{\Phi}_d$ and $\mathbf{\Phi}_i$ will remain the same after noise reduction, but the correlation matrix for the noise part will be changed to $\mathbf{\Phi}_{\hat{v}}$ with size $MJ \times MJ$. Then, the $MJ \times MJ$ correlation matrix $\mathbf{\Phi}_{\hat{x}}$ after noise reduction can be expressed as:

$$\mathbf{\Phi}_{\hat{x}} = \mathbf{\Phi}_d + \mathbf{\Phi}_i + \mathbf{\Phi}_{\hat{v}} \, . \tag{3.36}$$

$\mathbf{\Phi}_{\hat{v}}$ can be obtained from (3.34) and partition it into $M \times M$ submatrices (each submatrix is $J \times J$),

$$\mathbf{\Phi}_{\hat{v}} = \begin{bmatrix} \mathbf{\Phi}_{\hat{v}_{0,0}} & \cdots & \mathbf{\Phi}_{\hat{v}_{0,M-1}} \\ \vdots & \ddots & \vdots \\ \mathbf{\Phi}_{\hat{v}_{M-1,0}} & \cdots & \mathbf{\Phi}_{\hat{v}_{M-1,M-1}} \end{bmatrix} . \tag{3.37}$$

where $\mathbf{\Phi}_{\hat{v}_{i_1,i_2}} = E\left[\hat{\mathbf{x}}^*_{v_{i_1}} \hat{\mathbf{x}}^T_{v_{i_2}}\right]$. The delay between two adjacent taps in a TDL is $T_0 = \frac{\pi r}{2\Omega_0}$, where Ω_0 is the normalised centre frequency and r is the number of quarter-wave delays in T_0 at frequency Ω_0. Hence the delay between the i-th and the k-th taps is $\tau = (i-k)T_0$. Therefore, the correlation value $\left[\mathbf{\Phi}_{\hat{v}_{i_1,i_2}}\right]_{i,k}$ between the noise (after the proposed processing) at the i-th tap of the i_1-th element and that at the k-th tap of the i_2-th element is given by

$$\left[\mathbf{\Phi}_{\hat{v}_{i_1,i_2}}\right]_{i,k} = E\left[\hat{v}^*_{i_1,i}[n]\hat{v}_{i_2,k}[n]\right] = R_{\hat{v}(i_1,i_2)}\left[(i-k)T_0\right] \, . \tag{3.38}$$

From (3.34) and (3.38),

$$\begin{aligned} \left[\mathbf{\Phi}_{\hat{v}_{i_1,i_2}}\right]_{i,k} = \frac{\sigma_v^2}{M} \sum_{l=0}^{M-1} \frac{\pi - \hat{\Omega}_{l,L}}{\pi} e^{j\frac{2\pi}{M}(i_1-i_2)l} e^{j\frac{\pi+\hat{\Omega}_{l,L}}{2}(i-k)T_0} \\ \times \operatorname{sinc}\left(\frac{\pi - \hat{\Omega}_{l,L}}{2}(i-k)T_0\right) . \end{aligned} \tag{3.39}$$

Now all the correlation values required for calculating the $\mathbf{w}_{opt}$ in (2.6) is determined and the beamformer output $y[n]$ is

$$y[n] = \mathbf{w}_{opt}^T \hat{\mathbf{x}} \,, \tag{3.40}$$

with its power given by

$$P = \frac{1}{2} E\left[\|y[n]\|^2\right] = \frac{1}{2} \mathbf{w}_{opt}^H \mathbf{\Phi}_{\hat{x}} \mathbf{w}_{opt} \,. \tag{3.41}$$

The output SINR is given by

$$\text{SINR} = \frac{P_d}{P_i + P_{\hat{v}}} \,, \tag{3.42}$$

where

$$P_d = \frac{1}{2} \mathbf{w}_{opt}^H \mathbf{\Phi}_d \mathbf{w}_{opt} \,, \tag{3.43}$$

$$P_i = \frac{1}{2} \mathbf{w}_{opt}^H \mathbf{\Phi}_i \mathbf{w}_{opt} \,, \tag{3.44}$$

$$P_{\hat{v}} = \frac{1}{2} \mathbf{w}_{opt}^H \mathbf{\Phi}_{\hat{v}} \mathbf{w}_{opt} \,. \tag{3.45}$$

3.3.2 Linearly constrained minimum variance adaptive beamformer

In practice, the reference signal assumed in Section 2.2 may be unavailable. However, when some information on the DOAs as well as the bandwidth limits of the desired signal and/or the interferences is available, the LCMV beamformer can be employed for effective beamforming [2, 49]. The LCMV beamformer is formulated as follows (based on the recovered signal $\hat{\mathbf{x}}$ after the proposed noise reduction method),

$$\min_{\mathbf{w}} \mathbf{w}^H \mathbf{\Phi}_{\hat{x}} \mathbf{w} \qquad \text{subject to} \qquad \mathbf{C}^H \mathbf{w} = \mathbf{f} \,, \tag{3.46}$$

where $\mathbf{w}$ and $\mathbf{\Phi}_{\hat{x}}$ are defined as before in Section 2.2 and Section 3.3.1, $\mathbf{C}$ is the $MJ \times J$ constraint matrix and $\mathbf{f}$ is the $J \times 1$ response vector. The solution to (3.46) can be obtained using the Lagrange multipliers method,

$$\mathbf{w}_{opt} = \mathbf{\Phi}_{\hat{x}}^{-1}\mathbf{C}(\mathbf{C}^H\mathbf{\Phi}_{\hat{x}}^{-1}\mathbf{C})^{-1}\mathbf{f}\,. \tag{3.47}$$

Suppose the desired signal comes from the broadside, i.e., $\theta_d = 0^\circ$. Then, $\mathbf{C}$ and $\mathbf{f}$ have a very simple form, and they are same as (2.51) and (2.52). With the optimal weight vector determined, the output SINR can be obtained as in Section 2.2.

3.4 Compressive Sensing Based DOA Estimation

To further demonstrate the improved array processing performance with an improved TSNR, the effect of the developed method on the performance of the wideband DOA estimation problem is considered in this section by employing a compressive sensing based method.

3.4.1 Introduction to compressive sensing

The DOA estimation techniques are widely used for different applications such as radars. Most of the DOA estimation scenarios are sparse, since only a small fraction of the azimuth-range or the elevation-range cells are occupied by objects of interest. Therefore, compressive sensing (CS) [58, 59] is a suitable approach to solve the DOA estimation problem.

By employing the compressive sensing it is possible to reconstruct a sparse signal $\mathbf{f}$ from an under-determined linear system of equations $\mathbf{Bf} = \mathbf{g}$. Assuming $\mathbf{f}$ is a sparse vector with length L, the number of non-zero elements of f satisfies, $\|f\|_0 \ll L$, where $\|\cdot\|_0$ denotes the l_0 norm, which is the number of non-zero elements of a vector. Assume $\mathbf{B}$ is a $K \times L$ matrix of rank K, with $K < L$, so $\mathbf{B}$ is under-determined. $\mathbf{f}$ is considered to be sparse, hence, it can be computed from,

$$\begin{aligned} &\min_{\mathbf{f}} \ \|\mathbf{f}\|_0 \\ &\text{subject to } \mathbf{Bf} = \mathbf{g} \,, \end{aligned} \tag{3.48}$$

which is a non-deterministic polynomial-time (NP) hard problem. Therefore, solving (3.48) is not practically feasible. By using convex relaxation [60], also known as Basis Pursuit [61], the l_0 norm in (3.48) is relaxed by l_1 norm. So, (3.48) is written as,

$$\begin{aligned} &\min_{\mathbf{f}} \ \|\mathbf{f}\|_1 \\ &\text{subject to } \mathbf{Bf} = \mathbf{g} \,, \end{aligned} \tag{3.49}$$

where $\|\cdot\|_1$ denotes the l_1 norm. (3.49) can be solved by convex optimization methods [62]. Two conditions have to be satisfied, so that (3.49) can be solvable. One condition is that $\mathbf{B}$ must satisfy the isotropy property, which states that the components of each row of $\mathbf{B}$ have unit variance and they are uncorrelated. Another condition is that $\mathbf{B}$ should have a small coherence. The coherence is defined as the maximum inner product between normalised columns of $\mathbf{B}$ [63].

The compressive sensing based DOA estimation method adopted in this chapter is a direct adaptation and extension of the method developed in [29] and [32] for co-prime arrays.

3.4.2 Signal model for DOA estimation

First, for the received vector signal in (3.4), it is divided into P non-overlapping groups with length L, and an L-point DFT is then applied. The l-th frequency bin samples of the p-th group are placed into one vector as:

$$\mathbf{X}[l,p] = [X_0[l,p], X_1[l,p], \cdots, X_{M-1}[l,p]]^T \ , \tag{3.50}$$

where

$$X_n[l,p] = \sum_{i=0}^{L-1} x_n[Lp+i] e^{-j\frac{2\pi}{L}il}, \tag{3.51}$$

with $p = 0, \cdots, P-1$ and $l = 0, \cdots, L-1$.

Define $\bar{S}_k[l,p]$ and $V_m[l,p]$ as the DFT of the p-th group impinging signals $\bar{s}_k[n]$ and noise $v_m[n]$, respectively. $\bar{\mathbf{S}}[l,p] = \left[\bar{S}_0[l,p], \cdots, \bar{S}_{K-1}[l,p]\right]^T$ is a column vector holding signals from the l-th frequency bin, and $\mathbf{V}[l,p] = [V_0[l,p], \cdots, V_{M-1}[l,p]]^T$ is the column noise vector of the array. Then, the output signal model in the DFT domain can be expressed as:

$$\mathbf{X}[l,p] = \mathbf{D}(l,\theta)\bar{\mathbf{S}}[l,p] + \mathbf{V}[l,p], \tag{3.52}$$

where $\mathbf{D}(l,\theta) = [\mathbf{d}(l,\theta_0), ..., \mathbf{d}(l,\theta_{K-1})]$ is the steering matrix at frequency Ω_l corresponding to the l-th frequency bin. The column vector $\mathbf{d}(l,\theta_k)$ is the steering vector at frequency Ω_l and angle θ_k, which is given by

$$\mathbf{d}(l,\theta_k) = \left[1, \ e^{-j\frac{d}{cT_s}\Omega_l \sin\theta_k}, \ \cdots, \ e^{-j\frac{(M-1)d}{cT_s}\Omega_l \sin\theta_k}\right]. \tag{3.53}$$

By considering each frequency bin of interest separately, (3.52) is a narrowband signal model.

3.4.3 Generating the virtual array

The auto-correlation matrix of the observed array vector $\mathbf{X}[l,p]$ is:

$$\begin{aligned}\mathbf{R_{xx}}[l] &= E\left\{\mathbf{X}[l,p]\mathbf{X}^H[l,p]\right\} \\ &= \sum_{k=0}^{K-1}\sigma_k^2[l]\mathbf{d}(l,\theta_k)\mathbf{d}^H(l,\theta_k)+\sigma_v^2[l]\mathbf{I}_M\ ,\end{aligned} \tag{3.54}$$

where $\mathbf{I}_M$ is the $M\times M$ identity matrix. $\sigma_k^2[l]$ represents the power of the k-th impinging signal of the l-th frequency bin and $\sigma_v^2[l]$ is the corresponding noise power. In practical applications, it can be assumed that,

$$\mathbf{R_{xx}}[l]\approx\frac{1}{P}\sum_{p=0}^{P-1}\mathbf{X}[l,p]\cdot\mathbf{X}^H[l,p], \tag{3.55}$$

and it is assumed that the directional signals are wide-sense stationary.

Vectorising $\mathbf{R_{xx}}[l]$ yields:

$$\mathbf{u}[l]=\mathrm{vec}\{\mathbf{R_{xx}}\}=\tilde{\mathbf{D}}[l]\tilde{\mathbf{s}}[l]+\sigma_v^2\tilde{\mathbf{I}}_M\ , \tag{3.56}$$

where $\tilde{\mathbf{D}}[l]=[\tilde{\mathbf{d}}(l,\theta_0),\cdots,\tilde{\mathbf{d}}(l,\theta_{K-1})]$, $\tilde{\mathbf{d}}(l,\theta_k)=\mathbf{d}^*(l,\theta_k)\otimes\mathbf{d}(l,\theta_k)$ ($\otimes$ is the Kronecker product), and $\tilde{\mathbf{s}}[l]=\{\sigma_0^2[l],\sigma_1^2[l],\cdots,\sigma_{K-1}^2[l]\}^T$. $\tilde{\mathbf{I}}_M$ is an $M^2\times 1$ column vector obtained by vectorising the identity matrix $\mathbf{I}_M$. Eq. (3.56) characterises a virtual array with $\tilde{\mathbf{D}}[l]$ and $\tilde{\mathbf{s}}[l]$ as its steering matrix and impinging signal vector, respectively. Eq. (3.56) can be reduced to:

$$\mathbf{u}[l]=\tilde{\mathbf{D}}^{\circ}[l]\tilde{\mathbf{s}}^{\circ}[l], \tag{3.57}$$

where $\tilde{\mathbf{D}}^{\circ}[l]=\left[\tilde{\mathbf{D}}[l],\tilde{\mathbf{I}}_M\right]$ and $\tilde{\mathbf{s}}^{\circ}=\left[\tilde{\mathbf{s}}^T[l],\sigma_v^2[l]\right]^T$.

3.4.4 Narrowband DOA estimation

For the l-th frequency, with a search grid of K_g potential arriving angles $(\theta_{g,0}, \cdots, \theta_{g,K_g-1})$, the steering matrix is

$$\tilde{\mathbf{D}}_g[l] = \left[\tilde{\mathbf{d}}(l, \theta_{g,0}), \cdots, \tilde{\mathbf{d}}(l, \theta_{g,K_g-1})\right]. \tag{3.58}$$

Constructing a column vector $\tilde{\mathbf{s}}_g[l]$ consisting of K_g elements, with each representing a potential arriving signal, yields

$$\tilde{\mathbf{D}}_g^{\circ}[l] = \left[\tilde{\mathbf{D}}_g[l], \tilde{\mathbf{I}}_M\right]; \quad \tilde{\mathbf{s}}_g^{\circ}[l] = \left[\tilde{\mathbf{s}}_g[l], \sigma_v^2[l]\right]^T. \tag{3.59}$$

Since noise power is not known, $\sigma_v^2[l]$ is also considered to be a variable. In [29], a compressive sensing based DOA estimation was proposed for co-prime arrays, which can be applied directly for the ULA case. Therefore, for the l-th frequency bin, the narrowband DOA estimation is formulated as:

$$\begin{aligned} &\min_{\tilde{\mathbf{s}}_g^{\circ}[l]} \ \left\|\tilde{\mathbf{s}}_g^{\circ}[l]\right\|_1 \\ &\text{subject to } \left\|\mathbf{u}[l] - \tilde{\mathbf{D}}_g^{\circ}[l]\tilde{\mathbf{s}}_g^{\circ}[l]\right\|_2 \leq \varepsilon \ , \end{aligned} \tag{3.60}$$

where ε denote the error bound.

3.4.5 Wideband DOA estimation

The narrowband DOA estimation in (3.60) can be used for wideband case by applying the estimation to each frequency bin, and then averaging the results.

For each frequency bin, the impinging signals have the same spatial characteristics, although the amount of power regarding each DOA might

be different. This is known as the group sparsity concept [64, 65]. Therefore, a more effective alternative is to apply the DOA estimation over the frequency range of interest simultaneously.

It is assumed Q frequency bins are covering the frequency range of interest in the DFT domain, where $Q \leq L$, and the same search grid K_g is assumed for each frequency bin l_q, $0 \leq q \leq Q-1$.

Two matrices should be constructed here, a block diagonal matrix $\bar{\mathbf{D}}_g$ using $\tilde{\mathbf{D}}_g^{\circ}[l_q]$,

$$\bar{\mathbf{D}}_g = \text{blkdiag}\{\tilde{\mathbf{D}}_g^{\circ}[l_0], \tilde{\mathbf{D}}_g^{\circ}[l_1], \cdots, \tilde{\mathbf{D}}_g^{\circ}[l_{Q-1}]\}\,, \tag{3.61}$$

and a $(K_g+1)\times Q$ matrix $\mathbf{R}$ using $\tilde{\mathbf{s}}_g^{\circ}[l_q]$ with $\mathbf{R} = \left[\tilde{\mathbf{s}}_g^{\circ}[l_0], \tilde{\mathbf{s}}_g^{\circ}[l_1], \cdots, \tilde{\mathbf{s}}_g^{\circ}[l_{Q-1}]\right]$. Then, the following wideband virtual array model $\tilde{\mathbf{u}} = \bar{\mathbf{D}}_g \tilde{\mathbf{r}}$ can be obtained, where $\tilde{\mathbf{u}} = \left[\mathbf{u}^T[l_0], \cdots, \mathbf{u}^T[l_{Q-1}]\right]^T$ and $\tilde{\mathbf{r}} = \text{vec}(\mathbf{R})$ is a $(K_g+1)\cdot Q \times 1$ column vector by vectorising $\mathbf{R}$. The row vector $\mathbf{r}_k$, $0 \leq k \leq K_g$, is used to represent k-th row of matrix $\mathbf{R}$. Then, a new $(K_g+1)\times 1$ column vector $\hat{\mathbf{r}}$ is formed based on the l_2 norm of $\mathbf{r}_k$, $0 \leq k \leq K_g$, as given below

$$\hat{\mathbf{r}} = \left[\|\mathbf{r}_0\|_2, \|\mathbf{r}_1\|_2, \cdots, \left\|\mathbf{r}_{K_g}\right\|_2\right]^T. \tag{3.62}$$

Finally, the group sparsity based wideband DOA estimation is formulated as follows

$$\begin{aligned} &\min_{\tilde{\mathbf{r}}} \ \ \|\hat{\mathbf{r}}\|_1 \\ &\text{subject to} \ \ \left\|\tilde{\mathbf{u}} - \bar{\mathbf{D}}_g \tilde{\mathbf{r}}\right\|_2 \leq \varepsilon\,. \end{aligned} \tag{3.63}$$

The problem in (3.63) can be solved using CVX, a software package for specifying and solving convex programs [66, 67]. The steps for calculating

the narrowband DOA estimation is provided in Algorithm 1, and the steps for calculating the wideband DOA estimation is provided in Algorithm 2.

The idea is to process the signal using the proposed noise reduction method and then applying the DOA estimation. The noise reduction method does not affect the directional signal, but it increases the input TSNR by reducing the white noise. Therefore, it is expected that by applying the noise reduction method, the conditions of the DOA estimation convergence should not change considerably. Since the TSNR is increased, higher accuracy in DOA estimation is expected. One idea is to analyse the impact of the noise reduction method by analysing its effect on the Cramer-Rao bound (CRB) [68]. Analysing the exact impact of the precessed noise on the accuracy of the DOA estimation is quite complicated, and it is the scope of future research.

Algorithm 1: Narrowband DOA estimation

Input : $\mathbf{X}[l,p], \varepsilon, K_g$

Output : $\tilde{\mathbf{s}}_g^{\circ}[l]$

Calculate : $\tilde{\mathbf{D}}_g[l] = \left[\tilde{\mathbf{d}}(l,\theta_{g,0}), \cdots, \tilde{\mathbf{d}}(l,\theta_{g,K_g-1})\right]$

$\tilde{\mathbf{D}}_g^{\circ}[l] = \left[\tilde{\mathbf{D}}_g[l], \tilde{\mathbf{I}}_M\right]$

$\mathbf{R}_{\mathbf{xx}}[l] = \frac{1}{P}\sum_{p=0}^{P-1}\mathbf{X}[l,p]\cdot\mathbf{X}^H[l,p]$

$\mathbf{u}[l] = \mathrm{vec}\{\mathbf{R}_{\mathbf{xx}}\}$

Begin CVX:

$$\min_{\tilde{\mathbf{s}}_g^{\circ}[l]} \ \left\|\tilde{\mathbf{s}}_g^{\circ}[l]\right\|_1$$

$$\text{subject to} \ \left\|\mathbf{u}[l] - \tilde{\mathbf{D}}_g^{\circ}[l]\tilde{\mathbf{s}}_g^{\circ}[l]\right\|_2 \leq \varepsilon$$

Return : $\tilde{\mathbf{s}}_g^{\circ}[l]$

Algorithm 2: Wideband DOA estimation

Input : $\mathbf{X}[l,p], \varepsilon, K_g$

Output : $\hat{\mathbf{r}}$

for *l=0:Q-1* **do**

$$\tilde{\mathbf{D}}_g[l] = \left[\tilde{\mathbf{d}}(l,\theta_{g,0}),\cdots,\tilde{\mathbf{d}}(l,\theta_{g,K_g-1})\right]$$

$$\tilde{\mathbf{D}}_g^{\circ}[l] = \left[\tilde{\mathbf{D}}_g[l],\tilde{\mathbf{I}}_M\right]$$

$$\mathbf{R}_{\mathbf{xx}}[l] = \tfrac{1}{P}\sum_{p=0}^{P-1}\mathbf{X}[l,p]\cdot\mathbf{X}^H[l,p]$$

$$\mathbf{u}[l] = \mathrm{vec}\{\mathbf{R}_{\mathbf{xx}}\}$$

end

Calculate : $\tilde{\mathbf{u}} = \left[\mathbf{u}^T[l_0],\cdots,\mathbf{u}^T[l_{Q-1}]\right]^T$

$$\bar{\mathbf{D}}_g = \mathrm{blkdiag}\{\tilde{\mathbf{D}}_g^{\circ}[l_0],\tilde{\mathbf{D}}_g^{\circ}[l_1],\cdots,\tilde{\mathbf{D}}_g^{\circ}[l_{Q-1}]\}$$

Begin CVX:

$$\min_{\tilde{\mathbf{r}}} \ \|\hat{\mathbf{r}}\|_1$$

$$\text{subject to} \ \left\|\tilde{\mathbf{u}} - \bar{\mathbf{D}}_g\tilde{\mathbf{r}}\right\|_2 \le \varepsilon$$

Return : $\hat{\mathbf{r}}$

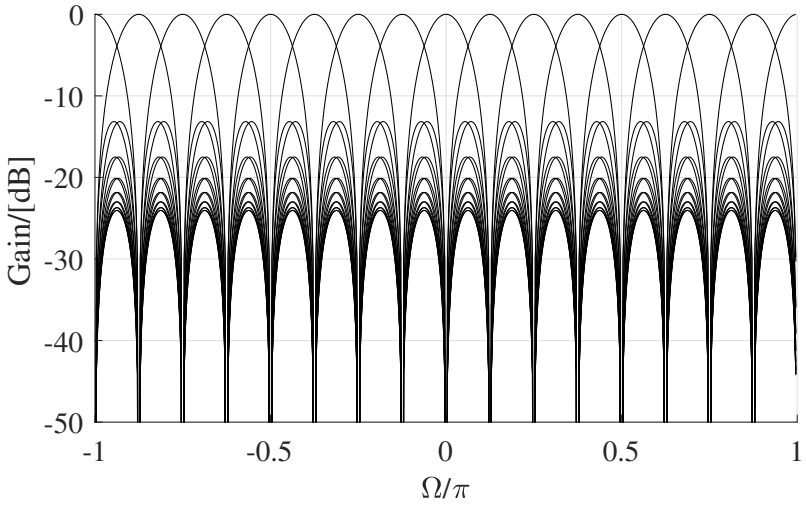

Fig. 3.5: The frequency response of the 16×16 DFT matrix.

3.5 Simulation Results

The simulation results are based on a 16-sensor ($M = 16$) ULA and the desired signal arrives from the broadside ($\theta_d = 0^\circ$). The received signals are processed by the 16×16 DFT-based transformation matrix, and its frequency response is shown in Fig. 3.5. Consider the frequency response of one of its row vectors shown in Fig. 3.6. The beam response of this row vector with respect to normalised signal frequency Ω and DOA angle θ is shown in Fig. 3.7. The high-pass behaviour can be seen clearly from this beam pattern.

Then, the transformed signals pass through the corresponding high-pass filters. It has been assumed that the high-pass filters have an ideal brick-wall shape response and to have a close approximation, linear-phase 101-tap FIR filters with a common delay of 50 samples are employed, and their frequency response is shown in Fig. 3.8.

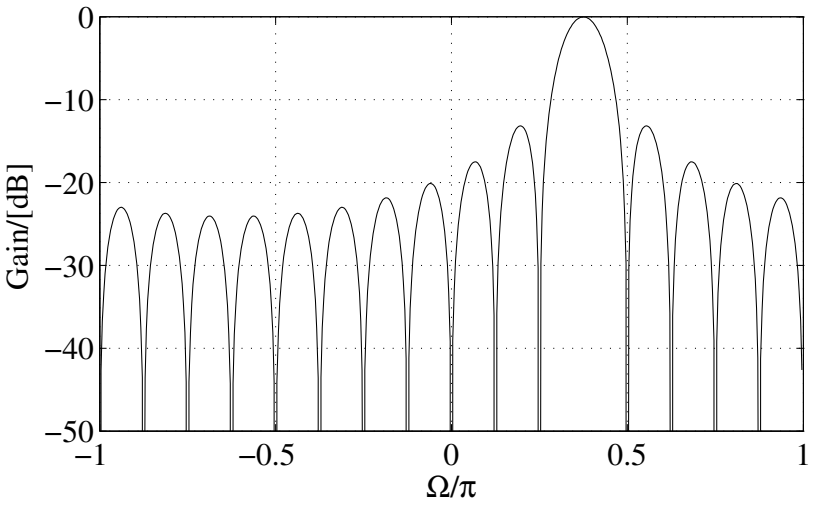

Fig. 3.6: Frequency response of an example band-pass filter with M=16.

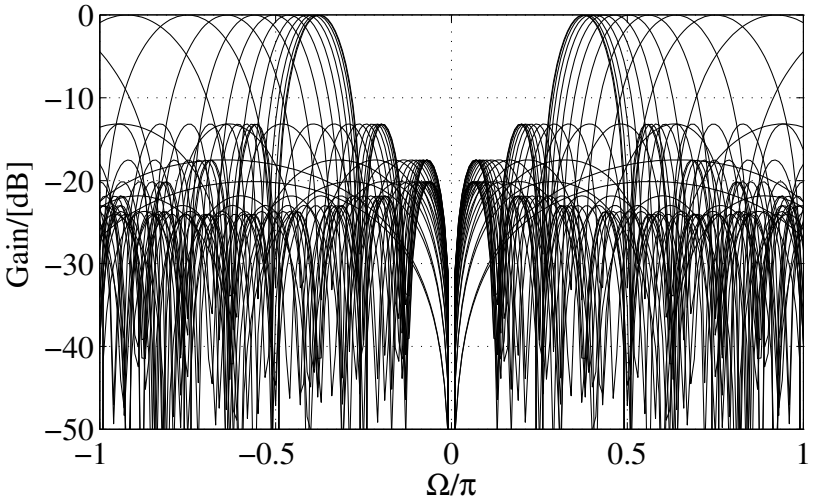

Fig. 3.7: Frequency response of the resultant beamformer with respect to normalised signal frequency and DOA angle, when applying the filter coefficients in Fig. 3.6 to the received array signal.

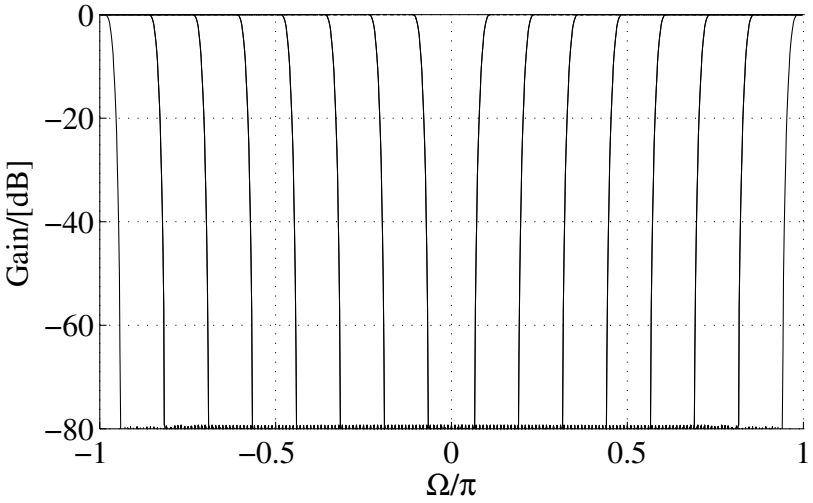

Fig. 3.8: Frequency response of the 16 linear-phase 101-tap FIR high-pass filters.

The 3D beam pattern of a sample row vector with respect to normalised signal frequency Ω and DOA angle θ before and after high-pass filtering is shown in Fig. 3.9.

3.5.1 The effect of the method on noise and directional signals

To see the effect of the whole system on noise, spatially and temporally white noise at the array sensors is generated with unit power. The power spectrum density of noise before and after the proposed noise reduction process is shown in Fig. 3.10a and Fig. 3.10b, respectively. It can be seen that the noise power has been reduced significantly at lower frequencies, while for higher frequencies, the reduction becomes less and less. Overall the power of noise has been reduced clearly.

For the received directional signals, as discussed before, there should not be any change after the proposed processing in the ideal case. However,

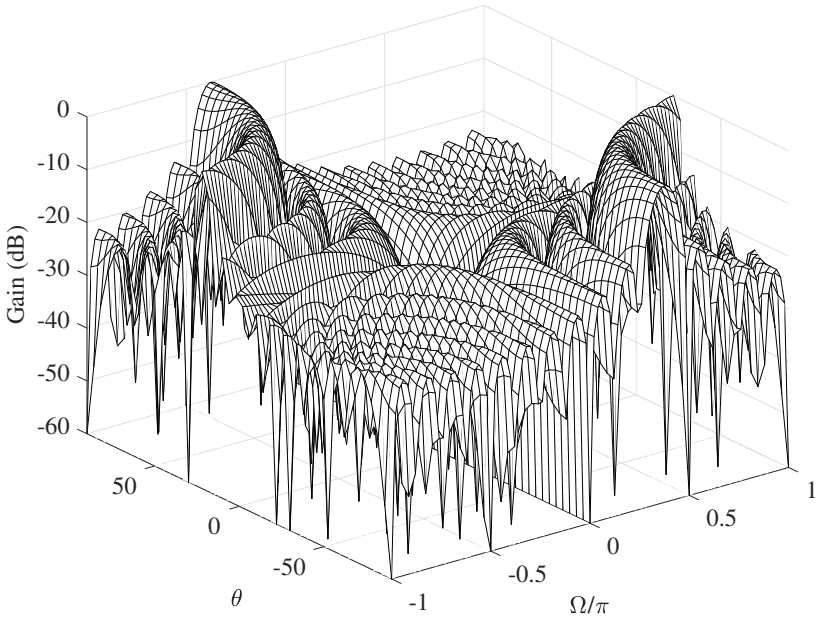

(a) Before high-pass filtering.

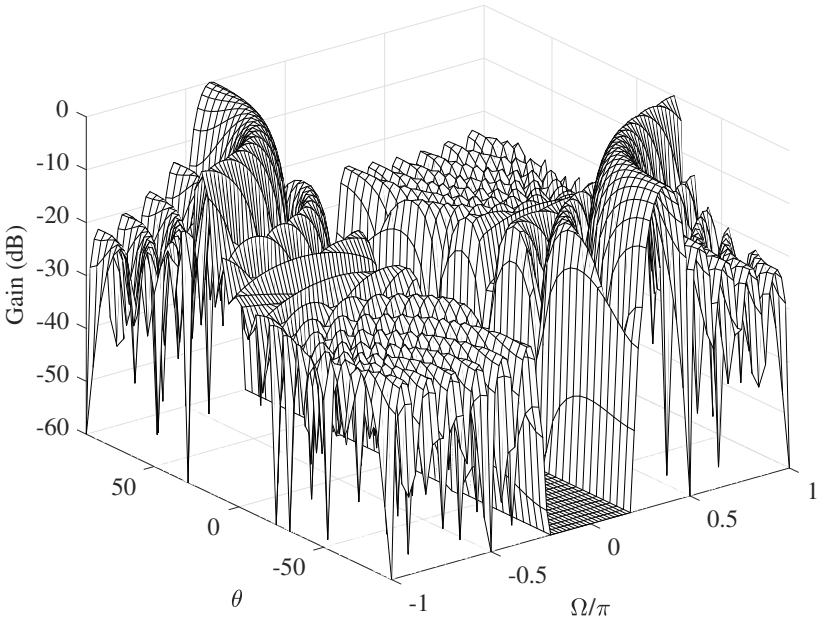

(b) After high-pass filtering.

Fig. 3.9: The beam pattern of a sample row vector before and after high-pass filtering (ULA, M=16).

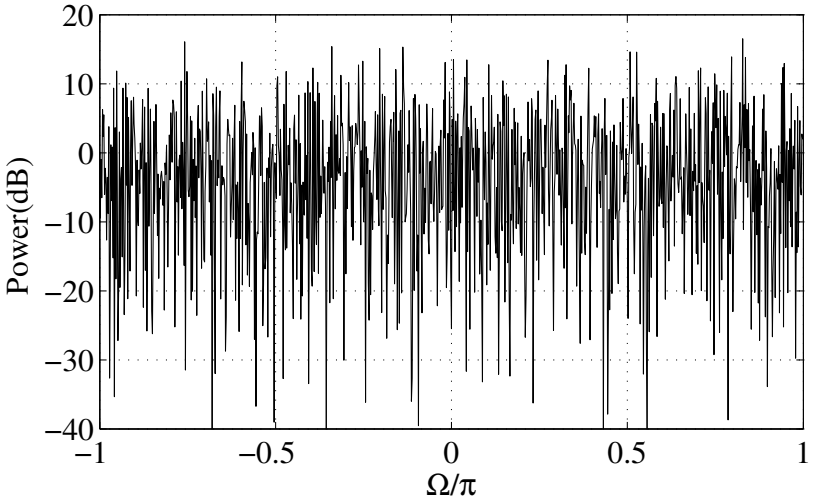

(a) Power spectrum density of noise before processing.

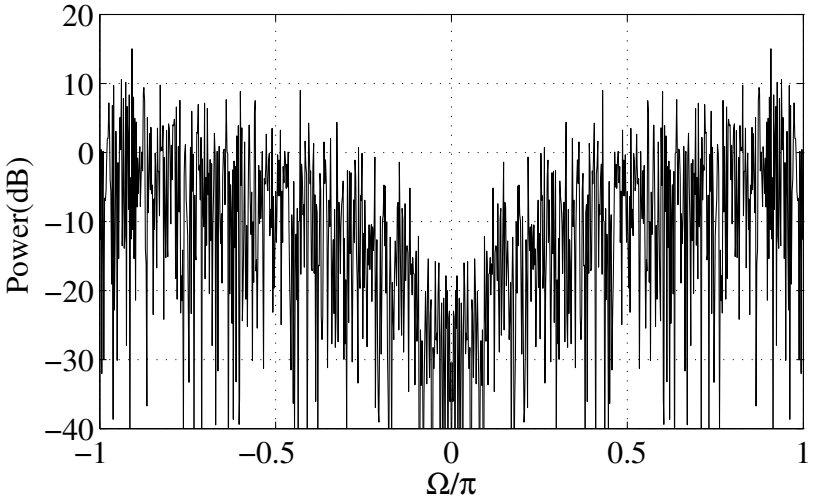

(b) Power spectrum density after processing.

Fig. 3.10: The power spectrum density of the spatially and temporally white noise before and after processing (M=16).

the response of the row vectors of the transformation is not ideal and as a result, a small amount of the directional signals will exist at the lower side-lobe region and it will be removed by the following high-pass filters.

In order to show this effect, a wideband signal with unit power is applied to the array from the broadside. The number of signals N sampled in the time domain at each sensor is 32768. The MSE for the directional signals before and after the proposed processing is calculated by,

$$\text{MSE} = \frac{1}{MN} \sum_{m=0}^{M-1} \sum_{n=0}^{N-1} \left(x_m[n] - \hat{x}_m[n] \right)^2 . \tag{3.64}$$

The results for different array size (M) are shown in Table 3.1, where it can be seen that the effect on the directional signal can be ignored for $M \geqslant 16$. Therefore, the directional signal is recovered with less distortion by increasing M, since by increasing the array size, less signal is available in the side-lobes which will be removed by the corresponding high-pass filters.

The output noise power P_{vo} to the input noise power P_{vi} is calculated and presented in Table 3.2. It can be seen that the power ratio which is presented in (3.14) is getting closer to the ideal case of -3 dB, as M increases. Therefore, larger array size M results in having a better recovery of the directional signal, and having a more effective white noise reduction.

M	MSE
10	0.0339
16	0.0205
20	0.0114
30	0.0069
40	0.0023

Table 3.1: MSE for the directional signal.

M	P_{vo}/P_{vi}(dB)	ideal P_{vo}/P_{vi}(dB)
10	-2.21	-2.26
16	-2.41	-2.53
20	-2.52	-2.62
30	-2.65	-2.74
40	-2.79	-2.80

Table 3.2: Power loss for the white noise.

3.5.2 The effect of the method on beamforming performance

The effect of the proposed method on the performance of both the RSB and the LCMV beamformers is examined here.

A desired band-limited wideband signal with bandwidth of $[0.3\pi : \pi]$ is received by the $M = 16$ array sensors from the broadside. An interfering signal with the same bandwidth and a -10 dB signal-to-interference ratio (SIR) arrives with a varying DOA angle. The received array signals are processed by the proposed noise reduction method and then the recovered array signals with an increased SNR are used as input to the beamformer.

The input SNR is 0 dB and the TDL length is $J = 100$.

The output SINR performances of both beamformers with and without the proposed pre-processing are compared in Fig. 3.11 as a function of the DOA angle θ_i of the interfering signal, where the theoretical value is based on the result derived in Sec. 3.3. It can be seen that the simulation result matches the theoretical one very well. With the change of the direction of the interfering signal, except for the region where DOA of the interfering signal is very close to the desired signal, an almost constant improvement of about 2 dB can be observed.

It is also important to analyse how the output SINR performance of the proposed method varies with different input SNRs. Seven interfering signals are applied to the system, each with a -10 dB input SIR, and their DOAs are $\theta_i = 10^\circ, 20^\circ, 30^\circ, 40^\circ, 50^\circ, 60^\circ$ and 70°, respectively. All the other settings are the same as before. The results are shown in Fig. 3.12. As expected, a higher output SINR has been achieved by the proposed method for both beamformers especially when the input SNR is larger than -10 dB and generally the improvement becomes larger when input SNR increases.

In general, the theoretical results should be the best one, but it can be seen in Fig. 3.11 and Fig. 3.12 that the simulated results are better than the theoretical results. The reason is that the band-pass response of the row vectors of the transformation is not ideal and therefore, the directional signal components which are available in the lower side-lobes are removed by the high-pass filters. So, the interfering signals are going to be slightly

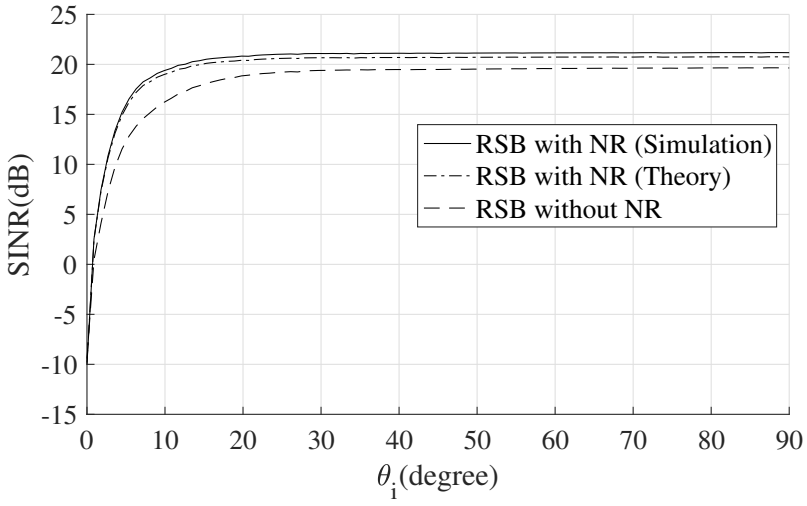

(a) RSB beamformer.

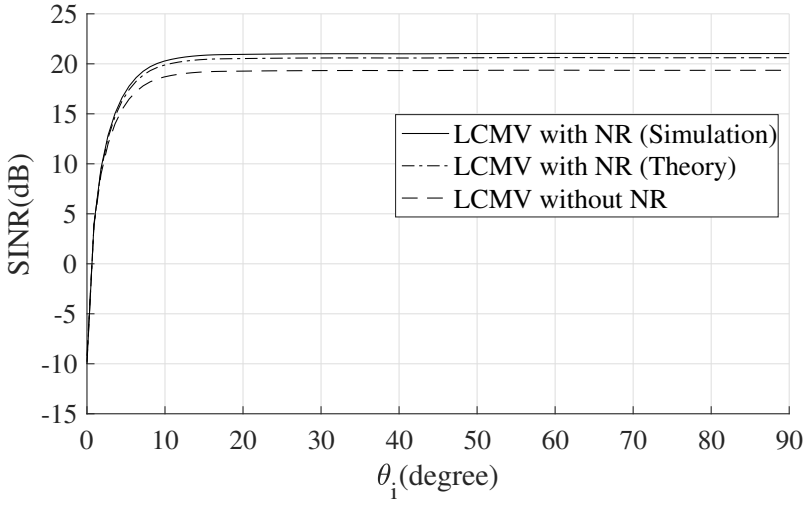

(b) LCMV beamformer.

Fig. 3.11: SINR performance of both beamformers with and without the proposed noise reduction (NR) method (M=16, J=100).

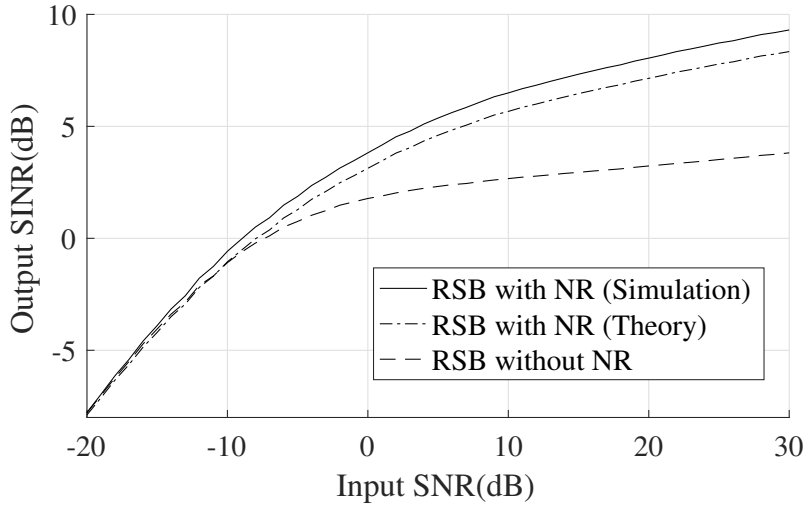

(a) RSB beamformer.

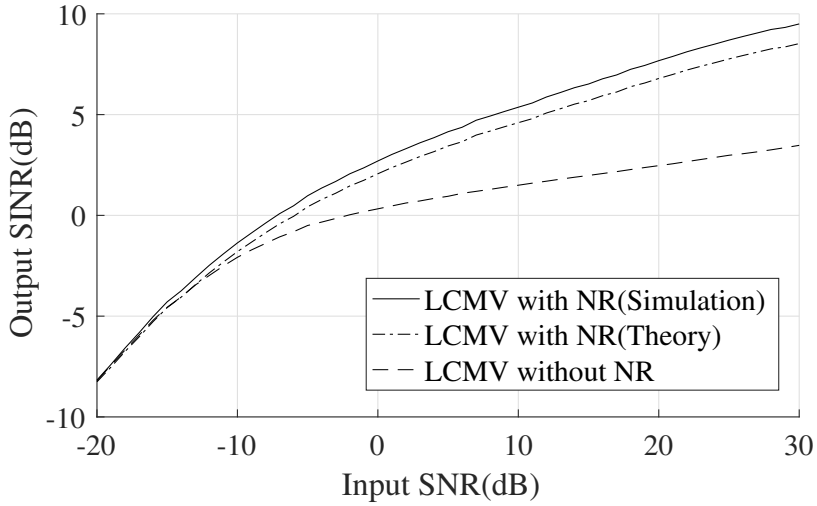

(b) LCMV beamformer.

Fig. 3.12: SINR performance of both beamformers with and without the proposed noise reduction method with regard to input SNR (M=16, J=100).

distorted, which contributes in the performance improvement of the beamformer. In the theoretical case, this distortion to interferences are not considered, and it is assumed that the interference after the pre-processing is exactly the same as before the processing, and only the effect of the method on the white noise is considered. Thus, the simulated results are showing a higher output SINR.

3.5.3 The effect of the method on DOA estimation performance

There are 12 band-limited impinging signals with a normalised frequency range from 0.5π to π and 0 dB SNR, and their DOAs are uniformly distributed between -60 to 60 degrees. The number of signals sampled in the time domain at each sensor is 32768, and a DFT of $L = 64$ points is applied. The number of data blocks used for estimating $\mathbf{R_{xx}}[l]$ in (3.54) at each frequency bin is $P = 512$. The search grid is formed to cover the full DOA range with a step size of 0.05°. By applying the proposed noise reduction method, 2.41 dB improvement in SNR is achieved.

The DOA estimation results with and without noise reduction are shown in Fig. 3.13, where it can be seen that in Fig. 3.13a there are a few false directions detected and the results are not as accurate as Fig. 3.13b when the proposed noise reduction method is used.

To compare the performance with more accuracy the root mean square error (RMSE) for the DOA estimation result with respect to different SNRs is shown in Fig. 3.14. The results are averaged from running the simulation

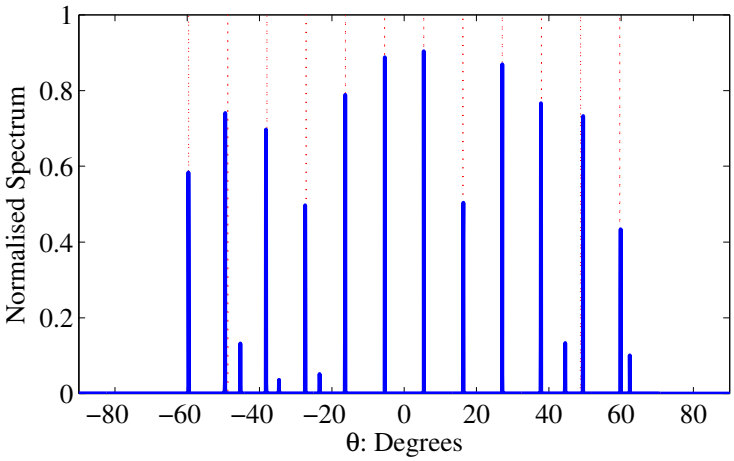

(a) Without white noise reduction.

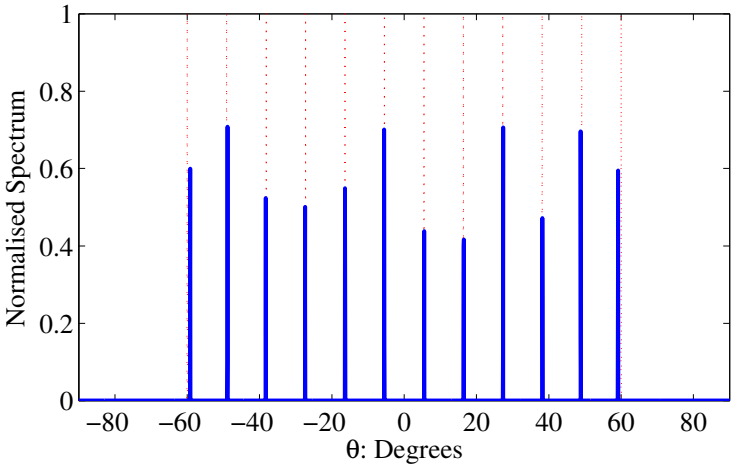

(b) With white noise reduction.

Fig. 3.13: DOA estimation results with and without the proposed white noise reduction.

100 times. It can be clearly seen that using the developed noise reduction method, the DOA estimation result has been improved significantly over the whole considered input SNR range.

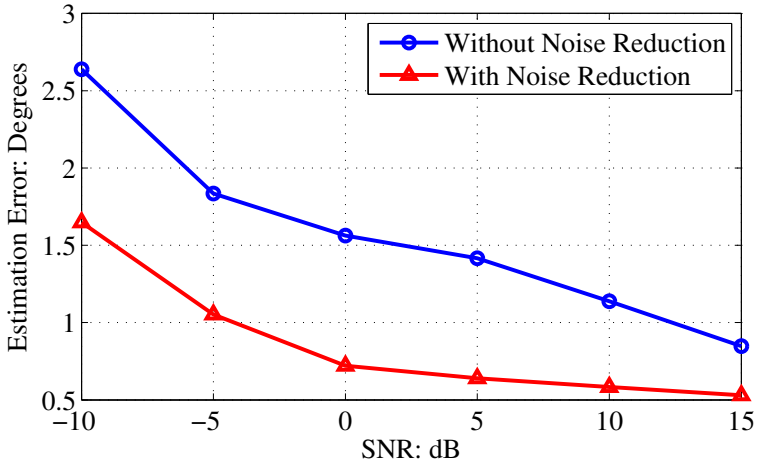

Fig. 3.14: RMSE vs input SNR.

3.6 Summary

In this chapter, a method for reducing the white noise level in wideband ULAs has been introduced. Initially, the general structure of the proposed method was explained, and each stage of the structure was analysed. It was shown that considering the array size is very large $M \to \infty$, a maximum of 3 dB improvement in TSNR can be achieve.

Since the DFT matrix is unitary, and it has good side-lobe attenuation, it was used as the transformation matrix. Then, the transfer function for the method was derived, and later, it was used to analyse the power spectrum and the auto-correlation of the noise after being processed.

Next, the performance of the proposed noise reduction method for adaptive wideband beamformers was analysed, considering the change in the correlation matrix of the noise. Then, as another example of the array signal processing applications, a compressive sensing based DOA estimation

for was reviewed.

In the simulation section, the effect of the method on the directional signal, and white noise presented. Then, the SINR performance of the RSB and LCMV beamformers with and without the noise reduction method was demonstrated, which confirmed the increased output SINR for beamformers using the proposed method. Also, simulation results showed an improvement in the accuracy of the compressive sensing based DOA estimation.

Chapter 4

Extension of the Noise Reduction Method for Non-uniform Linear Arrays

In Chapter 3, a method was developed for reducing the effect of white noise in wideband ULAs via a combination of a judiciously designed transformation followed by high-pass filters to improve the performance for wideband beamforming and DOA estimation. In this chapter, that idea is extended to non-uniform linear arrays (NLAs) and as a result, the transformation is re-designed using the least squares method to adjust the noise reduction method for the non-uniform sensor layout of NLAs.

To make sure the transformation is invertible, a prototype filter is first designed and then modulated to different subbands to cover the full normalised frequency band from $-\pi$ to π. The diagonal loading method is used to keep the condition number to a low level [69]. Similar to the ULA case, the overall SNR of the system can be improved by up to 3 dB, which then leads to performance enhancement for beamforming as demonstrated

using two well-known adaptive beamformers, namely the RSB [70,71] and the LCMV beamformers [2,49].

The contents of this chapter is published in [50] and is also presented at a conference [72].

4.1 The Proposed White Noise Reduction for Non-uniform Linear Arrays

The general structure of the proposed method for NLAs is same as the general structure for ULAs, as presented in Fig. 3.1. M array signals $x_m[n], m = 0, \cdots, M-1$, are received by the NLA sensors. Then, the received array signals are transformed by an $M \times M$ transformation $\mathbf{A}$. Next, the transformed signals $q_m[n], m = 0, \cdots, M-1$, are passed through the corresponding high-pass filters $h_m[n], m = 0, \cdots, M-1$. Finally, the high-pass filtered signals $z_m[n], m = 0, \cdots, M-1$ are block-transformed by the inverse of the transformation $\mathbf{A}^{-1}$.

The signal model is similar to the ULA case, and it can be presented by (3.1)–(3.4). By applying the $M \times M$ transformation to the signal vector $\mathbf{x}[n]$, the output signal vector is obtained as (3.5). Each row vector of $\mathbf{A}$ acts as a simple beamformer, with its output same as (3.6). The beam response $R_m(\Omega, \theta)$ of this beamformer for the NLA structure is given by:

$$R_m(\Omega, \theta) = \sum_{l=0}^{M-1} a_{m,l} e^{-j\frac{d_l}{cT_s}(\Omega \sin\theta)} = A_m(\Omega \sin\theta), \tag{4.1}$$

where d_l is the spacing between the zero-th sensor and the l-th sensor

(where d_0=0). Therefore, considering $\hat{\Omega} = \Omega \sin\theta$,

$$A_m(\hat{\Omega}) = \sum_{l=0}^{M-1} a_{m,l} e^{-j\frac{d_l}{cT_s}\hat{\Omega}}, \tag{4.2}$$

where $A_m(\hat{\Omega})$ is the frequency response of the m-th row vector of the transformation matrix $\mathbf{A}$, considering each row vector as the impulse response of an FIR filter. The frequency responses $A_m(\hat{\Omega}), m = 0, \cdots, M-1$, are set to have band-pass characteristics, each with a bandwidth of $2\pi/M$. Overall, the row vectors of $\mathbf{A}$ cover the entire normalised frequency band of $[-\pi : \pi]$.

By considering the entire range of the DOA θ of the received signals, the row vectors of $\mathbf{A}$ have high-pass filtering behaviour as explained in Sec. 3.1. According to the general structure in Fig. 3.1, each high-pass filter $h_l[n], l = 0, \cdots, M-1$, processes its corresponding input $q_l[n]$, $l = 0, \cdots, M-1$. The high-pass filters have the same high-pass frequency response as their corresponding row vectors of the transformation $\mathbf{A}$, and they cover the entire bandwidth of the directional signal. Therefore, in the ideal case, the directional signal is not affected by any distortion after being processed by the high-pass filters. On the contrary, the high-pass filters remove parts of the white noise which fall into their stop-band.

The output of the aforementioned high-pass filters which is denoted by $z_l[n]$, $l = 0, \cdots, M-1$, is then processed by the inverse transformation $\mathbf{A}^{-1}$, and the original array signals will be recovered without any distortion in the ideal case, while the noise power will be reduced leading to an

improved overall SNR. Following the same analysis for the ULA, as discussed in Sec. 3.1, when $\mathbf{A}$ is unitary, up to 3 dB total SNR improvement can be achieved by the proposed method. Although, in practice, the TSNR improvement will be less than 3 dB, due to limited number of sensors and difficulty in designing a unitary transformation matrix with the required band-pass responses for the NLA case.

The transformation matrix $\mathbf{A}$ is required to be unitary to make sure that the row vectors of both $\mathbf{A}$ and $\mathbf{A}^{-1}$ have unity norm and preserve the signal power after transforming the signal and also after transforming the signal back. If the transformation is not unitary, the noise might be amplified significantly during the process, even if some of it has been removed by high-pass filters, which subsequently leads to a reduced output SNR. Moreover, a unitary transformation ensures that $\mathbf{A}$ is of full rank.

In the next section, the design of the transformation for NLAs is presented, with required band-pass characteristics.

4.2 Least Squares Based Design for the Transformation Matrix

As an example for a unitary matrix with a good band-pass response, the DFT matrix in the ULA case is considered in this section. However, the DFT matrix is not applicable for the NLA case, since it does not have a uniform spacing, and the resultant beams by each row vector of such a

transformation will be significantly distorted.

Therefore, a different approach for designing the transformation matrix is used for NLAs by introducing a least squares based design method here. The idea is to use an ideal unitary beam response such as those of a DFT matrix as the reference response for the least squares method to design a prototype filter $\mathbf{p}$ (where $[\mathbf{p}]_l = p_l, l = 0, \cdots, M-1$), and then it is modulated into different subbands in a uniform way to form the required transformation matrix.

The least squares filter design method has been well studied in the past [2, 73]. Given the desired beam pattern $P_d(\hat{\Omega})$ and considering $\mathbf{d}(\hat{\Omega})$ as the steering vector of the NLA,

$$\mathbf{d}(\hat{\Omega}) = \left[1, \quad e^{-j\frac{d_1}{cT_s}\hat{\Omega}}, \quad \cdots, \quad e^{-j\frac{d_{M-1}}{cT_s}\hat{\Omega}}\right], \tag{4.3}$$

the problem can be solved by minimising the sum of squares of the error between $P_d(\hat{\Omega})$ and the designed response $P(\hat{\Omega})$ over the frequency range of interest, i.e.,

$$\min_{\mathbf{p}} \sum |P(\hat{\Omega}) - P_d(\hat{\Omega})|^2. \tag{4.4}$$

Minimising the above cost function with respect to the coefficients vector $\mathbf{p}$ gives the standard least squares solution,

$$\mathbf{p}_{opt} = \mathbf{G}_{ls}^{-1}\mathbf{g}_{ls}, \tag{4.5}$$

with

$$\mathbf{G}_{ls} = \sum_{\hat{\Omega}_{pb}} \mathbf{d}(\hat{\Omega})\mathbf{d}^H(\hat{\Omega}),$$

$$\mathbf{g}_{ls} = \sum_{\hat{\Omega}_{pb}} (\mathbf{d}_R(\hat{\Omega}) P_{d,R}(\hat{\Omega}) + \mathbf{d}_I(\hat{\Omega}) P_{d,I}(\hat{\Omega})),$$

where $\mathbf{d}_R(\hat{\Omega})$ and $P_{d,R}(\hat{\Omega})$ denote the real parts of $\mathbf{d}(\hat{\Omega})$ and $P_d(\hat{\Omega})$, and $\mathbf{d}_I(\hat{\Omega})$ and $P_{d,I}(\hat{\Omega})$ are their imaginary parts.

Then, $\mathbf{p}$ is modulated to different subbands to cover the whole normalised frequency band,

$$A_{m,l} = e^{-j\frac{2\pi}{M} m \frac{d_l}{cT_s}} p_l, \tag{4.6}$$

where $m = 0, \cdots, M-1$, $l = 0, \cdots, M-1$.

At this stage, if the condition number of the resultant transformation matrix is high, the diagonal loading method [69] can be used to reduce the condition number,

$$\mathbf{A}_L = \mathbf{A} + \alpha \mathbf{I}\,, \tag{4.7}$$

where α is a constant representing a small loading level.

Note that the transformation matrix obtained by the above procedure will not be unitary in general and how to design a unitary matrix for NLAs with the required band-pass filtering effect is still an open problem for the future research work. However, it is shown in the simulation that the transformation matrix obtained from the above procedure works well to some degree and provides a clear performance improvement.

4.3 Simulation Results

These simulation results are based on an $M = 15$ NLA example provided in [74], with the sensor locations listed in Table 4.1, where λ is the wavelength associated with the normalised frequency $\Omega = \pi$. The 15×15 transformation matrix is obtained by the design procedure described in Sec. 4.2, and its frequency response is shown in Fig. 4.1. The other settings are the same as in the ULA case.

n	1	2	3	4	5
d_n/λ	0	0.81	1.62	2.42	3.28
n	6	7	8	9	10
d_n/λ	4.09	4.24	5.00	5.81	5.96
n	11	12	13	14	15
d_n/λ	6.72	7.58	8.38	9.19	10

Table 4.1: Sensor locations for the wideband NLA example.

The received signals are processed by the designed sparse transformation matrix and then pass through the high-pass filters. For high-pass filters, 101-tap linear-phase FIR filters with a common delay of 50 samples are employed same as ULA. Then, the signals are transformed back by inverse of the transformation matrix.

The effect of the proposed method on the performance of both the RSB beamformer and the LCMV beamformer is examined. A desired band-limited wideband signal with a bandwidth of $[0.3\pi : \pi]$ is received by the previously mentioned NLA from the broadside. Same as the ULA case,

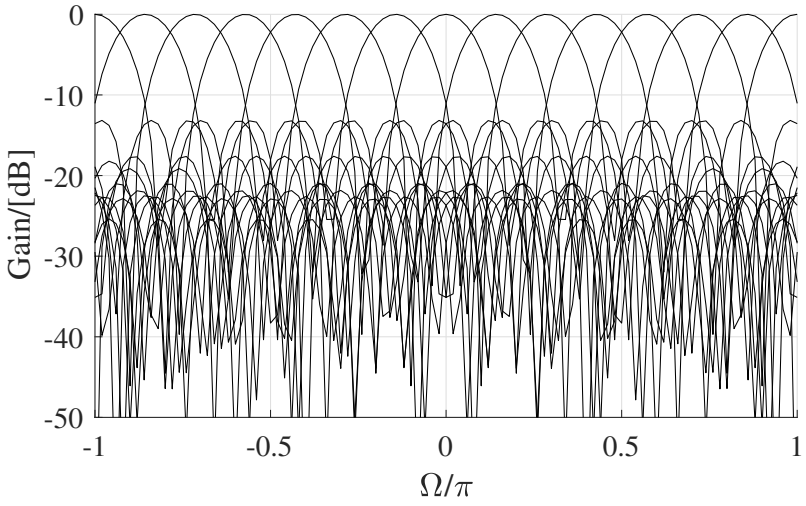

Fig. 4.1: Frequency response of the row vectors of the 15×15 designed transformation matrix for NLAs.

seven interfering signals are applied to the system, each with a -10 dB input SIR and their DOAs are $\theta_i = 10^\circ$, 20°, 30°, 40°, 50°, 60° and 70°, respectively. A TDL length of $J = 100$ is used for these beamformers [2].

The results are shown in Fig. 4.2, and it can be seen that a higher output SINR is achieved by the proposed method for both beamformers, especially when the input SNR is larger than 0 dB and generally the improvement becomes larger when input SNR increases. However, compared to the ULA case, for input SNR smaller than 0 dB, there is not as much improvement. Moreover, the improvement becomes smaller when the input SNR is roughly larger than 25 dB, which is difficult to explain. After checking the designed transformation matrix, it is been found that it is far away from being unitary and has a large condition number, which could be the reason for such a behaviour. A method for reducing the condition

number even further is introduced in Sec. 4.4 but as mentioned at the end of Sec. 4.2, further research is needed for designing a unitary transformation matrix for NLAs with the desired frequency responses.

4.4 Fixing Ill Conditioned Transformation Matrix With Singular Value Decomposition

It has been mentioned before that, it is important that the transformation matrix is well conditioned and ideally unitary. A well conditioned matrix has a low condition number. In section 4.2, the least squares method is used to design a transformation for NLAs by employing the least squares filter design method, and then using the diagonal loading method, the condition number of the transformation is reduced. As it was seen in previous section, an improvement in the performance of the NLAs was achieved but for low input SNRs the performance was not satisfactory and by analysing the transformation, it was realised that the condition number of the transformation is still high (around 9). In this section, the singular value decomposition (SVD) is used to decompose the transformation and subsequently to modify the transformation to be well-conditioned and as close to unitary as possible by replacing the low value singular values.

An $M \times M$ transformation matrix $\mathbf{A}$ is assumed, which is not unitary. The SVD of $\mathbf{A}$ is

$$\mathbf{A} = \mathbf{U}\Sigma\mathbf{V}^H, \tag{4.8}$$

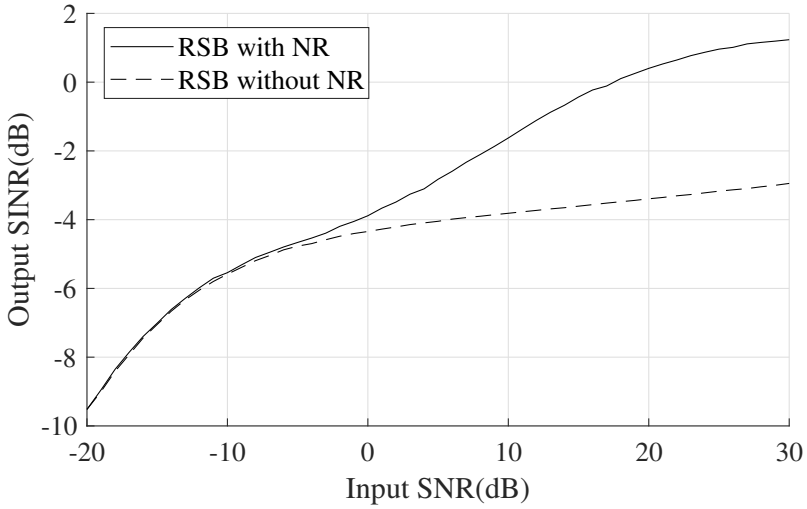

(a) RSB beamformer.

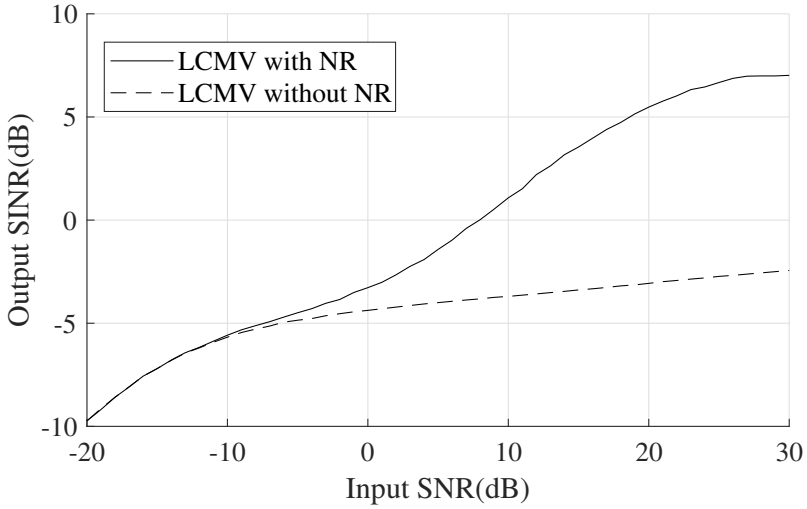

(b) LCMV beamformer.

Fig. 4.2: SINR performance of both beamformers with and without the proposed noise reduction method for the NLA.

where $\mathbf{U}$ and $\mathbf{V}$ are $M \times M$ unitary matrices and Σ is a diagonal rectangular $M \times M$ matrix with singular values $\sigma_i, i = 0, \cdots, M-1$, on the diagonal.

The condition number of a matrix is the largest singular value divided by the smallest one:

$$\kappa = \frac{\sigma_0}{\sigma_{M-1}} . \tag{4.9}$$

Therefore, small singular values result in a large condition number.

The unitary matrix $\mathbf{B}$ which minimises $||\mathbf{A} - \mathbf{B}||_F^2$ is $\mathbf{B} = \mathbf{U}\mathbf{V}^H$, where $||.||_F$ defines the Frobenius norm, and therefore, the closest unitary matrix to $\mathbf{A}$ is $\mathbf{B}$ [75,76]. This is actually, equal to replacing all the singular values with 1, $\sigma_i = 1, i = 0, \cdots, M-1$.

The problem with this method is that, if all singular values are replaced with 1, the beam-pattern of the row vectors of the transformation may be changed significantly. Therefore, it is not suitable for transforming the signal, although the transformation is unitary.

The alternative approach is to replace the singular values smaller than a threshold value. Using this method, the condition number is reduced but the singular values which are bigger than the threshold are kept the same.

4.4.1 Simulation

As an example, the NLA case which was mentioned before is considered, the threshold is set to 0.5, and all the $(\sigma_i, i = 0, \cdots, M-1) \leq 0.5$ are replaced with 0.5. After replacing the small singular values, the condition number is reduced to 2.45, which is much better than 9 achieved by the

diagonal loading previously. In order to analyse the effect on the beam pattern, the side-lobe attenuation and 3 dB beamwidth are calculated before and after the singular value modification of the transformation. The average 3 dB beamwidth before the modification is 0.162 in the normalised frequency. The average 3 dB beamwidth after the modification is also 0.162, and therefore, there is no change in 3 dB beamwidth. Moreover, The average side-lobe attenuation before the modification is 12.59 dB, and after the modification is 12.73 dB. So, there is no major change in the beam-pattern for the transformation, and the proposed modification method works quite well.

Next, the performance of the noise reduction method is analysed with the modified transformation with low condition number, when used as a pre-processing step for TDL beamformers. The NLA array structure has 15 sensors ($M = 15$) and the desired signal arrives from the broadside ($\theta_d = 0^\circ$). The transformation is a 15×15 matrix obtained by the modified design procedure described. For high-pass filters, 101-tap linear-phase FIR filters with a common delay of 50 samples are employed. A desired band-limited wideband signal with a bandwidth of $[0.3\pi, \pi]$ is received by the aforementioned NLA from the broadside. Four interfering signals are applied to the system, each with a -20 dB input SIR and their DOAs are $\theta_i = 10^\circ, 30^\circ, 50^\circ, 70^\circ$, respectively. A tapped delay line with length $J = 5$ is used for these beamformers. Fig. 4.3, illustrates the performance of the two well-known RSB and LCMV beamformers when used with and with-

out the modified noise reduction method. It is clear that for both RSB and LCMV beamformers the performance of the beamformer with the modified noise reduction pre-processing is increased significantly.

4.5 Summary

In this chapter, the noise reduction method introduced in Chapter 3 was re-designed based on the structure of NLAs. Same as the ULA case, a maximum of 3 dB improvement in output TSNR was achieved. This TSNR improvement leads to possible performance enhancement in many array signal processing applications.

Due to the non-uniform spacing of the NLA, the resultant beam-patterns of the row vectors are significantly distorted. Therefore, the DFT matrix is not applicable. The least squares method was used for re-designing the transformation for NLA. The beam response of DFT matrix was used as the reference response for the least squares method to design a prototype filter, and then the prototype was modulated to different subbands to form the transformation matrix.

Diagonal loading method was used to reduce the condition number of the designed transformation, and simulation results presented an improvement in output SINR performance for the RSB and LCMV beamformers, when the noise reduction method is used as a pre-processing step.

Later, the SVD was used to decompose the transformation. By replac-

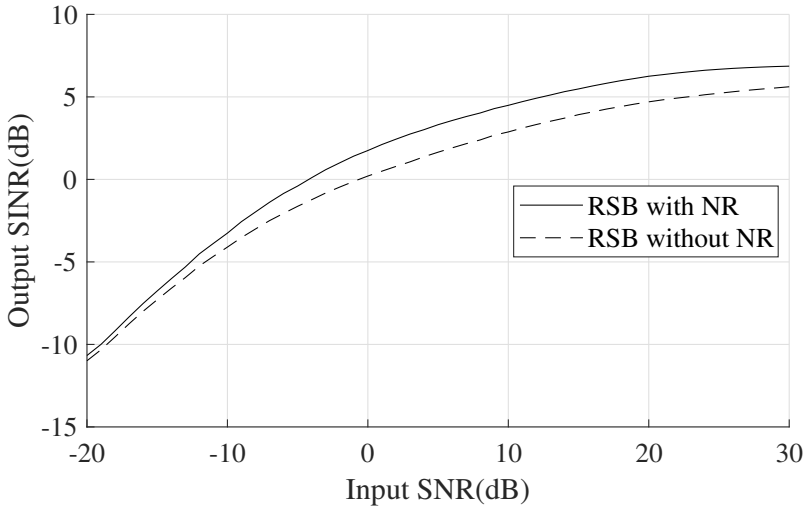

(a) RSB beamformer.

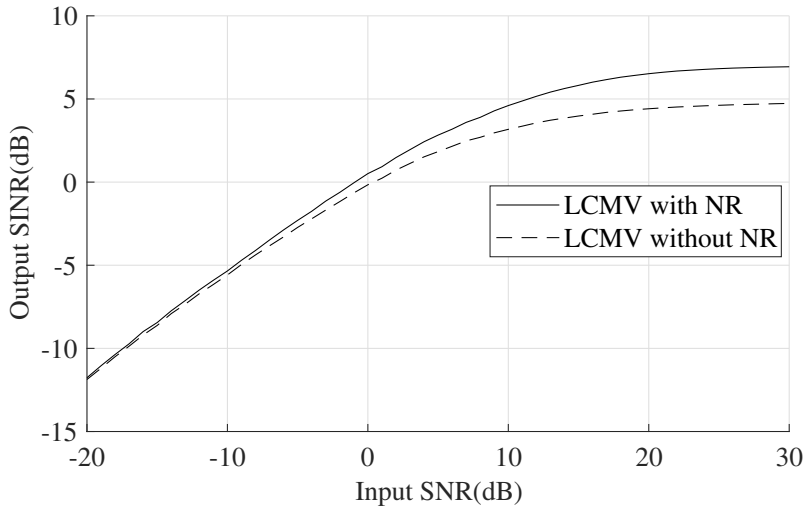

(b) LCMV beamformer.

Fig. 4.3: SINR performance of both beamformers with and without the modified noise reduction (NR) methods for the NLA.

ing the low value singular values, the transformation was modified to be well-conditioned and as close to unitary as possible. The simulation results showed a steady improvement for RSB and LCMV beamformers for a wide range of input SNRs from -20 dB to 30dB.

In the following chapter transformation is re-designed for the structure of planar arrays.

Chapter 5

Extension of the Method to Planar Arrays

In Chapter 3, a method was developed for reducing the effect of white noise in wideband ULAs via a combination of a judiciously designed transformation followed by high-pass filters to improve the performance for wideband beamforming and DOA estimation. In this chapter, the idea is extended to the case of planar arrays, and focus on two major types of planar arrays, namely, uniform rectangular arrays (URAs) [77, 78] and uniform circular arrays (UCAs) [79, 80]. As a result, the transformation matrix has to be re-designed to adjust the noise reduction method to the structure of URAs and UCAs.

In particular, two noise reduction methods are introduced in this chapter for URAs and for each one, a different transformation is designed. The first method is based on a two-dimensional (2D) transformation. The second method is an adaptation of the method introduced in Chapter 3, which

is based on one-dimensional (1D) transformation of the signals received by the URA. The transformations must be invertible and ideally, unitary. As representative examples for unitary transformations, 2D-DFT (discrete Fourier transform) and 1D-DFT are used in simulation.

Later, a method is introduced for the UCAs based on a 1D transformation. The transformation is re-designed for the UCA structure, by changing the modulation of the prototype filter to match the structure of the UCA.

All the methods can increase the overall signal-to-noise ratio (SNR) of the array. This improvement leads to performance enhancement of various array signal processing applications such as beamforming, which is demonstrated by simulation using two well-known adaptive beamformers, namely the RSB [39, 40], and the LCMV beamformers [2, 49].

Part of the contents of this chapter was presented at a conference [81].

5.1 White Noise Reduction for URAs with a 2D Transformation

The linear arrays are used to resolve the azimuth angle θ of the received signal, whereas the URA allows to resolve the elevation angle ϕ in addition to the azimuth angle θ [82]. Both structures are widely used for developing different smart antennas.

The structure of a URA is shown in Fig. 5.1, and a block diagram for the general structure of the proposed noise reduction method is shown in

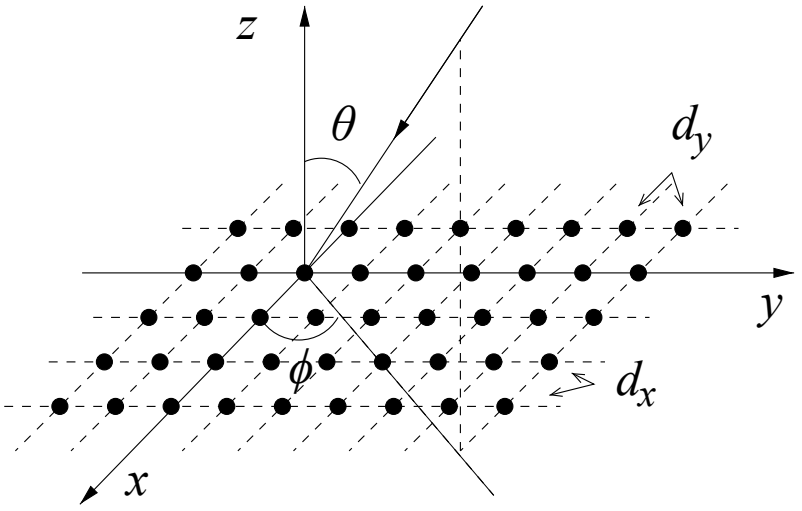

Fig. 5.1: The structure of a URA, where a signal impinges from azimuth angle θ and elevation angle ϕ .

Fig. 5.2. Suppose there are M sensors along the x-axis and N sensors along the y-axis. The received array signals $x_{m,l}[n]$, $m = 0,\ldots,M-1$, $l = 0,\ldots,N-1$, are first transformed by a 2D transformation and then its outputs $q_{m,l}[n], m = 0,\cdots,M-1, l = 0,\cdots,N-1$, pass through a set of high-pass filters with impulse responses given by $h_{m,l}[n], m = 0,\cdots,M-1$, $l = 0,\cdots,N-1$. The outputs of the high-pass filters $z_{m,l}, m = 0,\cdots,M-1$, $l = 0,\cdots,N-1$, are then transformed by the inverse of the 2D transformation.

There are two components for the received array signal $x_{m,l}[n]$ at the (m,l)-th sensor: the directional signal part $s_{m,l}[n]$ and the white noise part $v_{m,l}[n]$, i.e.,

$$x_{m,l}[n] = s_{m,l}[n] + v_{m,l}[n] \; . \tag{5.1}$$

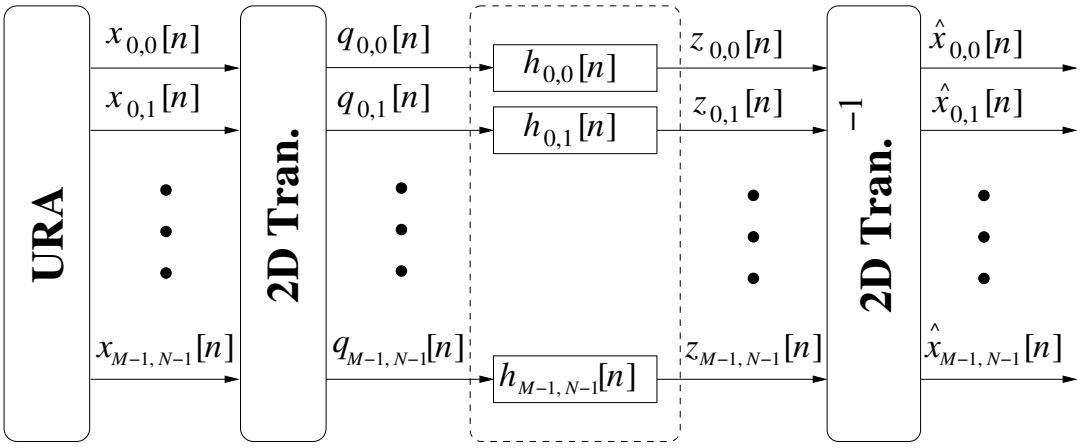

Fig. 5.2: A block diagram of the proposed noise reduction method based on a 2D transformation.

The complete $M \times N$ signal matrix $\mathbf{X}[n]$ can be expressed as

$$\mathbf{X}[n] = \mathbf{S}[n] + \mathbf{V}[n] \,, \tag{5.2}$$

where

$$\mathbf{X}[n] = [\mathbf{x}_0[n], \mathbf{x}_1[n], \cdots, \mathbf{x}_{N-1}[n]] \,,$$

$$\mathbf{S}[n] = [\mathbf{s}_0[n], \mathbf{s}_1[n], \cdots, \mathbf{s}_{N-1}[n]] \,,$$

$$\mathbf{V}[n] = [\mathbf{V}_0[n], \mathbf{V}_1[n], \cdots, \mathbf{V}_{N-1}[n]] \,.$$

and

$$\mathbf{x}_l[n] = [x_{0,l}[n], x_{1,l}[n], \cdots, x_{M-1,l}[n]]^T,$$

$$\mathbf{s}_l[n] = [s_{0,l}[n], s_{1,l}[n], \cdots, s_{M-1,l}[n]]^T,$$

$$\mathbf{V}_l[n] = [v_{0,l}[n], v_{1,l}[n], \cdots, v_{M-1,l}[n]]^T,$$

with $l = 0, 1, \cdots, N-1$.

In this method, the array signal $\mathbf{X}[n]$, which is received by an $M \times N$ URA, is transformed with a 2D unitary transformation. The output matrix

$\mathbf{Q}[n]$ of the transformation is [7, 83],

$$\mathbf{Q}[n] = \mathbf{A}\mathbf{X}[n]\mathbf{B}, \tag{5.3}$$

where $\mathbf{A}$ and $\mathbf{B}$ are $M \times M$ and $N \times N$ transform matrices, respectively, and they are assumed to be unitary and together form the 2D transformation.

The element of $\mathbf{A}$ at the m-th row and i-th column is denoted by $a_{m,i}$, i.e., $[\mathbf{A}]_{m,i} = a_{m,i}$, and the element of $\mathbf{B}$ at the k-th row and l-th column is denoted by $b_{k,l}$, i.e., $[\mathbf{B}]_{k,l} = b_{k,l}$. Each pair of a row vector of $\mathbf{A}$ and a column vector of $\mathbf{B}$ acts as a simple beamformer, and its output $q_{m,l}$ is given by

$$q_{m,l}[n] = \sum_{i=0}^{M-1} \sum_{k=0}^{N-1} a_{m,i} b_{k,l} x_{i,k}[n] \, . \tag{5.4}$$

The beam response $R_{m,l}(\Omega, \theta, \phi)$ of this beamformer as a function of the normalised frequency Ω, azimuth angle θ and elevation angle ϕ is [84]

$$R_{m,l}(\Omega, \theta, \phi) = \sum_{i=0}^{M-1} \sum_{k=0}^{N-1} a_{m,i} b_{k,l} e^{-j\Omega \sin\theta (i\mu_x \cos\phi + k\mu_y \sin\phi)} \, , \tag{5.5}$$

where $\mu_x = \frac{d_x}{cT_s}$, $\mu_y = \frac{d_y}{cT_s}$ and $\Omega = \omega T_s$, with c being the wave propagation speed, T_s the sampling period, d_x and d_y the array spacings along the x-axis and y-axis, and ω the angular frequency of signals.

With $\Omega_1 = \mu_x \Omega \sin\theta \cos\phi$ and $\Omega_2 = \mu_y \Omega \sin\theta \sin\phi$,

$$A_{m,l}(\Omega_1, \Omega_2) = \sum_{i=0}^{M-1} \sum_{k=0}^{N-1} a_{m,i} b_{k,l} e^{-ji\Omega_1 - jk\Omega_2} \, , \tag{5.6}$$

where $A_{m,l}(\Omega_1, \Omega_2)$ is the frequency response of the pair of the m-th row vector of the transformation matrix $\mathbf{A}$ and the l-th column vector of the

transformation **B**, considering each row vector and column vector pair as defining the impulse response of a separable 2D FIR filter.

Equation (5.6) can be rearranged as

$$\sum_{i=0}^{M-1} a_{m,i} e^{-ji\Omega_1} \sum_{k=0}^{N-1} b_{k,l} e^{-jk\Omega_2} = A_m(\Omega_1) A_l(\Omega_2) \,, \tag{5.7}$$

where $A_m(\Omega_1)$ is the frequency response of the m-th row vector of the transformation matrix **A** and $A_l(\Omega_2)$ is the frequency response of the l-th column vector of the transformation matrix **B**. By substituting $\Omega_1 = \mu_x \Omega \sin\theta \cos\phi$ and $\Omega_2 = \mu_y \Omega \sin\theta \sin\phi$ in (5.7) and considering (5.5),

$$R_{m,l}(\Omega, \theta, \phi) = A_m(\mu_x \Omega \sin\theta \cos\phi) A_l(\mu_y \Omega \sin\theta \sin\phi) \,. \tag{5.8}$$

So, the beam pattern of the (m,l)-th 2D transformation is the frequency response of the m-th row vector of **A** multiplied by frequency response of the l-th column vector of **B**.

By assuming that the sampling frequency is twice the highest frequency component of the wideband signal and the array spacings (d_x, d_y) are half the wavelength of the highest frequency component, hence $\mu_x = \mu_y = 1$ [2]. The frequency responses $A_{m,l}(\Omega_1, \Omega_2), m = 0, \cdots, M-1, l = 0, \cdots, N-1$, are arranged to be band-pass, each with a bandwidth of $2\pi/M$ for Ω_1 and $2\pi/N$ for Ω_2 in the normalised 2D frequency domain. The row vectors of **A** and column vectors of **B** all together cover the whole 2D frequency band, which is $\Omega_1, \Omega_2 \in [-\pi : \pi]$. An ideal example of the 2D band-pass filter responses in the 2D frequency domain is shown in Fig. 5.3.

The 2D band-pass filters have a high-pass filtering effect on the received

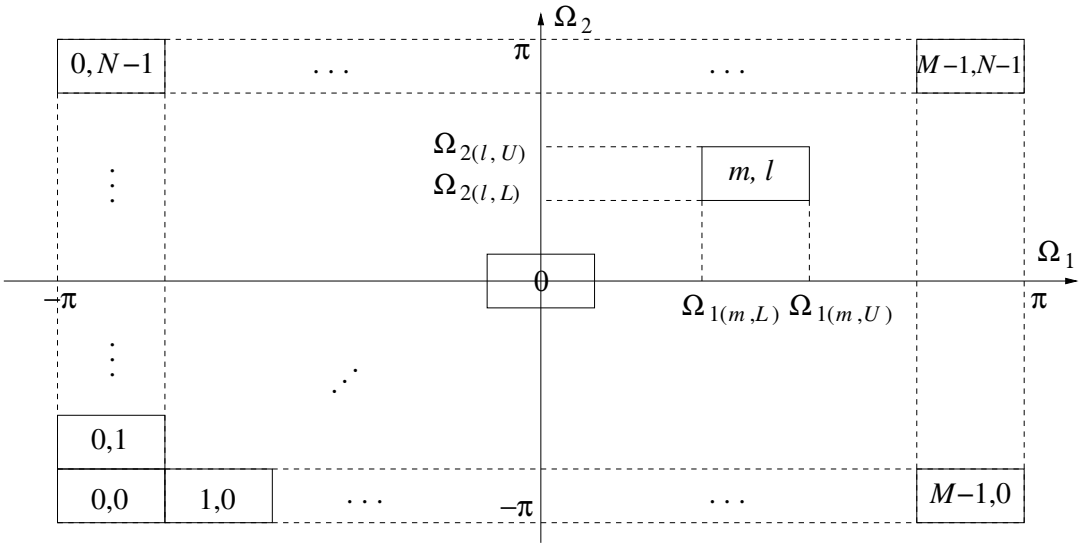

Fig. 5.3: Frequency responses of the 2D transformation applied to an $M \times N$ URA.

array signals. Taking the pair of the m-th row vector of $\mathbf{A}$ and the l-th column vector of $\mathbf{B}$ as an example, its frequency repsonse is

$$\left|A_{m,l}(\Omega_1,\Omega_2)\right| = \begin{cases} 1, & \text{for } \Omega_1 \in [\Omega_{1(m,L)};\Omega_{1(m,U)}] \\ & \;\&\; \Omega_2 \in [\Omega_{2(l,L)};\Omega_{2(l,U)}] \\ 0, & \text{otherwise.} \end{cases} \tag{5.9}$$

Considering the above frequency response, the received array signal components with frequency of $\Omega \in [-\Omega_{1(m,L)} : \Omega_{1(m,L)}] \& [-\Omega_{2(l,L)} : \Omega_{2(l,L)}]$ will not pass through this row vector, since $\Omega_1 = \Omega \sin\theta \cos\phi$ and $\Omega_2 = \Omega \sin\theta \sin\phi$ does not fall into the passband of $[\Omega_{1(m,L)} : \Omega_{1(m,U)}]$ and $[\Omega_{2(l,L)} : \Omega_{2(l,U)}]$, no matter what value the DOA angles (θ, ϕ) take. Therefore, the frequency range of the output is $|\Omega| \geq \min(\Omega_{1(m,L)}, \Omega_{2(l,L)})$ and the lower bound is determined by $\min(\Omega_{1(m,L)}, \Omega_{2(l,L)})$ when $\Omega_{1(m,L)}$ and $\Omega_{2(l,L)} \geq 0$. The negative values for Ω_1 and Ω_2 needs to be considered as well. Therefore, more generally, the frequency range of the output is $|\Omega| \geq$

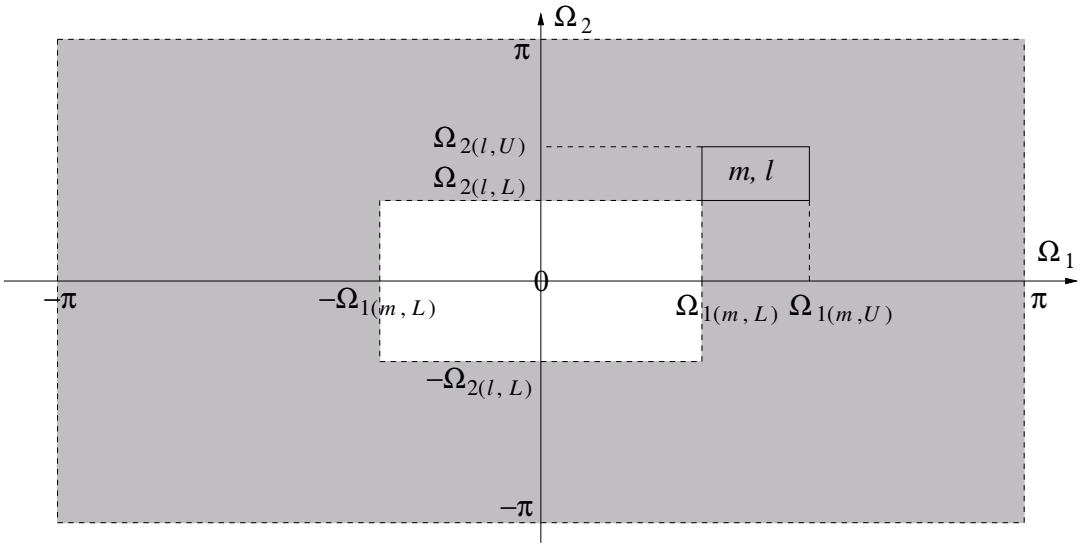

Fig. 5.4: The high-pass filtering effect of the (m,l)-th 2D filter in the ideal case.

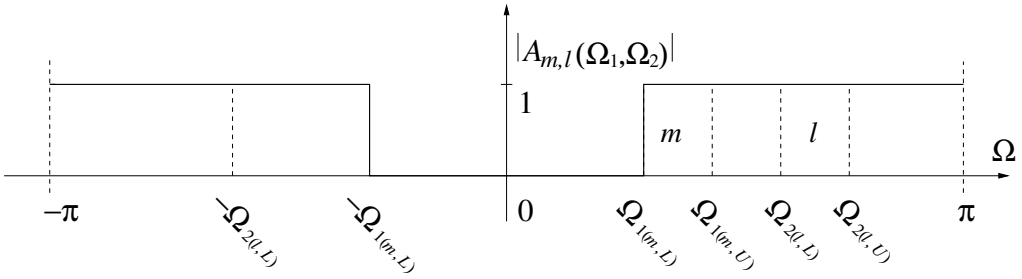

Fig. 5.5: The high-pass filtering effect of the (m,l)-th 2D filter in the signal frequency domain in the ideal case.

$\min(|\Omega_{1(m,L)}|, |\Omega_{1(m,U)}|, |\Omega_{2(l,L)}|, |\Omega_{2(l,U)}|)$, with lower bound determined by $\min(|\Omega_{1(m,L)}|, |\Omega_{1(m,U)}|, |\Omega_{2(l,L)}|, |\Omega_{2(l,U)}|)$.

Therefore, the output spectrum of the directional signal part of $q_{m,l}[n]$ from (3.6) corresponding to the m-th row vector of $\mathbf{A}$ and the l-th column vector of $\mathbf{B}$ is high-pass filtered as demonstrated in Fig. 5.4 in the 2D frequency domain, and its effect on the signal frequency domain is shown in Fig. 5.5. Since the noise part at the array sensors is spatially white, the output noise spectrum of each pair of transformation vectors is still a con-

stant, covering the whole spectrum. Assuming the row vectors of $\mathbf{A}$ and the column vectors of $\mathbf{B}$ are normalised to unity norm, there would be no change to the total noise power after the transformation.

Each $q_{m,l}[n], m = 0, \cdots, M-1, l = 0, \cdots, N-1$, is the input to the corresponding high-pass filter $h_{m,l}[n], m = 0, \cdots, M-1, l = 0, \cdots, N-1$, and that filter should cover the whole bandwidth of the signal part, i.e., having the same high-pass frequency response as shown in Fig. 5.5. Therefore, ideally the high-pass filters will not have any effect on the signal part and the signal part should pass through the high-pass filters without any distortion. But the frequency components of the white noise which fall into the stopband of the high-pass filters will in fact be removed. The output of these high-pass filters is given by

$$\mathbf{Z}[n] = \begin{bmatrix} z_{0,0}[n] & \cdots & z_{0,N-1}[n] \\ \vdots & \ddots & \vdots \\ z_{M-1,0}[n] & \cdots & z_{M-1,N-1}[n] \end{bmatrix}, \tag{5.10}$$

where $z_{m,l}[n] = q_{m,l}[n] \circ h_{m,l}[n], m = 0, \cdots, M-1, l = 0, \cdots, N-1$.

By applying the 2D inverse transformation to $\mathbf{Z}[n]$, the estimates of the original input sensor signals $\hat{x}_{m,l}[n], m = 0, \cdots, M-1, l = 0, \cdots, N-1$ will be obtained. Therefore, in matrix form,

$$\hat{\mathbf{X}}[n] = \mathbf{A}^{-1}\mathbf{Z}[n]\mathbf{B}^{-1}, \tag{5.11}$$

where $\mathbf{A}^{-1}$ and $\mathbf{B}^{-1}$ are the inverse of the corresponding transformation matrices. The original directional array signal will be recovered without

distortion in the ideal case, while the noise power will be reduced, leading to an improved TSNR.

Considering the stopband of each high-pass filter, the total effect of the high-pass filters on the total noise power can be calculated. By using numeric methods, it has been calculated that when $M, N \to \infty$, the power of noise will be reduced by 1.76 dB. Therefore, up to a maximum of 1.76 dB improvement in TSNR can be achieved. However, in practice, the TSNR improvement will be less than that, due to the limited number of sensors in the URA. This TSNR improvement is less than the 3 dB improvement which was achieved for ULAs using a 1D unitary transformation as in Chapter 3. In the next section, as an alternative approach, the noise reduction method for ULAs is adapted to be applicable to URAs, in order to achieve a higher output TSNR.

5.2 White Noise Reduction for URAs with a 1D Transformation

In this approach, the method developed for ULAs in Chapter 3 is adapted for the URA structure. Each column of the sensors of a URA is actually a ULA. Therefore, each column of the sensors is taken separately as a ULA and the previously developed noise reduction method is applied for the ULAs to each column. As a result, along each column of sensors a 3 dB improvement in the SNR of that column is achieved. Considering the

whole URA structure, the TSNR is improved by 3 dB. In the following, this approach is explained in more details.

Assume the l-th column of sensors along the x-axis, is considered for processing. $\mathbf{x}_l[n]=[x_{0,l}[n],\ x_{1,l}[n],\ \cdots,\ x_{M-1,l}[n]]^T$ is the signal vector according to this column. $\mathbf{x}_l[n]$ is transformed with a 1D transformation matrix such as $\mathbf{A}$, with size $M \times M$. After transforming $\mathbf{x}_l[n]$, the output signal vector $\mathbf{q}_l[n]$ is obtained as

$$\mathbf{q}_l[n] = \mathbf{A}\mathbf{x}_l[n], \tag{5.12}$$

where $\mathbf{q}_l[n] = [q_{0,l}[n], \cdots, q_{M-1,l}[n]]^T$.

The high-pass filtering effect of the transformation for ULAs has been shown in Chapter 3. Because of the high-pass filtering effect of the transformation on the directional signal, the output spectrum of the directional signal part of $q_{m,l}[n]$ corresponding to the m-th row vector of $\mathbf{A}$ is high-pass filtered. As the noise part of the array sensors is spatially white, the output noise spectrum of the row vector is still a constant, covering the whole spectrum. Since $\mathbf{A}$ is assumed to be unitary and the row vectors of $\mathbf{A}$ are normalised to unity norm, therefore, there would be no change to the total noise power after transformation.

Similar to the explanation for (5.10), each $q_{m,l}[n], m = 0, \cdots, M-1$, is the input to the corresponding high-pass filter $h_{m,l}[n], m = 0, \cdots, M-1$, and the high-pass filter should cover the whole bandwidth of the signal part, i.e., having the same high-pass frequency response. Therefore, ide-

ally the high-pass filters will not have any effect on the signal part and the signal part should pass through the high-pass filters without any distortion. However, frequency components of the white noise which fall into the stopband of the high-pass filters will be removed. The output of these high-pass filters is given by

$$\mathbf{z}_l[n] = \begin{bmatrix} z_{0,l}[n] \\ z_{1,l}[n] \\ \vdots \\ z_{M-1,l}[n] \end{bmatrix} = \begin{bmatrix} q_{0,l}[n] \circ h_{0,l}[n] \\ q_{1,l}[n] \circ h_{1,l}[n] \\ \vdots \\ q_{M-1,l}[n] \circ h_{M-1,l}[n] \end{bmatrix}. \tag{5.13}$$

By applying the inverse of the transformation matrix ($\mathbf{A}^{-1}$) to $\mathbf{z}_l[n]$, the estimates of the original input sensor signals $\hat{x}_{m,l}[n]$, $m = 0, \cdots, M-1$ is obtained. Therefore, in vector form,

$$\hat{\mathbf{x}}_l[n] = \mathbf{A}^{-1}\mathbf{z}_l[n], \tag{5.14}$$

where $\hat{\mathbf{x}}_l[n] = [\hat{x}_{0,l}[n], \hat{x}_{1,l}[n], \cdots, \hat{x}_{M-1,l}[n]]^T$. After going through these processing stages, ideally, there is no change in the signal part in the final output $\hat{x}_{m,l}[n]$, $m = 0, \cdots, M-1$, compared to the original signal part in $x_{m,l}[n]$, $m = 0, \cdots, M-1$. However, since $\mathbf{A}^{-1}$ is also unitary, the total noise power stays the same between $\hat{\mathbf{x}}_l[n]$ and $\mathbf{z}_l[n]$. Following the same analysis for the ULA case as discussed in Chapter 3, the same conclusion can be drawn that up to 3 dB TSNR improvement can be obtained by the proposed method. However, in practice, the SNR improvement will be less than 3 dB due to the limited number of sensors. The same process needs to

be applied to all the columns of sensors of the URA across the x-axis, and for each column of sensors a 3 dB improvement in TSNR will be achieved.

However, one important point is that, although the TSNR improvement is 3 dB and much higher than the case of the 2D transformation developed in the last section, the side-lobe attenuation of the 1D case will be much less than the 2D case. Because as shown in (5.8), the beam-pattern of the 2D transformation is the multiplication of the beam-patterns of its corresponding row/column vectors. A direct consequence will be more distortion to the signal part using the 1D transformation when discarding the noise components using the high-pass filters. As a result, the performance improvement may be less than the method directly based on the 2D transformation. This will be demonstrated in simulation section.

5.3 White Noise Reduction for UCAs

In this section, the method is extended to uniform circular arrays (UCAs) which is another type of planar arrays. Therefore, the transformation is re-designed to adjust the noise reduction method to the structure of UCAs.

The method introduced in this section is based on a 1D transformation and is an adaptation of the method introduced in Chapter 3. Same as before, the transformation should be invertible and ideally, unitary. The circular arrays have a sparse structure naturally. Therefore, designing an ideal unitary transformation is not always possible. First, the transforma-

tion matrix is designed with the required bandwidth characteristics for the UCA structure. Then, same as section 4.4, the singular values of the transformation which are lower than a threshold are replaced with a higher value to improve the condition number of the transformation.

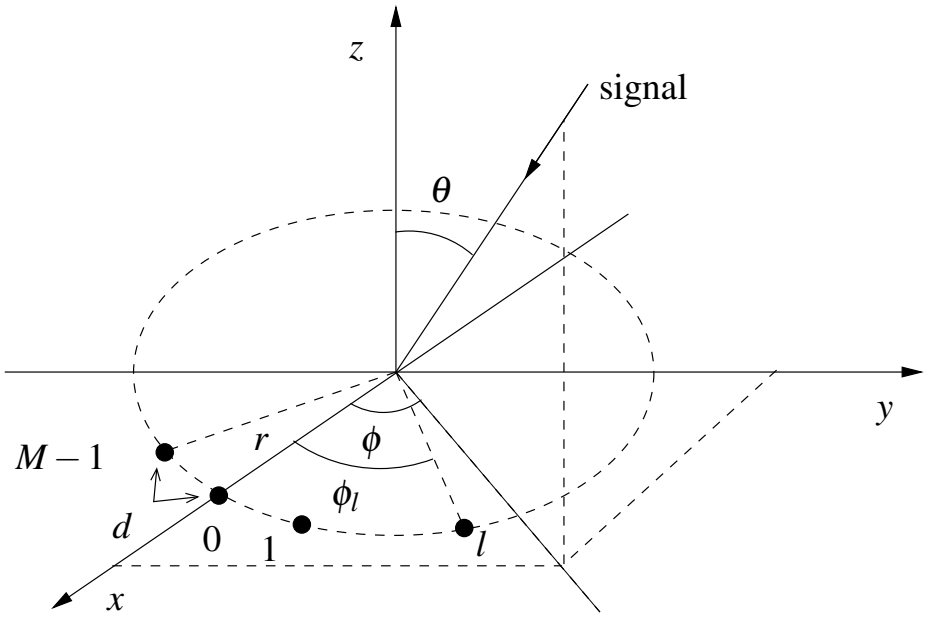

Fig. 5.6: The general structure for UCA.

The structure of a UCA is shown in Fig. 5.6. The general structure of the method for UCA is same as the structure for ULA, and is shown in Fig. 3.1. Suppose there are M sensors along the perimeter of the UCA, with a circumferential spacing of d, the radius r of the UCA is:

$$r = \frac{Md}{2\pi} . \tag{5.15}$$

The position of the l-th sensor is $(r\cos\phi_l, r\sin\phi_l, 0)$, $l = 0, 1, \cdots, M-1$, where $\phi_l = l2\pi/M$ is the angle between the x-axis and the m-th sensor. The

spacing d is $\alpha/2$ times the wavelength of the highest frequency component of the signal λ_{min}, and therefore, $d = \alpha\lambda_{min}/2$, where α is a scalar value. So, r is [85, 86]:

$$r = \alpha\frac{\lambda_{min}}{2}\frac{M}{2\pi} . \tag{5.16}$$

Considering $\beta = M/2\pi$,

$$r = \alpha\beta\frac{\lambda_{min}}{2} . \tag{5.17}$$

The phase difference between the centre of the UCA and the l-th sensor is:

$$\Phi = \omega\frac{r\sin\theta\cos(\phi-\phi_l)}{c} , \tag{5.18}$$

where ω is the angular frequency of the signal and c is the wave propagation speed. By plugging (5.16) into (5.18),

$$\Phi = \frac{\omega\lambda_{min}}{2c}\alpha\beta\sin\theta\cos(\phi-\phi_l) . \tag{5.19}$$

$\Omega = \omega T_s$ by considering the sampling frequency of $T_s = \lambda_{min}/2c$. Therefore, the l-th element of $\mathbf{d}(\Omega,\theta,\phi)$ which is the steering vector of the UCA is [79, 87]:

$$d_l = e^{j\alpha\beta\Omega\sin\theta\cos(\phi-\phi_l)} . \tag{5.20}$$

The transformation can be designed for the UCA using the steering vector. The row vectors of the transformation matrix are each a band-pass filter and together they cover the entire normalised frequency range of the signal. Same as before, first a low-pass filter with the required characteristics is designed as the prototype filter. Then, the prototype filter is modulated to each subband of the transformation. Considering $\mathbf{p}$ is the prototype

filter with length M, $\mathbf{p}$ can be modulated to cover the entire normalised frequency band, using

$$a_{m,l} = e^{-j\alpha\beta\frac{2\pi}{M}m\cos(\phi-\phi_l)}p_l \ , \tag{5.21}$$

where $m = 0,\cdots,M-1$, $l = 0,\cdots,M-1$. Note that, for different elevation angles ϕ, the transformation changes, and the design gives different results. Therefore, the elevation angle ϕ of the desired signal should be known to design the transformation. For the signals not coming from ϕ used for the design, the frequency response of the transformation is different, so in here, it is assumed that the impinging signals are coming from the same ϕ. If the elevation angle ϕ of the desired signal changes, the transformation should be re-designed, or alternatively, pre-steering can be used to adjust the impinging signal to the transformation.

In this work, it is assumed that $\phi = \pi/2$. Therefore, (5.21) can be written as:

$$a_{m,l} = e^{-j\alpha\beta\frac{2\pi}{M}m\cos(\frac{\pi}{2}-\phi_l)}p_l \ . \tag{5.22}$$

The beam response $R_m(\Omega,\theta)$ of a row vector of the transformation is:

$$R_m(\Omega,\theta) = \sum_{l=0}^{M-1} a_{m,l}e^{j\alpha\beta\Omega\sin\theta\cos(\frac{\pi}{2}-\phi_l)} \ . \tag{5.23}$$

With $\hat{\Omega} = \Omega\sin\theta$, $R_m(\Omega,\theta)$ can be represented in the following form:

$$A_m(\hat{\Omega}) = \sum_{l=0}^{M-1} a_{m,l}e^{j\alpha\beta\hat{\Omega}\cos(\frac{\pi}{2}-\phi_l)}, \tag{5.24}$$

where $A_m(\hat{\Omega})$ is the frequency response of the m-th row vector of the transformation.

The frequency responses are designed to be band-pass, each with a bandwidth of $2\pi/M$, and altogether they cover the entire normalised frequency band. The band-pass filters have high-pass filtering effect on the received signals with $\phi = \pi/2$, and different values for θ. The examination of the high-pass behaviour is same as the examination provided for the ULA case in Sec. 3.1.

The transformation should be invertible and ideally unitary. The circular arrays are sparse in general [88]. Therefore, if the transformation matrix is ill-conditioned, the approach introduced in Sec. 4.4 can be used to reduce the condition number of the transformation, without causing a significant change in the beam pattern of the transformation.

After designing a well-conditioned transformation with the required frequency responses, the high-pass filters are applied and then the signal is transformed back, similar to the block diagram illustrated in Fig. 3.1.

5.4 Simulation Results

In this section, simulation results will be provided and compared to verify the effectiveness of the proposed noise reduction pre-processing methods for the URA and UCA structures.

5.4.1 Simulation for the URA structure

For simplicity, the same number of sensors is used across the x-axis and y-axis ($M = N$), with the same array spacings ($d_x = d_y$). The URA has 16 sensors along each axis ($M = 16$) and the desired signal arrives from the broadside ($\theta_d, \phi_d = 0$). The transformation matrix $\mathbf{A} = \mathbf{B}$ is a 16×16 DFT matrix, as an example of unitary transformation. For the high-pass filters, linear phase 101-tap FIR filters with a common delay of 50 samples are employed. Then, the array signals are transformed back by the inverse of the transformation matrix ($\mathbf{A}^{-1}$).

As mentioned before, by using the 2D transformation method, up to 1.76 dB and by using the 1D transformation method, up to 3 dB TSNR improvement can be achieved. Despite lower TSNR improvement, the 2D transformation method has less distortion on the directional signal, because the 2D transformation vectors have a higher side-lobe attenuation, due to the dual filtering process along both axes. Frequency responses of an example 2D-DFT vector in the frequency domain and its corresponding 1D-DFT vector, for the directional signal arriving from $\theta = 90^\circ$ and $\phi = 45^\circ$ are shown in Fig. 5.7. It can be clearly seen that the side-lobe attenuation for the 2D-DFT is around 26 dB, whereas the side-lobe attenuation for the 1D-DFT is around 13 dB. This results to less amount of directional signals available in the lower side-lobes of the 2D-DFT, to be removed by the high-pass filters compared to the 1D-DFT. Therefore, a better recovery for

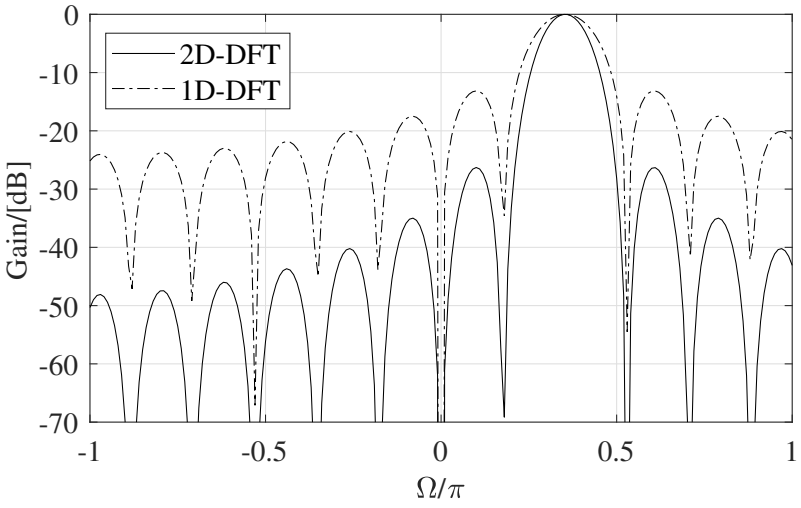

Fig. 5.7: Frequency responses of an example 2D-DFT vector and its corresponding 1D-DFT vector, for the directional signal arriving from $\theta = 90^\circ$ and $\phi = 45^\circ$.

the directional signals after the inverse transformation is achieved.

In order to compare the performance of the two methods in recovering the directional signal, wideband signals with unit power from random directions are applied to the URA, and then processed by the noise reduction methods. The MSE between the original signal and the recovered one by both methods is calculated for different URA sizes (M) with 10,000 Monte Carlo runs [89], and the results are presented in Table 5.1. It is clear that the effect on the directional signal for the method using the 2D-DFT is much smaller compared to the method using the 1D-DFT, and hence better recovery.

Here, the effect of the two proposed methods on the performance of both the RSB beamformer and the LCMV beamformer is examined. When the directional signal is arriving from the broadside, there is no delay be-

M	2D-DFT	1D-DFT
10	8.25×10^{-4}	2.04×10^{-2}
16	6.63×10^{-4}	1.85×10^{-2}
20	5.66×10^{-4}	1.75×10^{-2}
30	3.79×10^{-4}	1.43×10^{-2}
40	2.80×10^{-4}	1.20×10^{-2}

Table 5.1: MSE for the directional signal before and after the proposed noise reduction process for different URA sizes.

tween the received array signals. Therefore, most of the signal power appears in the output of the transformation covering the zero frequency, which is not affected by the corresponding high-pass filter. This leads to an almost distortionless output for both methods. In the following simulation, the desired signal is first assumed to be arriving from the broadside. Otherwise, pre-steering can be used to change the look direction. When the desired signal is arriving from a direction other than broadside, both methods will have a small distortion on the desired signal. The method with a 1D-DFT has a higher SNR improvement, and so for low input SNR values, it is expected that the beamformer will have a higher SINR performance compared to the method with a 2D-DFT. On the other hand, when the input SNR is high enough, the 2D-DFT method should have a higher SINR performance, as it has less distortion on the desired signal. For very high SNR values, as the effect of noise is almost negligible, higher beamforming performance is expected by not applying any noise reduction.

First, it is assumed that a desired band-limited signal with bandwidth of $[0.3\pi, \pi]$ is received by the URA from the broadside. Seven interfering signals are applied to the system, each with a -10 dB input SIR and their DOAs are $\theta_i = 10^\circ$, 20°, 30°, 40°, 50°, 60° and 70°, respectively, all with $\phi = 45^\circ$. A TDL with length of $J = 30$ is used for the beamformers.

The results are shown in Fig. 5.8. A higher output SINR is achieved by both proposed noise reduction methods for both beamformers for all the input SNR range and generally the improvement becomes larger when the input SNR increases. As the SNR improvement of the noise reduction method with a 1D-DFT is higher than the SNR improvement of the method with a 2D-DFT, a higher SINR improvement is achieved for both beamformers using the method with a 1D-DFT.

At last, an example is given to show the effect caused by the different distortions using the two different noise reduction methods. The SINR performance of the RSB beamformer is shown in Fig. 5.9, with the desired signal arriving from $\theta_d = 5^\circ$ and $\phi_d = 0^\circ$, and other conditions are the same. As it is shown in Table 5.1, when the direction of desired signal is not form the broadside, it is affected by some degree of distortion. For low SNR values, the performance is higher using a 1D-DFT noise reduction method, since it has a higher SNR improvement compared to the 2D-DFT noise reduction method. Although the 2D-DFT noise reduction method has a lower SNR improvement, but it causes less distortion to the desired signal. Therefore, for the input SNR values higher than 12 dB, the

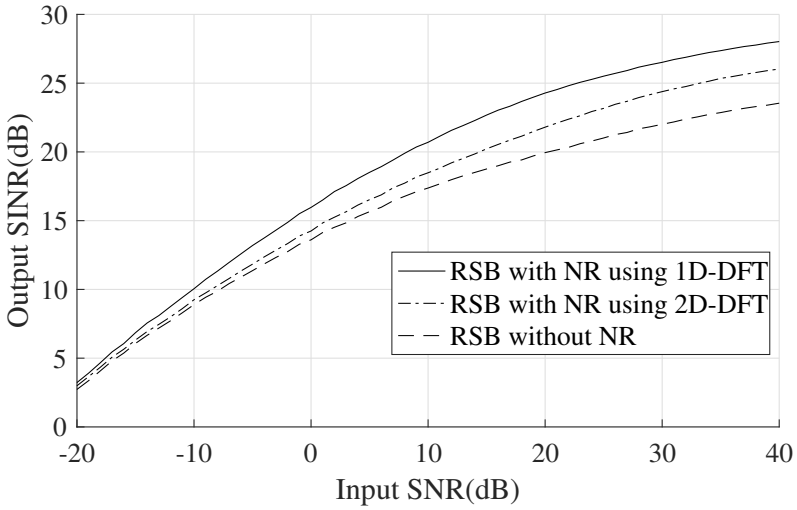

(a) RSB beamformer.

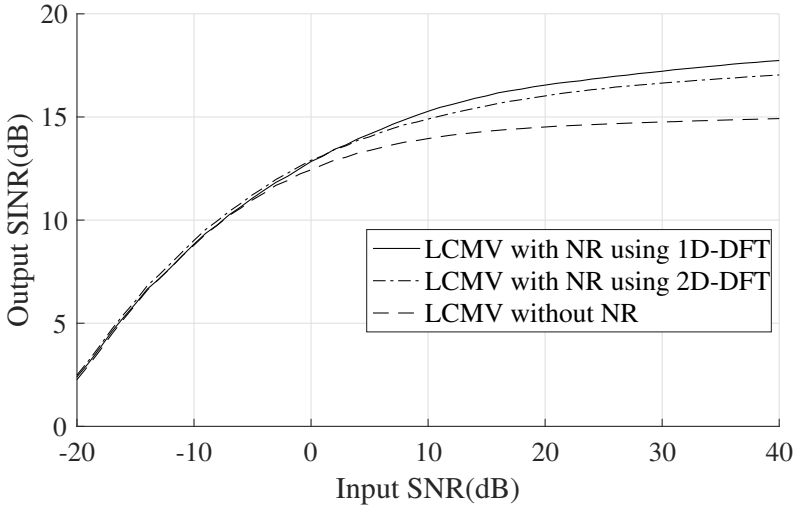

(b) LCMV beamformer.

Fig. 5.8: SINR performance of both beamformers with and without the proposed noise reduction (NR) methods for the URA.

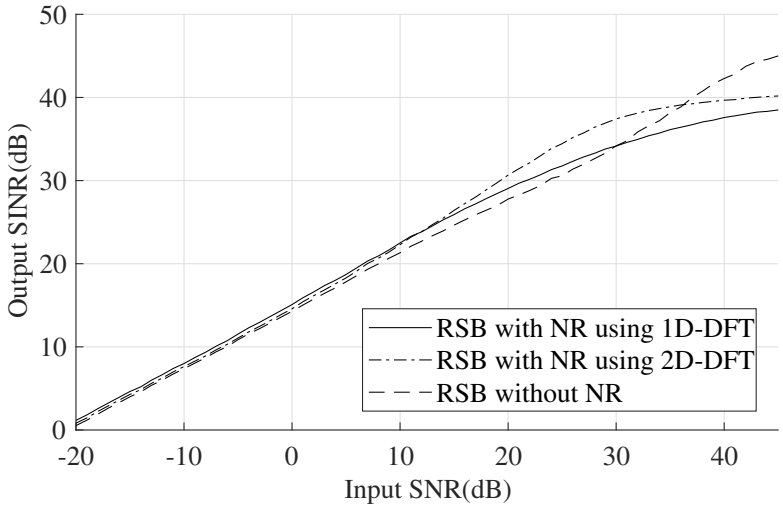

Fig. 5.9: SINR performance of the RSB beamformer with the desired signal arriving from $\theta_d = 5^\circ$ and $\phi_d = 0^\circ$.

less distortion to the desired signal becomes the dominant factor, and the beamformer using the 2D-DFT noise reduction achieves a higher output SINR performance.

For very high SNR values the effect of noise is almost negligible, while the distortion to the desired signal caused by the noise reduction methods becomes the dominant factor. Therefore, when the input SNR value is higher than 30 dB, the beamformer with 1D-DFT noise reduction has a lower performance compared to the beamformer without the noise reduction. Also, for the input SNR values higher than 36 dB, both beamformers employing the noise reduction have a lower performance compared to the beamformer without the noise reduction.

5.4.2 Simulation for the UCA structure

For simulation, a UCA with $M = 30$ sensors is considered, and for designing the transformation, it is assumed that $\phi = \pi/2 = 90^\circ$. Then, the method explained in Sec. 4.4 is employed to reduce the condition number. The threshold is set to 1, i.e., the singular values $\sigma_i = 1, \cdots, M-1$ smaller than 1 are replaced with 1. After replacing the small singular values, the condition number is reduced to 2.25. Now the effect of reducing the condition number, on the beam-pattern of the transformation matrix is analysed. The average 3 dB beamwidth before and after the condition number modification is 0.15 in normalised frequency, and it is not affected. The average side-lobe attenuation before the modification is 7.90 dB, and it is 8.02 dB after the modification. Therefore, the beam-pattern of the transformation matrix has not changed considerably. Fig. 5.10 illustrates the beam-pattern of the transformation before and after modifying the condition number. It is clear that there is almost no considerable change in the beam-pattern.

Now, the effect of the noise reduction method with the modified transformation on the performance of the RSB and LCMV beamformers is analysed. A desired band-limited wideband signal with a bandwidth of $[0.3\pi : \pi]$ is received by the UCA from the broadside ($\theta_d = 0^\circ, \phi_d = 90^\circ$). Seven interfering signals are received by the array each with a -10 dB input SIR and DOAs of $\theta_i = 10^\circ, 20^\circ, 30^\circ, 40^\circ, 50^\circ, 60^\circ$ and 70°, respectively, all with $\phi_i = 90^\circ$. For the high-pass filters, linear phase 101-tap FIR filters

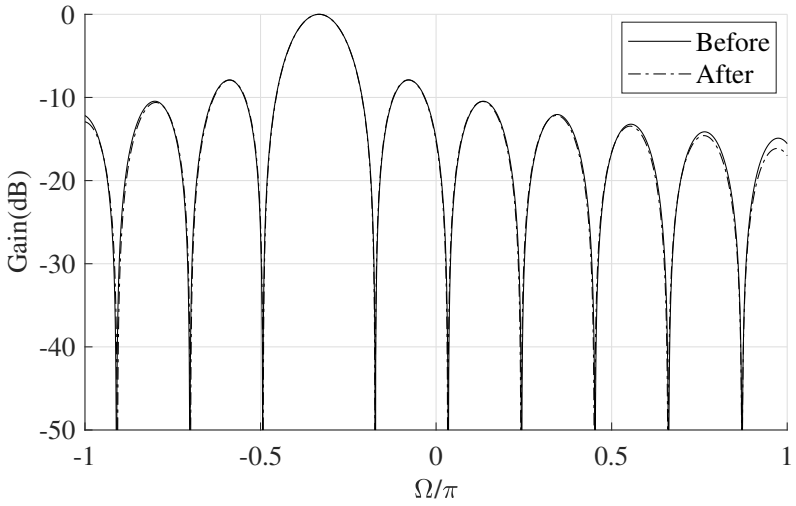

Fig. 5.10: The beam-pattern of a sample row vector of the transformation designed for UCA, before and after modifying the condition number, $M = 30$, $\phi = 90°$.

with a common delay of 50 samples are employed. A TDL of length $J = 5$ is used for these beamformers.

The results are shown in Fig. 5.11. A higher output SINR is achieved by the proposed noise reduction method for both beamformers for the input SNR range. The improvement becomes larger when the input SNR increases.

5.5 Summary

In this chapter, the idea for white noise reduction was extended to the planar arrays. As representative examples of the planar arrays, two types of planar arrays were considered which have been widely used for different applications, namely, URA and UCA.

Two methods for mitigating the effect of white noise without affecting

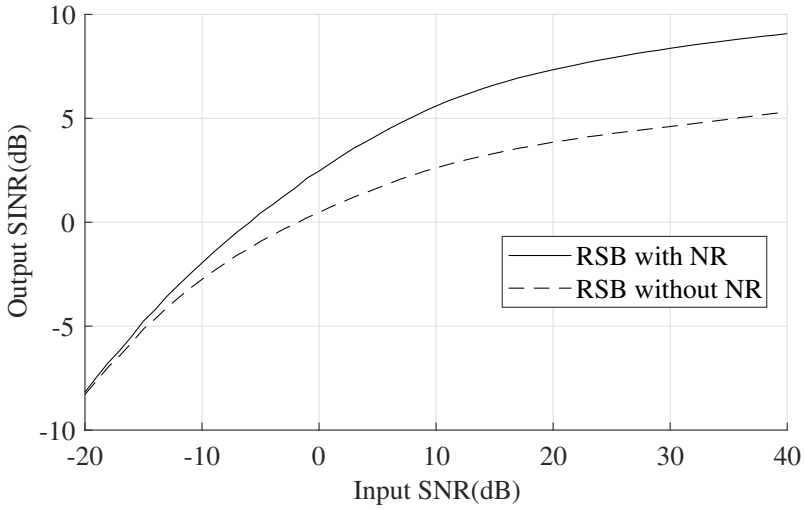

(a) RSB beamformer.

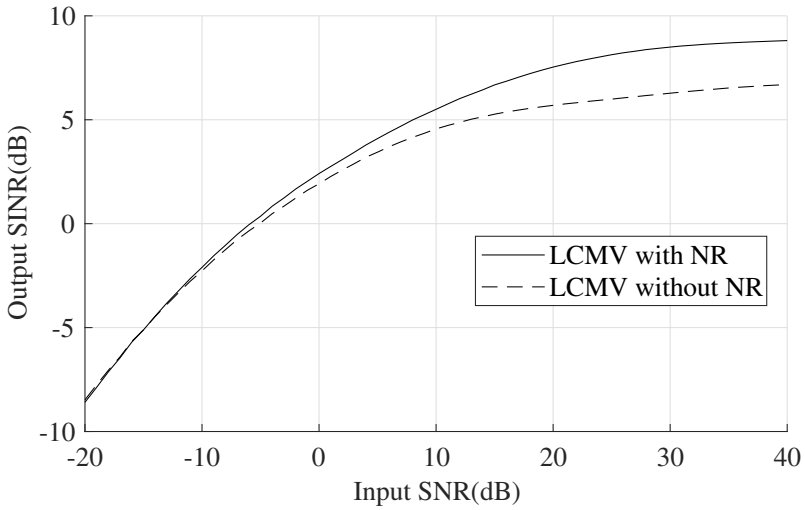

(b) LCMV beamformer.

Fig. 5.11: SINR performance of both beamformers with and without the modified noise reduction (NR) methods for the UCA, $M = 30$, $J = 5$.

the directional signal in wideband URAs have been introduced. With the proposed method using a 2D transformation, a maximum of 1.76 dB improvement in TSNR can be achieved in the ideal case, which is less than the 3 dB improvement previously achieved for ULAs. As an alternative, the noise reduction method using a 1D transformation for the URAs was proposed, which is a direct adaptation of the method used for ULAs, with a 3 dB improvement achieved. Despite lower improvement in TSNR, the 2D transformation method has less distortion for directional signals.

Later, a method based on 1D transformation was introduced for the UCAs, with a maximum of 3 dB improvement in TSNR. Due to the sparse nature of the UCA structure, the transformation is not unitary, and the condition number of the transformation is high. Therefore, same as Chapter 4, the transformation was modified by replacing the low value singular values of the transformation.

The increased TSNR can be translated into performance improvement in various planar array signal processing applications and as an example its effect on adaptive beamforming was studied. As demonstrated by simulation results, a clear improvement in performance in terms of output SINR has been achieved for a range of input SNR values.

Chapter 6

Further Insights into the Proposed Noise Reduction Method

As it can be seen from the proposed structure in Chapter. 3, no prior information is needed about the impinging signals to reduce the noise level and increase the overall SNR by about 3 dB. However, although the SNR has been improved, the noise is not white any more, as specified in (3.34), whose effect on the ultimate performance of the system can not be seen directly. That is why both theoretical analyses and computer simulation are provided to show that indeed by the proposed method, the performance of the two studied beamformers has been improved.

The result in the previous chapters is obtained from the viewpoint of reducing the noise level of the received signals. In this chapter, the benefits of the method is discussed from a broader point of view.

The contents of this chapter is published in [50].

6.1 The TDL Equivalent Structure

Actually by studying the structure further, it is realised that the proposed structure is equivalent to a traditional TDL system, but with a much larger TDL length. As a result, by applying the same LCMV beamformer (with the same TDL length) to both the original set of array signals and the new set of array signals after the proposed pre-processing, the latter one will be equivalent to a kind of LCMV beamformer but with much longer TDLs, and hence the improved performance. From this viewpoint, the proposed method can also be considered as a low-complexity approach to adaptive beamforming. Certainly another advantage is that the proposed pre-processing is standard and can be applied to the original array signals, whatever the following processing (either beamforming or DOA estimation, or tracking, etc.) is. As shown in the study for DOA estimation based on the proposed structure in [51], the improved SNR can be translated into improved DOA estimation performance too.

To show that the overall combination of the proposed noise reduction part and the following TDL-based beamformer is equivalent to a new beamformer with a much longer TDL, i.e., the noise reduction method alongside the TDL attached can be modelled as an equivalent TDL with a larger length, first the following is derived:

$$y[n] = \sum_{k=0}^{M-1} \sum_{n_0=0}^{l_{hp}+J-2} x_k[n-n_0] \sum_{p=0}^{M-1} a_{pk} \sum_{m=0}^{M-1} \tilde{a}_{mp} \sum_{j=0}^{J-1} w_{mj} h_p[n_0-j], \quad (6.1)$$

where l_{hp} is the length of the high-pass filters and $[\mathbf{A}^{-1}]_{mp} = \tilde{a}_{mp}$.

By arranging (6.1),

$$y[n] = \sum_{k=0}^{M-1} \sum_{n_0=0}^{l_{hp}+J-2} \sum_{p=0}^{M-1} \sum_{m=0}^{M-1} \sum_{j=0}^{J-1} a_{pk}\tilde{a}_{mp}w_{mj}h_p[n_0-j]x_k[n-n_0] \; . \qquad (6.2)$$

By assuming $\tilde{w}_{k,n_0} = \sum_{p=0}^{M-1}\sum_{m=0}^{M-1}\sum_{j=0}^{J-1} a_{pk}\tilde{a}_{mp}w_{mj}h_p[n_0-j]$, (6.1) becomes

$$y[n] = \sum_{k=0}^{M-1} \sum_{n_0=0}^{l_{hp}+J-2} \tilde{w}_{k,n_0}x_k[n-n_0], \qquad (6.3)$$

which is the equivalent TDL of a length $J_{eq} = l_{hp} + J - 1$ for the noise reduction method combined with a TDL of length J.

The question is, since the noise reduction method can be modelled as a TDL, which one of the following provides a higher performance: using the noise reduction method and a TDL with length J or using a larger TDL with length $J_{eq} = l_{hp} + J - 1$. It might be thought that the latter one will give a higher performance, although it may have the highest implementation complexity, since a globally optimum solution can be found without constraints imposed by the proposed specific noise reduction process. However, the real picture is much complicated, due to numerical issues involved in calculating the optimum beamforming coefficients based on inversion of correlation matrices of difference sizes [90, 91]. The longer the TDL, the larger the dimension of the matrix involved and the more likely it will cause additional errors in performing matrix inversion.

6.2 Computational Complexity of the Method

To further investigate the performance of the method the computational complexity of the white noise reduction method is considered. The computational complexity of the proposed noise reduction method (including the beamforming part), and the directly implemented RSB and LCMV beamformers is presented in Table 6.1, where N is the number of signal samples at each sensor. As $J \ll J_{eq}$, the complexity with the proposed method is much smaller than the direct implementation case.

Algorithm	without NR	with NR
RSB	$\mathcal{O}(M^3J_{eq}^3)+M^2J_{eq}^2N+M^2J_{eq}^2$ $+MJ_{eq}N$	$\mathcal{O}(M^3J^3)+M^2J^2N+M^2J^2$ $+MJN+2M^2N+Ml_{hp}^2+MNl_{hp}$
LCMV	$\mathcal{O}(M^3J_{eq}^3)+\mathcal{O}(J_{eq}^3)+2M^2J_{eq}^3$ $+2MJ_{eq}^3+M^2J_{eq}^2N+MJ_{eq}^2$	$\mathcal{O}(M^3J^3)+\mathcal{O}(J^3)+2M^2J^3+2MJ^3$ $+M^2J^2N+MJ^2+2M^2N+Ml_{hp}^2+MNl_{hp}$

Table 6.1: Computational complexity of the noise reduction based implementation, the RSB and LCMV beamformers.

6.3 Simulation Results

Same as Chapter. 3, the simulation results are based on a 16 sensor ($M = 16$) ULA, and the number of signal samples N in the time domain at each sensor is 20000. Again, the two types of TDL-based beamformers, i.e., the RSB and the LCMV beamformers are considered. The desired signal arrives from the broadside ($\theta_d = 0^\circ$). The received signals are processed

by the 16×16 DFT-based transformation matrix. Seven interfering signals are applied to the system, each with a -10 dB input SIR, and their DOAs are $\theta_i = 10^\circ, 20^\circ, 30^\circ, 40^\circ, 50^\circ, 60^\circ$ and 70°, respectively.

The SINR performance of RSB beamformer with noise reduction method and without the method with the equivalent length J_{eq} is shown in Fig. 6.1, and for LCMV beamformer is shown in Fig. 6.2. All the simulation conditions are the same as in Section 3.5. When the length of the beamformer is short (J=10 and equivalent of J_{eq}=110) as in Fig. 6.1a and Fig. 6.2a, the performance of the beamformers without pre-processing is higher, as expected in theory. When the length of the beamformers is larger (J=50 and equivalent of J_{eq}=150) as in Fig. 6.1b and Fig. 6.2b, the performance of the beamformers with pre-processing is higher.

The SINR performance of the beamformers with noise reduction method and without the method with the equivalent length J_{eq}, with respect to number of taps J is shown in Fig. 6.3. In this simulation, the interfering signals are same as before but the input SNR is 10 dB. It is clear that when the number of taps is low, the performance of the beamformer without the pre-processing noise reduction is higher than the method with pre-processing, but as the number of taps increases, the beamformer with pre-processing has a higher performance.

A direct advantage of the proposed noise reduction pre-processing is in reducing the computational complexity of the beamformers. The computation time for processing a snapshot of the received signal with length

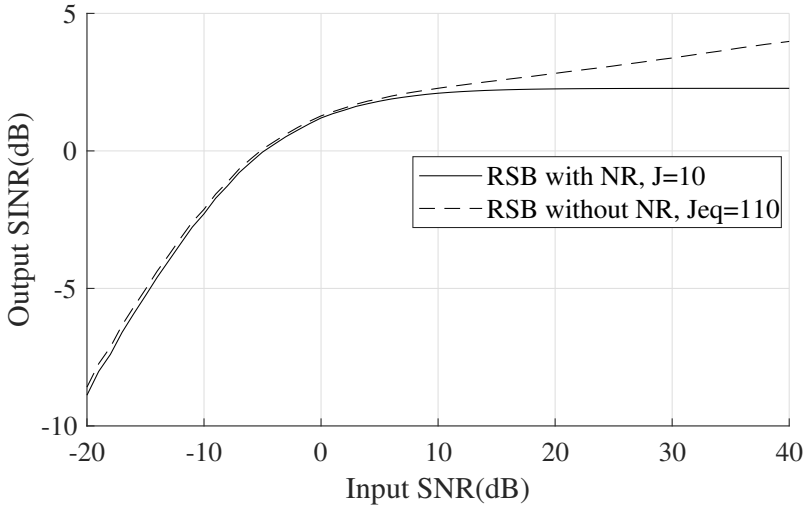

(a) $J = 10$ with NR, $J_{eq} = 110$ without NR.

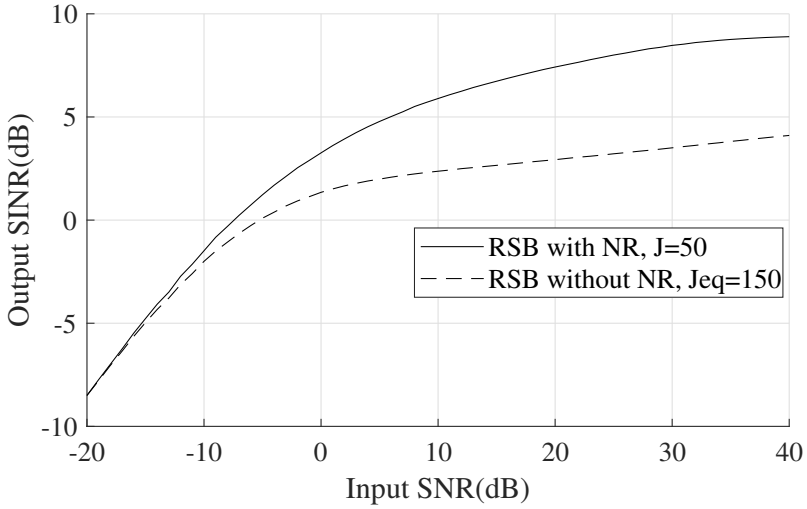

(b) $J = 50$ with NR, $J_{eq} = 150$ without NR.

Fig. 6.1: SINR performance of RSB beamformer with NR method and without NR with equivalent length, $l_{hp} = 101$.

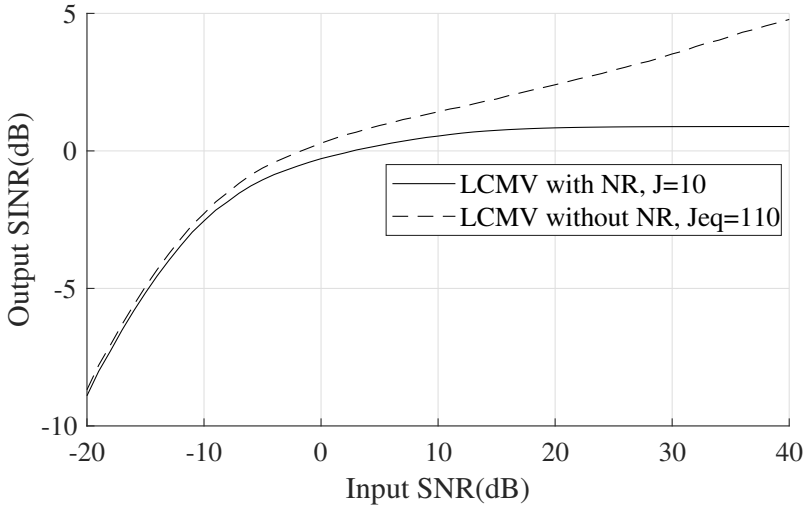

(a) $J = 10$ with NR, $J_{eq} = 110$ without NR.

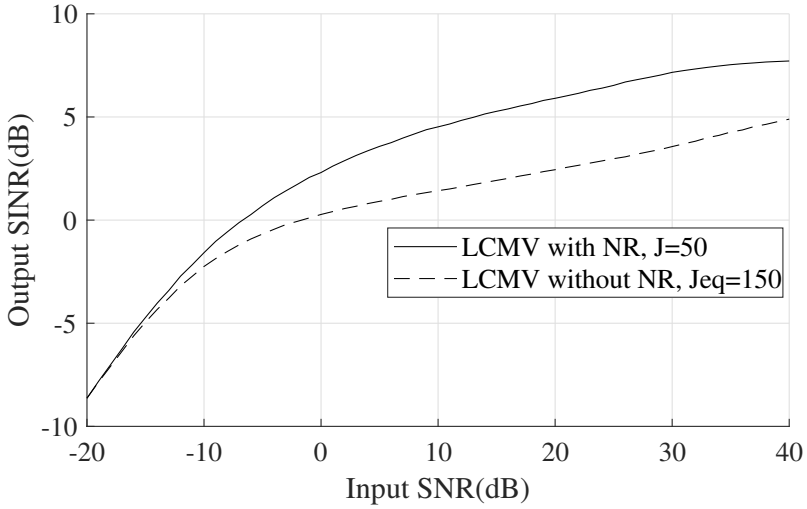

(b) $J = 50$ with NR, $J_{eq} = 150$ without NR.

Fig. 6.2: SINR performance of LCMV beamformer with NR method and without NR with equivalent length, $l_{hp} = 101$.

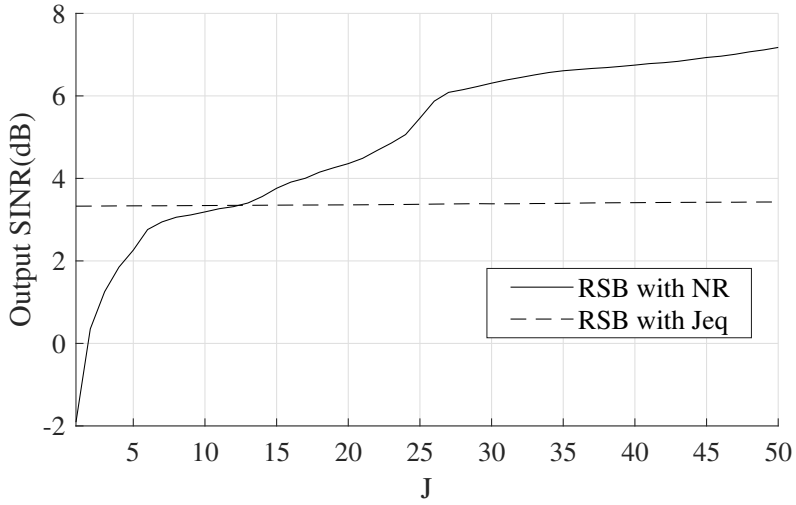

(a) RSB beamformer.

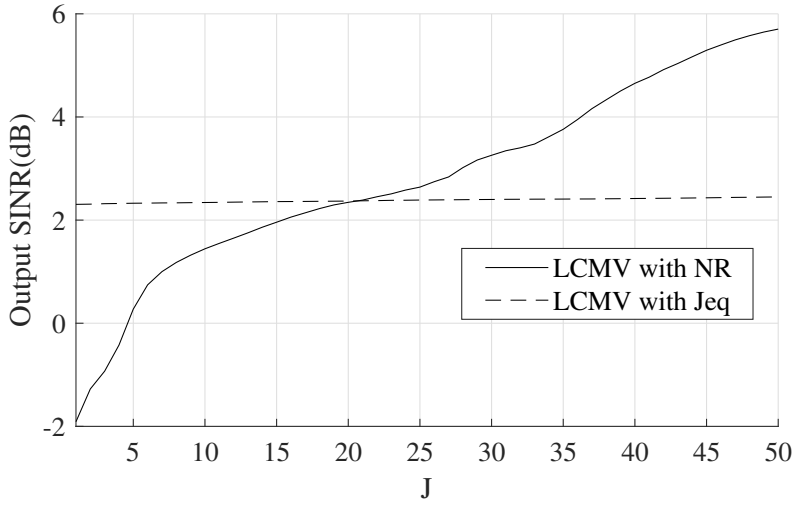

(b) LCMV beamformer.

Fig. 6.3: SINR performance of both beamformers with respect to number of taps, with NR method and without NR with equivalent length J_{eq}.

Algorithm	without NR $J_{eq} = 110$	with NR $J = 10$	without NR $J_{eq} = 150$	with NR $J = 50$
RSB	9.274s	3.635s	13.719s	5.527s
LCMV	9.104s	3.536s	13.874s	5.574s

Table 6.2: Computation time of the noise reduction based implementation, the RSB and LCMV beamformers.

$N = 20000$, calculated by the MATLAB R2017a under the environment of Intel CPU I5-2400 with a clock speed of 3.1 GHz and 4 GB RAM is presented in Table 6.2. As it can be seen in Table 6.1 and Table 6.2, since $J \ll J_{eq}$, the complexity of the noise reduction method including the beamforming part, is much smaller than the direct implementation of the beamformer. Also, using the noise reduction pre-processing the complications due to numerical issues involved in calculating the optimum beamforming coefficients based on inversion of correlation matrices can be avoided [90, 91]. Hence, a more robust beamforming is achieved with the noise reduction pre-processing.

6.4 Summary

In this chapter, the equivalent TDL structure of the noise reduction pre-processing method was analysed. By studying the structure of the method further, it was understood that if a classic beamformer such as RSB or LCMV is applied to a set of array signals which have been processed by

the noise reduction method, the pre-processing and the classic beamformer can be modelled as an equivalent beamformer with longer TDLs.

The weight vector of the equivalent TDL structure was derived, and the expressions for the computational complexity of the beamformers with and without the noise reduction method was presented.

The advantages of using the method as a pre-processing step for the beamformers compared to the direct usage of the classic adaptive beamformers with equivalent length J_{eq} from the viewpoint of computational complexity was discussed, and the performance of RSB and LCMV beamformers with noise reduction pre-processing method, and without the method with the equivalent length J_{eq} was compared by simulation results.

It was understood that the complexity of the noise reduction method including the beamformer part is less than the direct implementation with equivalent length J_{eq}. Also, with the noise reduction method, a more robust beamforming is achieved, since by using the noise reduction pre-processing the numerical issues due to calculating the optimum beamforming coefficients based on inversion of correlation matrices are avoided.

Chapter 7

Conclusions and Future Work

7.1 Conclusions

In this thesis, a method for mitigating the effect of white noise without affecting the directional signals in wideband arrays has been introduced. With the proposed method, a maximum 3 dB improvement in TSNR can be achieved in the ideal case. The increased TSNR can be translated into performance improvement in various array signal processing applications such as beamforming and DOA estimation.

The performance of the two well-known beamformers, namely, RSB and LCMV beamformers was briefly reviewed in Chapter 2. The proposed noise reduction method was introduced based on the ULA structure, and a detailed study of the proposed method was performed in Chapter 3. The analysis showed that the method does not have any effect on the spectra of the directional signal in the ideal case, but it will remove half of the noise power. Although in practice, the directional signal is distorted slightly

due to the presence of some signal components in lower side-lobes of the transformation. Also, due to the limitation of the size of the array, the improvement in TSNR is less than 3 dB.

The theoretical and simulated results for beamforming and DOA estimation showed that by using the noise reduction method as a pre-processing step, a higher output SINR performance for beamformers and a more accurate DOA estimation was achieved. Since the transformation for the ULA is unitary and the side-lobe attenuation of the DFT matrix which was used as the transformation is as high as 13 dB, the distortion to the directional signal caused by the method does not affect the performance considerably.

The method was re-designed to be applied to different array structures, namely, NLA, URA and UCA.

The least squares method was employed for the design of the transformation for the NLA to satisfy the required band-pass characteristics in Chapter 4. Since the NLA has a sparse array structure, designing a unitary or close to unitary transformation is a problematic issue. In addition to diagonal loading, a method based on replacing the small singular values was proposed to reduce the condition number of the transformation and still keeping the band-pass characteristics the same. Replacing the small singular values, reduces the condition number of the transformation which is in our interest. The improvement in the output SINR of the RSB and the LCMV beamformers was demonstrated by simulation. More research is needed to successfully design unitary transformations. Since transfor-

mations which are not unitary do not preserve the power of the signal after transformation, the transformed signals are prone to more significant distortion.

Two types of planar arrays were considered in Chapter 5, namely, URA and UCA. Two methods for mitigating the white noise for the URA were introduced. With the proposed method using a 2D transformation, a maximum of 1.76 dB improvement in TSNR can be achieved in the ideal case, which is less than the 3 dB improvement achieved for the linear arrays. Alternatively, the noise reduction method using a 1D transformation for URAs was also proposed, which is a direct adaptation of the method used for ULAs, with a 3 dB improvement achieved. Despite the lower TSNR, the 2D transformation method has less distortion for the directional signals. Therefore, depending on the application and the input SNR, either one of the methods can provide a satisfactory performance. The transformation was also re-designed for the UCA structure by modifying the modulation of the row vectors of the transformation. As demonstrated by simulation results, a clear improvement in performance, in terms of the output SINR has been achieved for a range of input SNR values.

As it was discussed in Chapter 6, the proposed structure is equivalent to a traditional TDL. Therefore, the noise reduction method and the corresponding beamformer can be considered as a beamformer with longer TDLs, but with lower computational complexity. There are different advantages and also disadvantages of using the proposed method. Based on

the application, one might find using the method beneficial or otherwise.

Overall, some the advantages of the proposed noise reduction method are:

- Improved TSNR by a maximum of 3 dB for different array structures.
- providing an alternative approach to beamforming with reduced computational complexity.
- Achieving a more robust beamforming solution, since the method does not involve the computation of the inverse of the signal correlation matrix which is normally needed for computing the optimal weight vector coefficients.
- Since no prior information of the impinging signal is needed, the method is quite flexible. Therefore, it can be used for different array signal processing applications.

On the other hand, the method has the following disadvantages:

- A unitary transformation design can only be achieved for uniform array structures.
- For non-uniform and sparse structures, the condition number needs to be reduced by either diagonal loading or replacing the small singular values, which can change the beam-pattern of the transformation and cause further complications in the design.

- The noise after being processed by the method is not white any more. This makes it more complicated to analyse the impact of the processed noise on the performance of the array signal processing applications, such as beamforming and DOA estimation.

7.2 Future Work

The following topics can be considered as future work.

The output noise spectrum is not white after being processed by the noise reduction processing, and it is correlated between the sensors. More research is needed to analyse the effect of the correlated and coloured noise on the performance of the beamformers, and the characteristics of the remaining noise need to be analysed further.

In Chapter 6, it was shown that the proposed structure is equivalent to a traditional TDL system with a larger TDL length and it was mentioned previously that the same beamforming techniques can be applied to the new set of array signals after the proposed processing, and it is equivalent to kind of adaptive beamformer but with longer TDLs. Therefore, the proposed method can be considered as a low-complexity approach to adaptive beamforming. This approach can be further studied and possibly new adaptive beamformers can be designed with lower complexity and optimal performance.

In addition, for every array structure, a transformation was designed

with the required band-pass characteristics. The transformation has to be invertible and ideally unitary. For the ULA and URA structure designing unitary transformations is not an issue, but with the increasing interest in sparse arrays, designing a unitary transformation is challenging. The transformation was designed for NLAs, with low condition number by either diagonal loading or replacing the small singular values, but designing a unitary or almost unitary transformation for sparse arrays is still an open problem. As the array becomes more sparse, the transformation design becomes more difficult. Some of the sparse arrays which are in focus for future work are co-prime arrays [92, 93], nested arrays [94] and super nested arrays [95, 96].

Another topic for further research can be designing unitary transformations with higher side-lobe attenuation. After the transformation, the directional signals which are available on the side-lobes are removed by consequent high-pass filters. So, the higher the side-lobe attenuation, the less distortion is caused to the directional signal. In this thesis, for ULA, 13 dB side-lobe attenuation has been achieved with DFT matrix as the transformation. By windowing techniques, higher side-lobe attenuation can be achieved, but the transformation will not be exactly unitary after applying the windows to the row vectors of the transformation. Therefore, further research is needed to design unitary transformation with higher side-lobe attenuation.

Appendix:

The relationship between cross correlation and convolution of two signals is [57]

$$E[x_m[n]\, x_n[n+m_0]] = x_m^*[-n] \circ x_n[n]\ , \tag{7.1}$$

where E, $\{\cdot\}^*$ and $\circ$ denote expectation, complex conjugate and convolution, respectively, and m_0 is the lag. Taking the DTFT of both sides yields:

$$\begin{aligned}
\mathrm{DTFT}\{E[x_m[n]\, x_n[n+m_0]]\} &= \mathrm{DTFT}\,\{x_m^*[-n] \circ x_n[n]\} \\
&= \mathrm{DTFT}\,\{x_m^*[-n]\}\,\mathrm{DTFT}\,\{x_n[n]\} \\
&= \sum_{n=-\infty}^{\infty} x_m^*[-n] e^{-j\Omega n} \sum_{n=-\infty}^{\infty} x_n[n] e^{-j\Omega n} \\
&= \sum_{n=-\infty}^{\infty} x_m^*[-n] \left(e^{-j\Omega(-n)}\right)^* \sum_{n=-\infty}^{\infty} x_n[n] e^{-j\Omega n} \\
&= \sum_{n=-\infty}^{\infty} \left(x_m[-n] e^{-j\Omega(-n)}\right)^* \sum_{n=-\infty}^{\infty} x_n[n] e^{-j\Omega n} \\
&= x_m^*(\Omega) x_n(\Omega).
\end{aligned} \tag{7.2}$$

Therefore,

$$\mathrm{DTFT}\{E[x_m[n]\, x_n[n+m_0]]\} = x_m^*(\Omega) x_n(\Omega), \tag{7.3}$$

which is the cross spectral density of $x_m[n]$ and $x_n[n]$.

Bibliography

[1] H. L. Van Trees, *Optimum Array Processing, Part IV of Detection, Estimation, and Modulation Theory*, Wiley, New York, April 2002.

[2] W. Liu and S. Weiss, *Wideband Beamforming: Concepts and Techniques*, John Wiley & Sons, Chichester, UK, March 2010.

[3] H. Krim and M. Viberg, "Two decades of array signal processing research: the parametric approach," *IEEE Signal Processing Magazine*, vol. 13, no. 4, pp. 67–94, July 1996.

[4] B. Allen and M. Ghavami, *Adaptive Array Systems, Fundamentals and Applications*, John Wiley & Sons, Chichester, England, February 2005.

[5] W. Yang, *Sensor Array*, InTech, DOI: 10.5772/2034, March 2012.

[6] B. Widrow, J. R. Glover, J. M. McCool, J. Kaunitz, C. S. Williams, R. H. Hearn, J. R. Zeidler, J. E. Dong, and R. C. Goodlin, "Adaptive noise cancelling: Principles and applications," *Proceedings of the IEEE*, vol. 63, no. 12, pp. 1692–1716, December 1975.

[7] A. K. Jain, *Fundamentals of digital image processing*, Prentice-Hall, Inc., January 1989.

[8] H. Ogawa and E. Oja, "Projection filter, Wiener filter, and Karhunen-Loeve subspaces in digital image restoration," *Journal of Mathematical analysis and applications*, vol. 114, no. 1, pp. 37–51, February 1986.

[9] Y. Kamamori, A. Kawamura, and Y. Liguni, "Zero phase signal analysis and its application to noise reduction," *IEICE Transactions on Fundamentals of Electronics, Communications and Computer Sciences*, vol. J93-A, pp. 658–666, October 2010.

[10] S. Kohmura, A. Kawamura, and Y. Iiguni, "An efficient zero phase noise reduction method for impact noise with damped oscillation," in *Proc. IEEE International Conference on Acoustics, Speech, and Signal Processing*, Vancouver, BC, Canada, 26 May 2013, IEEE, pp. 892–895.

[11] T. B. Spalt, C. R. Fuller, T. F. Brooks, and W. Humphreys, "A background noise reduction technique using adaptive noise cancellation for microphone arrays," in *Proc. 17th AIAA/CEAS Aeroacoustics Conference, American Institute of Aeronautics and Astronautics, Portland, OR*, 6 June 2011, pp. 2715–2731.

[12] J. Chen, J. Benesty, Y. Huang, and S. Doclo, "New insights into the noise reduction Wiener filter," *IEEE Transactions on audio, speech, and language processing*, vol. 14, no. 4, pp. 1218–1234, July 2006.

[13] J. S. Goldstein, I. S. Reed, and L. L. Scharf, "A multistage representation of the Wiener filter based on orthogonal projections," *IEEE Transactions on Information Theory*, vol. 44, no. 7, pp. 2943–2959, November 1998.

[14] S. Kohmura, A. Kawamura, and Y. Iiguni, "A zero phase noise reduction method with damped oscillation estimator," *IEICE Transactions on Fundamentals of Electronics, Communications and Computer Sciences*, vol. 97, no. 10, pp. 2033–2042, October 2014.

[15] W. Thanhikam, Y. Kamamori, A. Kawamura, and Y. Iiguni, "Stationary and non-stationary wide-band noise reduction using zero phase signal," *IEICE Transactions on Fundamentals of Electronics, Communications and Computer Sciences*, vol. 95, no. 5, pp. 843–852, May 2012.

[16] A. Tanaka and A. Kawamura, "Iterative zero phase method for white and impulse noise reduction," in *Proc. 22nd International Conference on Digital Signal Processing (DSP)*, London, UK, 23 August 2017, IEEE, pp. 1–5.

[17] R. Schmidt, "Multiple emitter location and signal parameter estimation," *IEEE Transactions on Antennas and Propagation*, vol. 34, pp. 276–280, March 1986.

[18] R. Roy and T. Kailath, "ESPRIT-estimation of signal parameters via rotational invariancetechniques," *IEEE Transactions on Acoustics, Speech, and Signal Processing*, vol. 37, no. 7, pp. 984–995, July 1989.

[19] B. Friedlander and A. J. Weiss, "Direction finding for wide-band signals using an interpolated array," *IEEE Transactions on Signal Processing*, vol. 41, no. 4, pp. 1618–1634, April 1993.

[20] J. Krolik and D. Swingler, "Focused wide-band array processing by spatial resampling,," *IEEE Transactions on Acoustics, Speech, and Signal Processing*, vol. 38, no. 2, pp. 356–360, February 1990.

[21] G. Su and M. Morf, "The signal subspace approach for multiple wide-band emitter location," *IEEE Transactions on Acoustics, Speech and Signal Processing*, vol. 31, no. 6, pp. 1502–1522, December 1983.

[22] H. Wang and M. Kaveh, "Coherent signal-subspace processing for the detection and estimation of angles of arrival of multiple wide-band sources," *IEEE Transactions on Acoustics, Speech, and Signal Processing*, vol. 33, pp. 823–831, August 1985.

[23] Y.-S Yoon, L. M. Kaplan, and J. H. McClellan, "TOPS: new DOA estimator for wideband signals," *IEEE Transactions on Signal Processing*, vol. 54, no. 6, pp. 1977–1989, June 2006.

[24] E. J. Candes, J. Romberg, and T. Tao, "Robust uncertainty principles: exact signal reconstruction from highly incomplete frequency information," *IEEE Transactions on Information Theory*, vol. 52, no. 2, pp. 489 – 509, February 2006.

[25] E. J. Candès, M. B. Wakin, and S. P. Boyd, "Enhancing sparsity by reweighted l_1 minimization," *Journal of Fourier Analysis and Applications*, vol. 14, pp. 877–905, December 2008.

[26] D. Malioutov, M. Çetin, and A. S. Willsky, "A sparse signal reconstruction perspective for source localization with sensor arrays," *IEEE Transactions on Signal Processing*, vol. 53, no. 8, pp. 3010–3022, August 2005.

[27] J. H. Yin and T. Q. Chen, "Direction-of-arrival estimation using a sparse representation of array covariance vectors," *IEEE Transactions on Signal Processing*, vol. 59, no. 9, pp. 4489–4493, September 2011.

[28] J. M. Zheng and M. Kaveh, "Sparse spatial spectral estimation: a covariance fitting algorithm, performance and regularization," *IEEE Transactions on Signal Processing*, vol. 61, no. 11, pp. 2767–2777, June 2013.

[29] Y. M. Zhang, M. G. Amin, and B. Himed, "Sparsity-based DOA estimation using co-prime arrays," in *Proc. IEEE International Conference on Acoustics, Speech, and Signal Processing*, Vancouver, Canada, May 2013, pp. 3967–3971.

[30] Z. M. Liu, Z. T. Huang, and Y. Y. Zhou, "Direction-of-arrival estimation of wideband signals via covariance matrix sparse representation," *IEEE Transactions on Signal Processing*, vol. 59, no. 9, pp. 4256–4270, Sept. 2011.

[31] Z.-M. Liu, Z.-T. Huang, and Y.-Y. Zhou, "Sparsity-inducing direction finding for narrowband and wideband signals based on array covariance vectors," *IEEE Transactions on Wireless Communications*, vol. 12, no. 8, pp. 1–12, August 2013.

[32] Q. Shen, W. Liu, W. Cui, S. L. Wu, Y. D. Zhang, and M. Amin, "Low-complexity direction-of-arrival estimation based on wideband co-prime arrays," *IEEE Trans. Audio, Speech and Language Processing*, vol. 23, pp. 1445–1456, September 2015.

[33] V. Ambegaokar and B. I. Halperin, "Voltage due to thermal noise in the dc josephson effect," *Physical Review Letters*, vol. 22, no. 25, pp. 1364, June 1969.

[34] H. Nyquist, "Thermal agitation of electric charge in conductors," *Physical review*, vol. 32, no. 1, pp. 110, July 1928.

[35] Y. M. Blanter and M. Büttiker, "Shot noise in mesoscopic conductors," *Physics reports*, vol. 336, no. 1-2, pp. 1–166, October 2000.

[36] R. H. Dicke, P. J. E. Peebles, P. G. Roll, and D. T. Wilkinson, "Cosmic Black-Body Radiation," *The Astrophysical Journal*, vol. 142, pp. 414–419, July 1965.

[37] C. Kipnis and S. R. S. Varadhan, "Central limit theorem for additive functionals of reversible markov processes and applications to simple exclusions," *Communications in Mathematical Physics*, vol. 104, no. 1, pp. 1–19, January 1986.

[38] W. Liu and R. J. Langley, "An adaptive wideband beamforming structure with combined subband decomposition," *IEEE Transactions on Antennas and Propagation*, vol. 89, pp. 913–920, July 2009.

[39] R. T. Compton, Jr., "The relationship between tapped delay-line and FFT processing in adaptive arrays," *IEEE Transactions on Antennas and Propagation*, vol. 36, no. 1, pp. 15–26, January 1988.

[40] R. T. Compton, "The bandwidth performance of a two-element adaptive array with tapped delay-line processing," *IEEE Transactions on Antennas and Propagation*, vol. 36, no. 1, pp. 4–14, January 1988.

[41] A. Jakobsson, S. R. Alty, and S. Lambotharan, "On the implementation of the linearly constrained minimum variance beamformer,"

IEEE Transactions on Circuits & Systems II: Express Briefs, vol. 53, no. 10, pp. 1059–1062, October 2006.

[42] M. E. Knox, "Single antenna full duplex communications using a common carrier," in *Wireless and microwave technology conference (WAMICON), 2012 IEEE 13th annual*, Cocoa Beach, FL, USA, 15-17 April 2012, IEEE, pp. 1–6.

[43] D. Yang, G. Xue, J. Zhang, A. Richa, and X. Fang, "Coping with a smart jammer in wireless networks: A stackelberg game approach," *IEEE Transactions on Wireless Communications*, vol. 12, no. 8, pp. 4038–4047, August 2013.

[44] S. R. Best, "The receiving and scattering properties of a finite dipole array," *IEEE Antennas and Propagation Magazine*, vol. 53, no. 6, pp. 9–17, December 2011.

[45] M. Wang, L. Lin, J. Chen, D. Jackson, W. Kainz, Y. Qi, and P. Jarmuszewski, "Evaluation and optimization of the specific absorption rate for multiantenna systems," *IEEE Transactions on Electromagnetic Compatibility*, vol. 53, no. 3, pp. 628–637, August 2011.

[46] L. Cohen, "The generalization of the Wiener-Khinchin theorem," in *Proceedings of the IEEE International Conference on Acoustics, Speech and Signal Processing*. IEEE, 15 May 1998, vol. 3, pp. 1577–1580.

[47] M. S. Brandstein and D. Ward, Eds., *Microphone Arrays: Signal Processing Techniques and Applications*, Springer, Berlin, April 2001.

[48] W. E. Rodgers and R. T. Compton, Jr., "Adaptive array bandwidth with tapped delay-line processing," *IEEE Trans. Areospace Electronic Systems*, vol. AES-15, no. 1, pp. 21–27, January 1979.

[49] O. L. Frost, III, "An algorithm for linearly constrained adaptive array processing," *Proceedings of the IEEE*, vol. 60, no. 8, pp. 926–935, August 1972.

[50] M. R. Anbiyaei, W. Liu, and D. C. McLernon, "White noise reduction for wideband linear array signal processing," *IET Signal Processing*, October 2017.

[51] M. R. Anbiyaei, W. Liu, and D. C. McLernon, "Performance improvement for wideband DOA estimation with white noise reduction based on uniform linear arrays," in *Proc. IEEE, Sensor Array and Multichannel Signal Processing Workshop (SAM)*, Rio de Janeiro, Brazil, July 2016.

[52] B. Noble and J. W. Daniel, *Applied Linear Algebra*, Prentice-Hall, Upper Saddle River, NJ, 1977.

[53] W. Liu, S. Weiss, and L. Hanzo, "A subband-selective broadband GSC with cosine-modulated blocking matrix," *IEEE Transactions on Antennas and Propagation*, vol. 52, pp. 813–820, March 2004.

[54] T. Sekiguchi and Y. Karasawa, "Wideband beamspace adaptive array utilizing FIR fan filters for multibeam forming," *IEEE Transactions on Signal Processing*, vol. 48, no. 1, pp. 277–284, January 2000.

[55] W. Liu, R. Wu, and R. Langley, "Design and analysis of broadband beamspace adaptive arrays," *IEEE Transactions on Antennas and Propagation*, vol. 55, no. 12, pp. 3413–3420, December 2007.

[56] B. Mulgrew, P. Grant, and J. Thompson, "Random signal analysis," in *Digital Signal Processing*, pp. 176–205. Macmillan Education UK, 1999.

[57] R. N. Bracewell, *The Fourier Transform and its applications*, McGraw-Hill Series in Electrical Engineering, Networks and Systems, New York, 2nd edition, February 1986.

[58] E. J. Candes and T. Tao, "Near-optimal signal recovery from random projections: Universal encoding strategies," *IEEE transactions on Information Theory*, vol. 52, no. 12, pp. 5406–5425, 30 November 2006.

[59] C. Y. Chen and P. P. Vaidyanathan, "Compressed sensing in MIMO radar," in *Proc. 42nd Asilomar Conference on Signals, Systems and Computers*. IEEE, October 2008, pp. 41–44.

[60] N. B. Karahanoglu and H. Erdogan, "A* orthogonal matching pursuit: Best-first search for compressed sensing signal recovery," *Digital Signal Processing*, vol. 22, no. 4, pp. 555–568, July 2012.

[61] S. S. Chen, D. L. Donoho, and M. A. Saunders, "Atomic decomposition by basis pursuit," *SIAM review*, vol. 43, no. 1, pp. 129–159, 2001.

[62] J. A. Tropp and S. J. Wright, "Computational methods for sparse solution of linear inverse problems," *Proceedings of the IEEE*, vol. 98, no. 6, pp. 948–958, April 2010.

[63] M. Rossi, A. M. Haimovich, and Y. C. Eldar, "Conditions for target recovery in spatial compressive sensing for MIMO radar," in *Proc. IEEE International Conference on Acoustics, Speech and Signal Processing (ICASSP)*. IEEE, May 2013, pp. 4115–4119.

[64] J. Kim, R. Monteiro, and H. Park, "Group sparsity in nonnegative matrix factorization," in *Proc. SIAM International Conference on Data Mining*, Anaheim, CA, USA, 2012, SIAM, pp. 851–862.

[65] J. Huang and T. Zhang, "The benefit of group sparsity," *The Annals of Statistics*, vol. 38, no. 4, pp. 1978–2004, 2010.

[66] M. Grant and S. Boyd, "CVX: Matlab software for disciplined convex programming, version 2.0 beta, build 1023," December 2013, Available: http://cvxr.com/cvx.

[67] M. Grant and S. Boyd, "Graph implementations for nonsmooth convex programs," in *Recent Advances in Learning and Control*, V. Blondel, S. Boyd, and H. Kimura, Eds., Lecture Notes in Control and Information Sciences, pp. 95–110. Springer-Verlag Limited, 2008, http://stanford.edu/ boyd/graph_dcp.html.

[68] P. Stoica and A. Nehorai, "MUSIC, maximum likelihood, and Cramer-Rao bound," *IEEE Transactions on Acoustics, Speech, and Signal Processing*, vol. 37, no. 5, pp. 720–741, May 1989.

[69] B. D. Carlson, "Covariance matrix estimation errors and diagonal loading in adaptive arrays," *IEEE Transactions on Aerospace and Electronic Systems*, vol. 24, pp. 397–401, July 1988.

[70] F. W. Vook and R. T. Compton, Jr., "Bandwidth performance of linear adaptive arrays with tapped delay-line processing," *IEEE Transactions on Aerospace and Electronic Systems*, vol. 28, no. 3, pp. 901–908, July 1992.

[71] N. Lin, W. Liu, and R. J. Langley, "Performance analysis of an adaptive broadband beamformer based on a two-element linear array with sensor delay-line processing," *Signal Processing*, vol. 90, pp. 269–281, January 2010.

[72] M. R. Anbiyaei, W. Liu, and D. C. McLernon, "Performance improvement for wideband beamforming with white noise reduction

based on sparse arrays," in *Proc. 25th European Signal Processing Conference (EUSIPCO)*, Kos Island, Greece, Aug 2017, pp. 2433–2437.

[73] Y. Zhao, W. Liu, and R. J. Langley, "An application of the least squares approach to fixed beamformer design with frequency invariant constraints," *IET Signal Processing*, pp. 281–291, June 2011.

[74] M. B. Hawes and W. Liu, "Sparse microphone array design for wideband beamforming," in *Proc. International Conference on Digital Signal Processing*, Santorini, Greece, July 2013.

[75] R. L. de Queiroz, "On unitary transform approximations," *IEEE Signal Processing Letters*, vol. 5, no. 2, pp. 46–47, February 1998.

[76] R. L. de Queiroz, "Approximating lapped transforms through unitary postprocessing," *IEEE Signal Processing Letters*, vol. 8, no. 12, pp. 307–309, December 2001.

[77] M. Ghavami, "Wideband smart antenna theory using rectangular array structures," *IEEE Transactions on Signal Processing*, vol. 50, no. 9, pp. 2143–2151, September 2002.

[78] W. Liu, "Design and implementation of a rectangular frequency invariant beamformer with a full azimuth angle coverage," *Journal of the Franklin Institute*, vol. 348, pp. 2556–2569, November 2011.

[79] S. C. Chan and K. S. Pun, "On the design of digital broadband beamformer for uniform circular array with frequency invariant characteristics," in *Proc. IEEE International Symposium on Circuits and Systems*, Phoenix, USA, May 2002, vol. 1, pp. 693–696.

[80] L. Yu and W. Liu, "Performance analysis of the data subtraction based robust beamformer," in *Proc. of the Sensor Signal Processing for Defence Conference*, London, UK, September 2011, pp. 21–24.

[81] M. R. Anbiyaei, W. Liu, and D. C. McLernon, "White noise reduction for wideband beamforming based on uniform rectangular arrays," in *Proc. 22nd International Conference on Digital Signal Processing (DSP)*, London, UK, Aug 2017, pp. 1–5.

[82] G. Sommerkorn, D. Hampicke, R. Klukas, A. Richter, A. Schneider, and R. Thomä, "Uniform rectangular antenna array design and calibration issues for 2-d ESPRIT application," in *Proceedings of the 4th European Personal Mobile Communications Conference*, Vienna, Austria, February 2001.

[83] J. S. Lim and A. V. Oppenheim, *Two-dimensional Signal and Image Processing*, Prentice Hall, Englewood Cliffs, New Jersey, 1990.

[84] W. Liu, "Design of a rectangular frequency invariant beamformer with a full azimuth angle coverage," in *Proc. European Signal Processing Conference*, Glasgow, Scotland, August 2009, pp. 579–582.

[85] P. Ioannides and C. A. Balanis, "Uniform circular and rectangular arrays for adaptive beamforming applications," *IEEE Antennas and Wireless Propagation Letters*, vol. 4, no. 1, pp. 351–354, 26 September 2005.

[86] C. A. Balanis, *Antenna Theory: Analysis and Design*, Wiley, February 2016.

[87] M. Abramowitz and I. A. Stegun, Eds., *Handbook of Mathematical Functions*, Dover Publications, New York, 1970.

[88] P. S. Naidu, *Sensor array signal processing*, CRC press, June 2009.

[89] C. P. Robert, *Monte Carlo Methods*, Wiley Online Library, August 2016.

[90] P. C. Hansen, *Rank-Deficient and Discrete Ill-Posed Problems. Numerical Aspects of Linear Inversion*, SIAM, Philadelphia, 1998.

[91] C. R. Vogel, *Computational Methods for Inverse Problems*, Society for Industrial and Applied Mathematics, Philadelphia, PA, USA, 2002.

[92] P. P. Vaidyanathan and P. Pal, "Sparse sensing with co-prime samplers and arrays," *IEEE Transactions on Signal Processing*, vol. 59, no. 2, pp. 573–586, Feb. 2011.

[93] S. Qin, Y. D. Zhang, and M. G. Amin, "Generalized coprime array configurations for direction-of-arrival estimation," *IEEE Trans-*

actions on Signal Processing, vol. 63, no. 6, pp. 1377–1390, March 2015.

[94] P. Pal and P. P. Vaidyanathan, "Nested arrays: A novel approach to array processing with enhanced degrees of freedom," *IEEE Transactions on Signal Processing*, vol. 58, no. 8, pp. 4167–4181, August 2010.

[95] C. L. Liu and P. P. Vaidyanathan, "Super nested arrays: Linear sparse arrays with reduced mutual coupling—Part I: Fundamentals," *IEEE Transactions on Signal Processing*, vol. 64, no. 15, pp. 3997–4012, August 2016.

[96] C. L. Liu and P. P. Vaidyanathan, "Super nested arrays: Linear sparse arrays with reduced mutual coupling—Part II: High-order extensions," *IEEE Transactions on Signal Processing*, vol. 64, no. 16, pp. 4203–4217, August 2016.